Design of an Automated On-Car Brake Lathe

by

Andrew Kirk Wilson

B.S.M.E., Santa Clara University (1999)

Submitted to the Department of Mechanical Engineering
in partial fulfillment of the requirements for the degree of

Master of Science in Mechanical Engineering

at the

MASSACHUSETTS INSTITUTE OF TECHNOLOGY

June 2001

Author_____
Department of Mechanical Engineering
May 23, 2001

Certified by_____
Samir A. Nayfeh
Assistant Professor of Mechanical Engineering
Thesis Supervisor

Accepted by_____
Ain A. Sonin
Professor of Mechanical Engineering
Chairman, Department Committee on Graduate Students

Design of an Automated On-Car Brake Lathe

by

Andrew Kirk Wilson

Submitted to the Department of Mechanical Engineering
on May 23, 2001, in partial fulfillment of the
requirements for the degree of
Master of Science in Mechanical Engineering

Abstract

An on-car brake lathe resurfaces disk-brake rotors by rotating them "in place" and making a light cut along the surface of the disk. The primary goal of this thesis is to develop an automated cutting head for an on-car brake lathe. The new cutting head must produce a surface finish that matches or exceeds that of the current (manual) cutting head. Pro-Cut International, a leading manufacturer of on-car brake lathes, developed functional requirements and cost constraints for the automated cutting head.

Technical challenges include design and fabrication of low-cost precision linear bearings and actuators with dynamic stiffness sufficient to suppress chatter.

During this thesis, two prototype cutting heads were designed, manufactured, and tested. The first prototype employed modular linear bearings, and produced unacceptable surface finish due to chatter. Cutting-tip vibration measurements combined with modal testing showed that chatter was caused by low structural stiffness of the modular bearing rails.

A second prototype employing a unitary ground bearing system produced an acceptable surface finish of 70 μ-inch at 0.015" depth of cut per side. The key components of this design can be extruded and sliced to form the assembly, thereby meeting cost constraints.

Thesis Supervisor: Samir A. Nayfeh
Title: Assistant Professor of Mechanical Engineering

Contents

List of Figures

Chapter 1

Introduction

1.1 Background

An on-car brake lathe resurfaces automotive disk-brake rotors "in place." The lathe mounts to the disk brake via a hub adaptor and spins the rotor on its bearings while cutting at a specified depth along the rotor's surface. This process eliminates alignment errors that may arise during assembly and disassembly of the disk brake system.

The goals of this thesis include design, fabrication, and analysis of an automated cutting head for the on-car brake lathe. Pro-Cut International currently sells manual brake lathes to various automotive repair shops around the world. They developed functional requirements and cost constraints for the new automated cutting head. In summary, the automated cutting head design must match or exceed the current manual cutting head's surface finish capabilities.

Technical challenges include: (1) design of a low-cost bearing set and actuators, and (2) combining these precision components while maintaining high dynamic stiffness in an environment with large vibration disturbances.

1.2 Current Design Usage

Pro-Cut's current brake lathe, seen in Figure 1-1, bolts to the car's rotor via a hub adaptor; the hub adaptor is not shown. Various size hub adaptors allow the brake lathe to be mounted to most foreign and domestic vehicles.

The cutting head's inboard-outboard placement relative to the vehicle (see Figure 2-5), is adjusted so as to roughly center the rotor between the cutting tips. This placement is accomplished by bolting the cutting head to either a "booster plate" for inboard placement, or to a "base plate" for outboard placement depending on the rotor's position within the wheel well. The technician brings the cutters into contact with the rotor and then adjusts the dials at the back of the cutting head to set the depth of cut. Feed is engaged to start the cutting process and these steps are repeated as needed.

1.3 Design Requirements

Many requirements restrict cutting head design options. A list follows

- New cutting head production cost is to be under $300. Production cost is the cost per machine in quantities of 2,000 units per year.

- No more than one sensor for depth of cut is allowed. Due to possible patent infringement, multiple depth of cut sensors are disallowed.

- The new cutting head must cut rotor thicknesses ranging from 2 mm (0.079 in) to 63.5 mm (2.5 in). Rotor thickness is the distance between the two braking surfaces.

- Resurfaced rotor thickness variation must be less than 0.0005".

- The cutting head must be able to make cuts as deep as 0.015" per side (0.030" total).

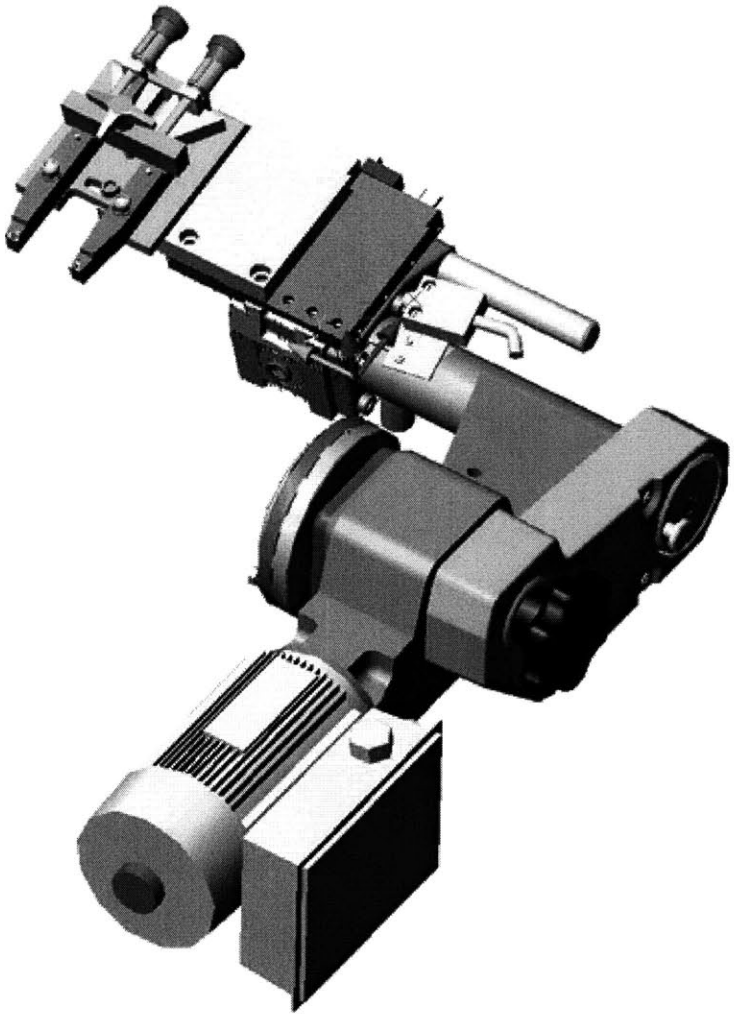

Figure 1-1: PFM900: Current brake lathe design

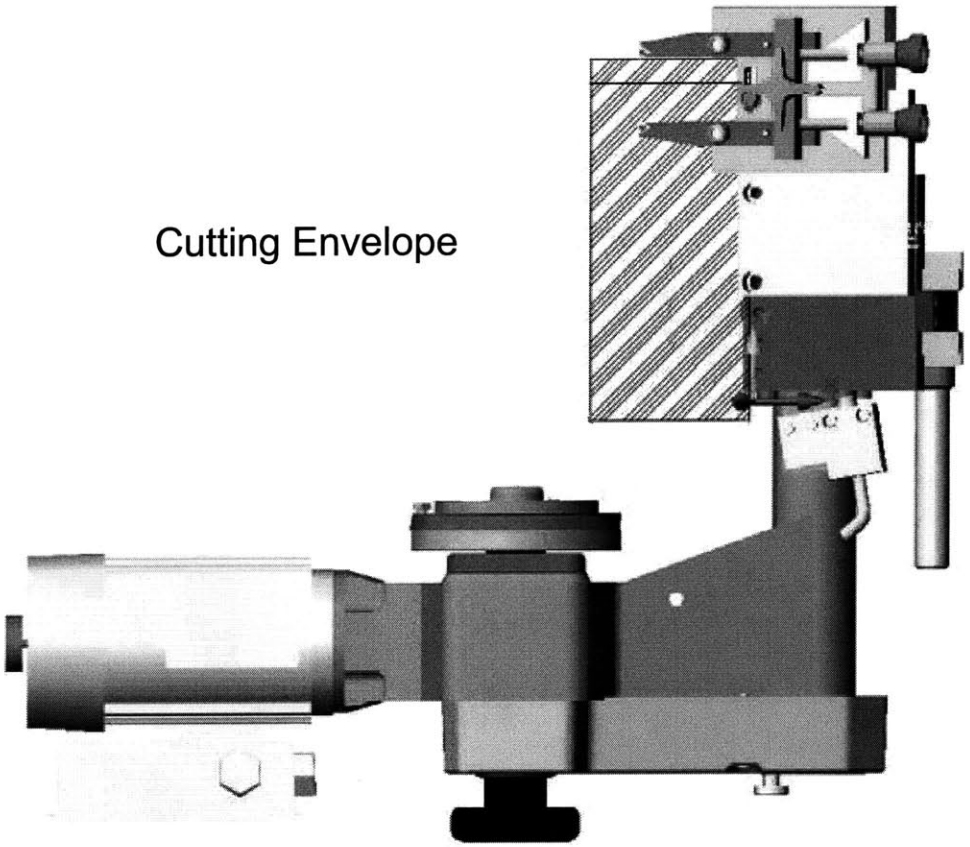

Figure 1-2: The cutting envelope is the hatched rectangle

- The system must determine rotor thickness before and after resurfacing and accordingly set the depth of cut.
- In case of controller failure, the machine must be operable in manual mode.
- The machine must measure lateral run-out non-intrusively. That is, it must determine rotor thickness variation without altering the freshly cut surface.
- The new cutting head must fit inside the wheel-well of various cars. Wheel-well rotor placement varies from automobile to automobile. Therefore, cutting head placement must encompass a broad range in order to meet this criterion. The cutting envelope is indicated by the hatched rectangle in Figure 1-2.

Chapter 2

Machine Design

2.1 Design Approach

A discussion of machine design and implementation follows. Bearing design, motor sizing, actuator selection, experimental results, interesting machine elements and designs are outlined in hopes of benefitting future machine designs of the reader and the writer.

2.1.1 Rotary vs. Linear

Rotary and linear cutting tip arrangements are the most obvious design solutions, shown in Figures 2-1 and 2-2.

Rotary

The rotary design appears to be the most simple to design and manufacture. A rotary encoder measures differential motion between cutting tips and a clutch mechanism switches actuator torque from one cutting tip to another so that only one motor is needed. The limitation of moving a single cutter at a time is moot: only differential motion can be measured according to design specifications, therefore only one cutter may move at a time for any design. We have a common pivot point and a single bearing set; therefore a minimal number of precision parts are needed. In addition,

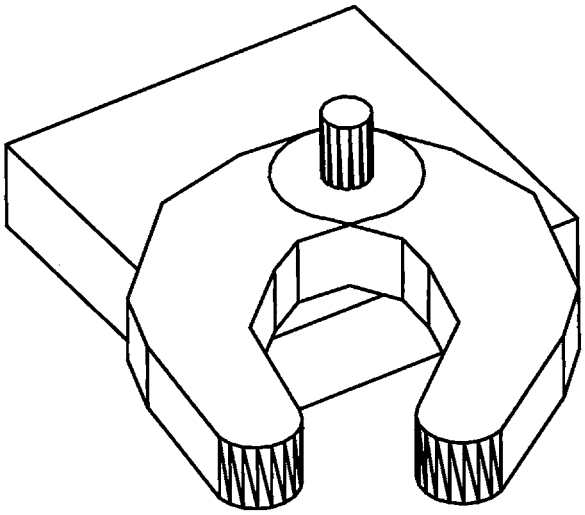

Figure 2-1: Rotary cutting head design

the rotary bearing is inherently easy to seal.

A rotary design is somewhat complicated to control. *Abbe* errors, although mathematically compensatable, can cause large errors because the cutting arms act like lever arms by amplifying angular errors. A very high-resolution encoder is therefore needed to accurately set depth of cut.

For example, if we specify the depth of cut to be 0.02" and let the rotor be placed symmetrically between the two cutting arms as they come into contact with the rotor surface. The arm length must be roughly 3" to cut the entire braking-surface radius. Depth of cut and arm rotation are related as follows

$$L \sin\theta = C \tag{2.1}$$

where C is the depth of cut, L is the arm length and θ is the cutting arm rotation.

With $C = 0.02$", and $L = 3$", the cutting arm must rotate 0.382°. A typical encoder has 2000 counts per revolution, which equates to 5.5 counts per degree or 0.18 degrees per count. It is feasible to move the system 2 or 3 counts, but cutting arm placement will not be robust to disturbances. For the case when the cutting arms are at an angle with respect to the rotor's surface, i.e., when the rotor is off-center from the two cutting tips, the required encoder resolution increases. With a standard

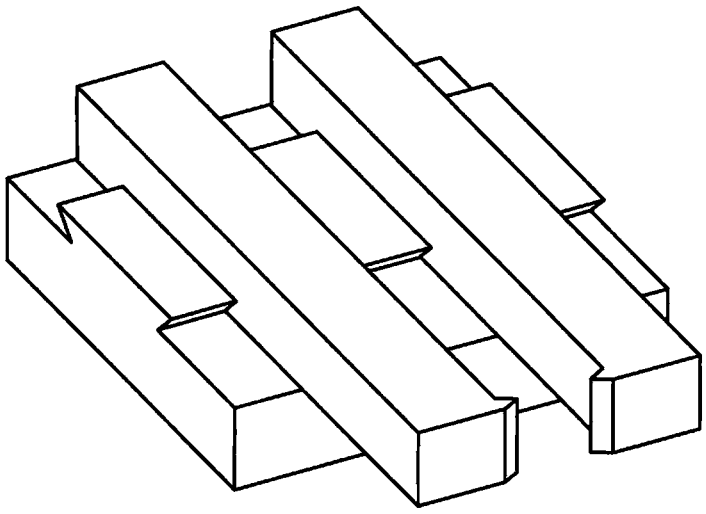

Figure 2-2: Linear Cutting Head Design

encoder, it becomes impossible to set depth of cut to the required accuracy.

To maintain rotor thickness variation less than 0.0005", each cutting tip must be held stationary to within ±0.00025", equivalently, the arm must not rotate more than $\pm 0.0048^{\circ}$. A 2000 count per revolution encoder cannot detect such motions, i.e., this system tries to hold position to $1/40$ of an encoder count. However, an anti-backlash worm-gear reduction easily allows the system to meet the criteria and is a simple solution.

For example, holding the cutting arms to within 15 counts requires a 570:1 gear reduction between the encoder and the cutting arms. Either a single 570:1 worm-gear reduction or two 24:1 worm-gear reductions placed in series would allow the system to meet the requirements.

In fact, the performance specification is easy to meet: we require only that the tools be stationary to within 0.0005", but this is achievable with a lower resolution if the system does not backdrive.

Linear

A simple linear-motion design is shown in Figure 2-2. Two motors, one for each cutting arm, rotate fine lead screws which transmit torque to the cutting arms via preloaded nuts. Multiple bearing surfaces means more precision parts and higher cost which are major drawbacks. The high resolution and zero backlash of preloaded fine lead screw mechanisms, allow for an inexpensive standard resolution encoder.

Although the linear system's mechanical part costs are higher than the rotary system's, ease of cutting tip placement and regulation afforded by the kinematics of the linear design's simplicity outweigh the rotary system's low cost advantage. Therefore, the new cutting head implements a linear arrangement.

2.1.2 Motor Type Selection

DC motors and stepper motors are the most reasonable lead screw actuators based on the design constraints. Pneumatics or hydraulics were ruled out by the sponsor. Stepper motors are extremely simple to control, relatively inexpensive, have a long life and are open loop stable. Their main drawbacks are very low stall torque and that large gear reductions are needed for smooth motions. Constant depth of cut is imperative; accordingly the system cannot be back drivable. A lockdown mechanism should be used in conjunction with a stepper motor drive.

In comparison, DC motors are relatively complicated to control, are open loop unstable, and on average cost slightly more than an equivalent stepper motor. DC motors have smooth motions and generate high torque output. They easily prevent the lead screws from being back-driven so a lockdown mechanism is not needed.

Both motor types have advantages and disadvantages. In summary, the system is either driven by a less expensive stepper motor with gear reduction accompanied by a lockdown mechanism for regulation, or a DC motor that is slightly more complicated to control without a lockdown mechanism. DC motors are chosen because of their high torque capabilities and even though they are more complicated to control, it is not overly difficult.

2.1.3 Lead Screw and Motor Sizing

Cutting tip placement requires precision actuation. Worm gear, or small lead lead-screw mechanisms produce the desired cutting tip placement at a reasonable cost. Worm gears are a good solution for specific applications but the backlash associated with meshing gears could be treacherous to cutting tip regulation due to fluctuating loads inherent to lathing. Therefore, a lead screw with a preloaded nut to prevent backlash is the choice actuator.

To regulate the cutting tips to within 0.00025", a fine lead lead screw must be used. Assuming that position can be accurately held to within 15 encoder counts, which equates to $\pm 1.35^\circ$ motor rotation, the motor shaft rotates no more than 2.7°. The desired lead of the lead screw is calculated as follows

$$\theta \times \frac{\text{rev.}}{360^\circ} \times \text{Lead} \leqslant D \tag{2.2}$$

where

θ = rotation of the shaft = 2.7°

D = distance travelled = 0.00025"

The lead must be less than 0.033"/rev. The project sponsor stipulated that the cutting tips must be at cutting position in under ten seconds. After examining the cutting envelope, it was determined that the maximum cutting tip travel is roughly 6" from maximum inboard to maximum outboard positions. Assuming that the motor will spin at a maximum of 3,000 rpm and that the cutting tip is attached to a lead screw with a lead of 0.025 inches, the tip will travel 6" in 10 seconds as shown in Figure 2-3.

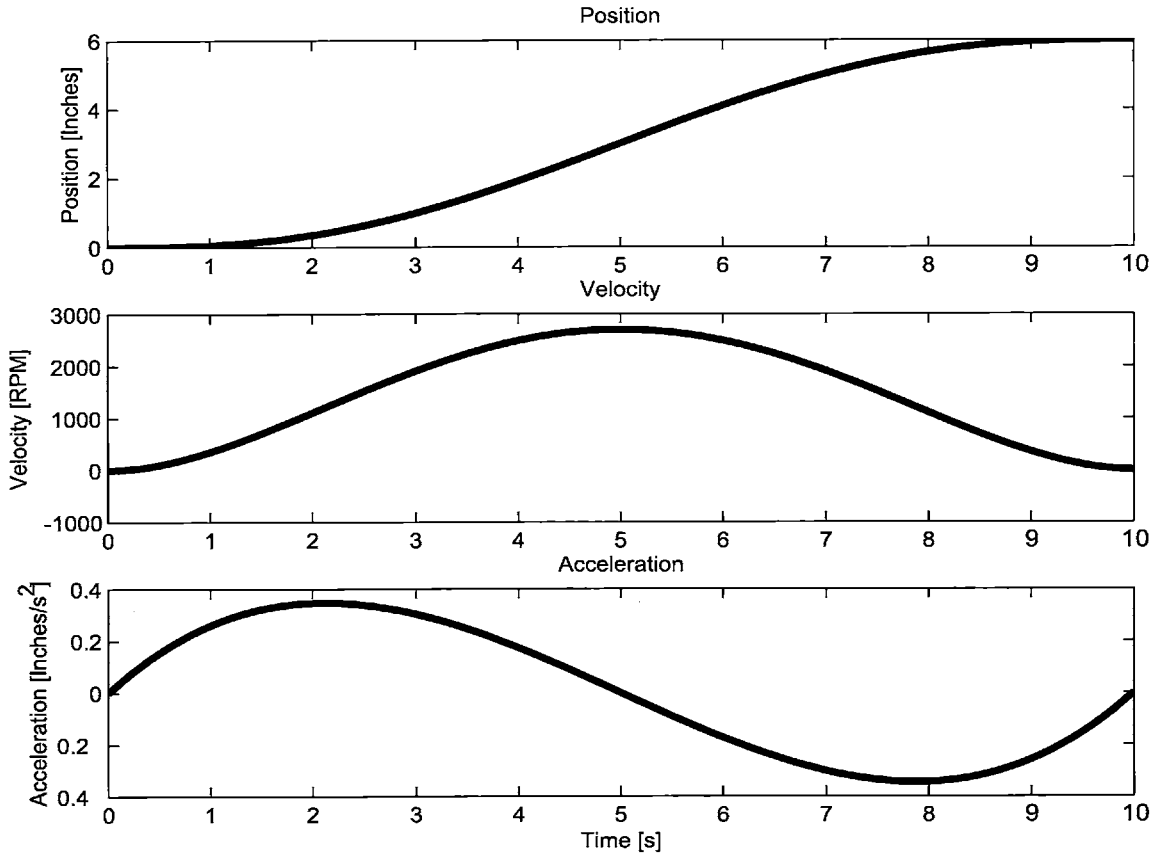

Figure 2-3: Cutting tip trajectory: position, velocity and acceleration

The lead screw must be stiff to ensure that its first mode is not excited as it rotates at 3,000 rpm. By intuition, the lead screw diameter should be large and its length should be short to increase stiffness. Looking at "off the shelf" lead screw mechanisms, the largest diameter shafts with 0.025" lead have 1/4" diameter.

The lead screw's first resonant frequency can be approximated using Rayleigh's method, which may be stated as follows: "In the fundamental mode of an elastic system, the distribution of vibration and potential energies is such as to make the frequency a minimum," [13]. This approximation is an energy based method and slightly overestimates a systems fundamental frequency; the fundamental frequency is approximated by equating average kinetic energy to the average potential energy and solving for ω.

The lead screw's potential energy T is

$$T = \frac{1}{2} EI \int_0^l \left(\frac{d^2 y}{dx^2} \right)^2 dx \tag{2.3}$$

The work done by the external system on the shaft is

$$W = \frac{1}{2} P \int_0^l \left(\frac{dy}{dx} \right)^2 dx \tag{2.4}$$

where y is the lateral displacement of the lead screw's axis at a distance x from one end, l is the lead screw's length, EI is its bending stiffness, and P is thrust load from the external system.

The available kinetic energy is calculated by subtracting Equation 2.4 from Equation 2.3. A shaft element has mass per unit length m/l, and a velocity $2\pi n y$, where n is the shaft's angular velocity. The kinetic energy, V, from bending about its axis is

$$V = 2\pi^2 n^2 m \int_0^l y^2 dx \tag{2.5}$$

Raleigh's Method then gives

$$2\pi^2 n^2 m \int_0^l y^2 dx = \frac{1}{2} EI \int_0^l \left(\frac{d^2y}{dx^2}\right)^2 dx - \frac{1}{2} P \int_0^l \left(\frac{dy}{dx}\right)^2 dx \tag{2.6}$$

Introducing non-dimensional variables

$$\lambda^2 = \frac{Pl^2}{EI} \tag{2.7}$$

$$\alpha^4 = \frac{4\pi^2 m n^2 l^4}{EI} \tag{2.8}$$

equation 2.6 may be written

$$\int_0^l \left(\frac{d^2y}{dx^2}\right)^2 dx = \left(\frac{\lambda}{l}\right)^2 \int_0^l \left(\frac{dy}{dx}\right)^2 dx + \left(\frac{\alpha}{l}\right)^4 \int_0^l y^2 dx \tag{2.9}$$

Ignoring the lateral stiffness of the nut, we can model the lead-screw mechanism as a cantilever beam. Therefore we need to come up with a deflection function $y(x)$ that matches a cantilever beam's boundary conditions. The shaft is clamped at $x = 0$ and free at $x = l$, thus the deflection y and slope $\frac{dy}{dx}$ are zero at $x = 0$. The bending moment $EI\frac{d^2y}{dx^2}$ and shear force $EI\frac{d^3y}{dx^3}$ are zero at $x = l$. Also, it can easily be seen that $EI\frac{d^4y}{dx^4} = 0$ at $x = l$.

A deflection function that matches these constraints is

$$y = 20l^3x^2 - 10l^2x^3 + x^5 \tag{2.10}$$

Solving Equation 2.9 for α gives

$$\alpha = 1.875$$

Plugging in the lead-screw parameters into Equation 2.8, the fundamental frequency is calculated as 95 Hz, equivalently 5710 rpm.

The lead screw parameters are listed as

α	=	1.875	clamped-free end condition
l	=	0.2032 m	lead screw length
E	=	2.1 E+011 N/m^2	Young's Modulus
I	=	8e-011 m^4	$\pi \times d^4/64$
d	=	0.005436 m	shaft diameter
ρ	=	7865 kg/m^3	material density
A	=	0.000023 m^2	shaft cross-sectional area

The shaft's first mode is well above the 50 Hz excitation caused by rotating the 3,000 rpm motor speed; therefore this system will be stable.

The cutting tip motion needs to be as smooth as possible to reduce the likelihood of exciting high frequency modes, and to minimize torque requirements. A 5$^{\text{th}}$ degree polynomial position trajectory allows the user to specify the cutting tip's initial and final positions, velocities, and accelerations [5]

$$\theta(t) = a_0 + a_1 t + a_2 t^2 + a_3 t^3 + a_4 t^4 + a_5 t^5 \tag{2.11}$$

where constraints are specified by constants a_0 through a_5 as

$$\begin{aligned}
\theta_0 &= a_0 \\
\theta_f &= a_0 + a_1 t_f + a_2 t_f^2 + a_3 t_f^3 + a_4 t_f^4 + a_5 t_f^5 \\
\dot{\theta}_0 &= a_1 \\
\dot{\theta}_f &= a_1 + 2a_2 t_f + 3a_3 t_f^2 + 4a_4 t_f^3 + 5a_5 t_f^4 \\
\ddot{\theta}_0 &= 2a_2 \\
\ddot{\theta}_f &= 2a_2 + 6a_3 t_f + 12a_4 t_f^2 + 20a_5 t_f^3
\end{aligned} \tag{2.12}$$

We have six equations and six unknowns. The solutions are

$$\begin{aligned}
a_0 &= \theta_0 \\
a_1 &= \dot{\theta}_0 \\
a_2 &= \frac{1}{2}\ddot{\theta}_0 \\
a_3 &= \frac{20\theta_f - 20\theta_0 - (8\dot{\theta}_f + 12\dot{\theta}_0)t_f - \left(3\ddot{\theta}_0 - \ddot{\theta}_f\right)t_f^2}{2t_f^3} \\
a_4 &= \frac{30\theta_0 - 30\theta_f + (14\dot{\theta}_f + 16\dot{\theta}_0)t_f + \left(3\ddot{\theta}_0 - 2\ddot{\theta}_f\right)t_f^2}{2t_f^4} \\
a_5 &= \frac{12\theta_f - 12\theta_0 - (6\dot{\theta}_f + 6\dot{\theta}_0)t_f - \left(\ddot{\theta}_0 - \ddot{\theta}_f\right)t_f^2}{2t_f^5}
\end{aligned} \tag{2.13}$$

The position, velocity and acceleration profiles can be seen in Figure 2-3.

The torque required to drive the load is defined as follows

$$T_{tot} = T_f + T_v + T_l + T_j \tag{2.14}$$

where

T_{tot} = required torque

T_f = nut drag torque

T_v = viscous torque

T_l = load torque

T_{jA} = torque to accelerate/decelerate inertia

Viscous torque T_v, is proportional to speed and is defined in Equation 2.15

$$T_v = K_d \times W \tag{2.15}$$

T_v = viscous torque

K_d = damping constant

W = speed

Load torque T_l is defined in Equation 2.16

$$T_l = \frac{\text{Load} \times \text{Lead}}{2\pi \times \text{Efficiency}} \tag{2.16}$$

Acceleration torque T_{jA} is defined in Equation 2.17

$$T_{jA} = J \times A \tag{2.17}$$

T_{jA} = acceleration torque

J = effective inertia of the motor shaft, coupling and lead screw

A = acceleration rate

Detailed trajectory and torque calculations can be found in Appendix C; the torque profile can be seen in Figure 2-4. To properly select a motor, the maximum required torque is multiplied by a safety factor. The motor's intermittent duty zone should match this value.

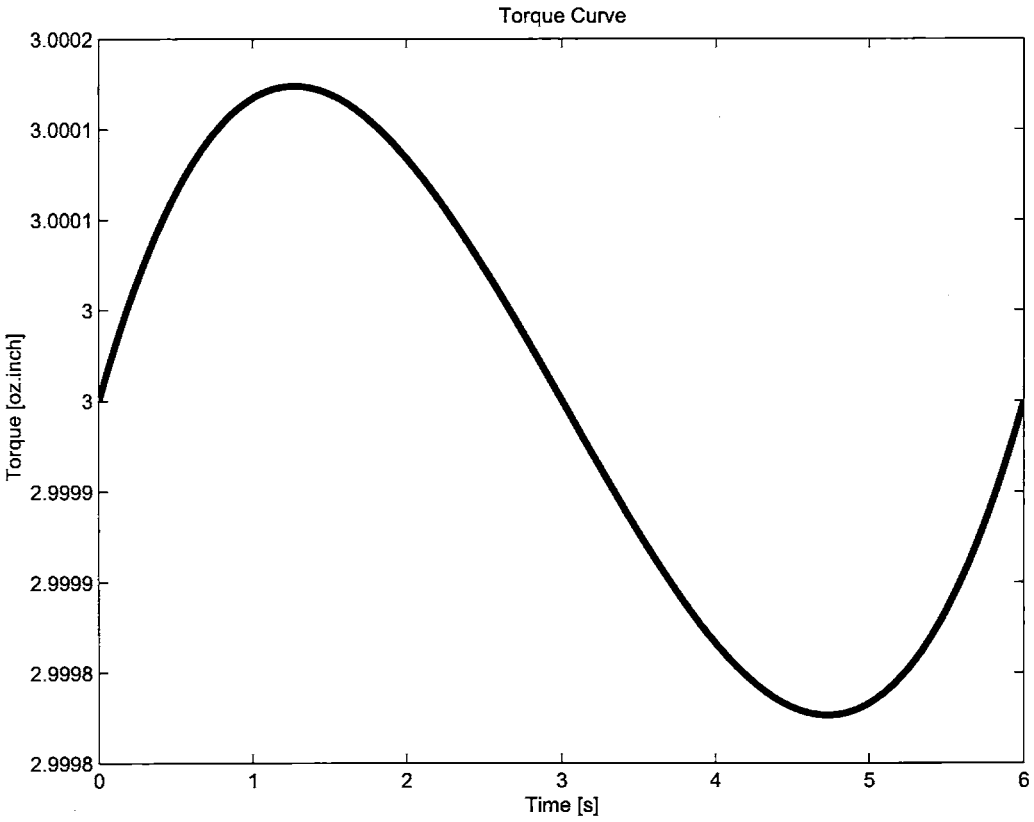

Figure 2-4: Torque profile for motor actuation of cutting tip

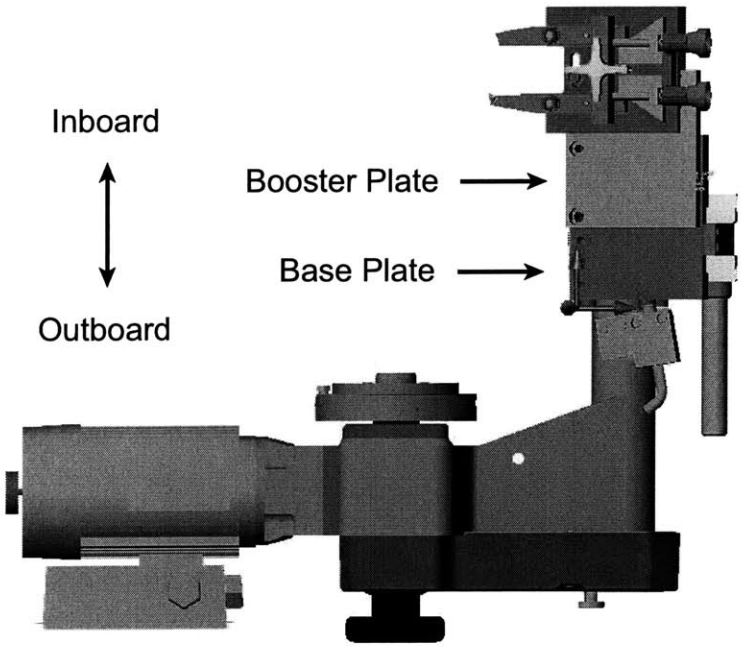

Figure 2-5: Inboard-outboard definition

2.1.4 Inboard-Outboard Positioning

Automatic vs. Manual Actuation

To minimize costs, coarse lateral movement (inboard-outboard movement) is manually set, see Figure 2-5. Although this does not allow for "hands free" lathe operation, the decision is straightforward. Similar to the setup of a standard CNC lathe, the machinist manually sets the tailstock, zeroes the machine, and sets depth of cut parameters in the computer. Likewise for the new brake lathe design the technician places the cutting tips within an inch of the rotor's surface, zeros the machine, and commands a depth of cut. This choice greatly reduces costs.

Sliding Contact Bearings

To set depth of cut and adjust inboard-outboard position, a minimum of one linear bearing system is needed. Cost limitations rule out rolling element bearings, and low traversal speeds do not require them. Sliding contact bearings are an adequate choice; they are simple, inexpensive, have high stiffness, and inherent damping. These

properties are well suited to machine tools [12].

The current brake lathe uses dovetail bearings for traversal along the feed direction (see Figure 2-6), but the project sponsor expressed interest in a gibless bearing system because vibrations cause the gib to become misadjusted.

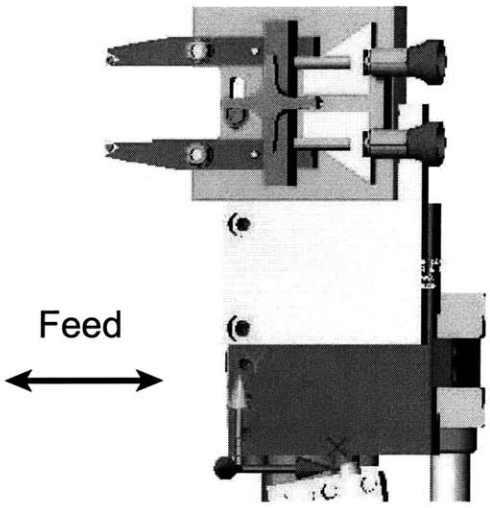

Figure 2-6: Feed definition

Chapter 3

Kinematic Design

3.1 Exact Constraint Theory

Accuracy, repeatability, and resolution are important measures affecting the quality of a machine. Accuracy is a measure of the maximum error between the average experimental value and the desired value. Repeatability is the measure of error between attempts on the same desired output. Resolution is the smallest mechanical step that the machine can make. For the brake lathe, accuracy is the difference between actual cut depths and desired cut depth, repeatability is the variance of cut depth between different cut sessions, and resolution is the minimum allowable cut depth. To minimize these quanta, exact-constraint bearing design is implemented. Properly executed, exact constraint bearings have high repeatability and smooth motions [12].

Three-dimensional objects have six degrees of freedom, three translation motions (referred to as X, Y and Z) and three rotary motions (referred to θ_x, θ_y and θ_z) as shown in Figure 3-1. These six degrees of freedom fully define the position and orientation of an object in space. When designing a machine, we must account for these six degrees of freedom so that the machine is high performance and low cost. The use of exact constraint design, "kinematic design," uniquely constrains these six degrees of freedom to obtain the desired precise and repeatable trajectory. Such mechanisms do not have "play," binding and assembly stresses, without the cost of tightly toleranced parts [2].

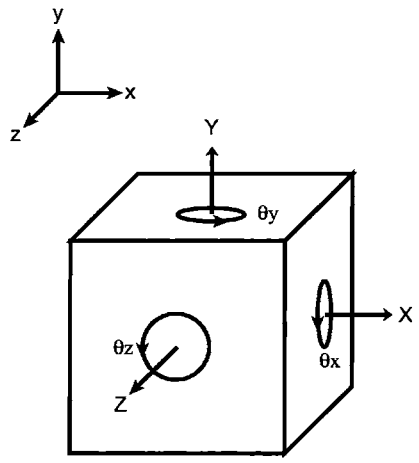

Figure 3-1: Six degrees of freedom

Overconstrained designs result when imposed constraints compete to control the same degree of freedom. These systems have three potential problems [2]

- Loose fit. That is, the dimensions of the bearings are such that there is "play" between the parts.
- Tight fit. The dimensions of the bearings are such that there is interference between the bearings and they bind against each other.
- Tolerance specification. To fix dimension problems, bearing tolerances can be tightened with a manufacturing cost penalty.

Overconstrained design by mating two perfectly dimensioned parts still results in built up stresses. For example, a doubly constrained plate in the x-direction as shown in Figure 3-2, generates internal stresses as temperature variations or external forces cause plate dimensions to vary. Thus it is better to avoid an overconstrained design to avoid internal stress buildup.

Use of nesting forces avoids overconstrained designs. Nesting forces are used to constrain a degree of freedom, therefore each constrained degree of freedom must have a nesting force and a contact point. Nesting forces are adjustable forces that preload the part against a hard constraint. Machine screws, flexures and balls in *vee grooves* are examples. Each constraint device has its own qualities: stiffness, manufacturability, ease of assembly, range of motion, and cost.

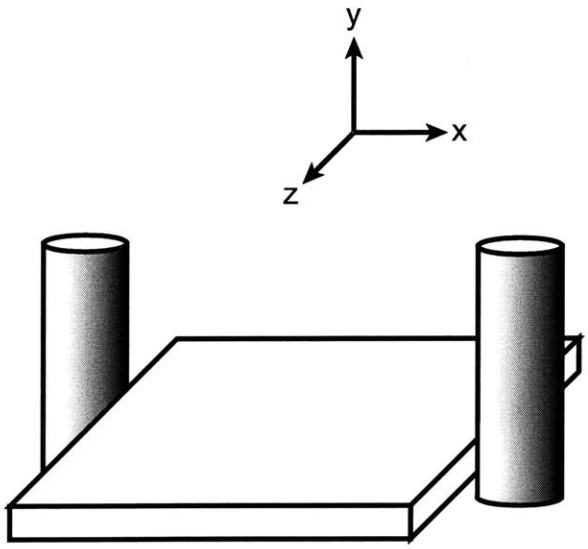

Figure 3-2: Overconstrained plate

Taking the example of the plate from Figure 3-2, by replacing one constraint with a flexure the object will be exactly constrained in the x-direction. As part dimensions change, the flexure deflects and does not damage the plate as would a hard restraint [11].

Flexures are higher performance elements than other constraint devices. Their simplicity is elegant; self-adjusting force application and zero friction are ideal nesting force mechanism properties. Drawbacks are that flexure element size is orders of magnitude larger than the displacement, and they need to be designed for maximum and minimum loading conditions [2].

3.2 Bearing Replication

Bearing replication is an inexpensive alternative to precision bearing manufacturing. It improves system accuracy and repeatability, simplifies manufacturing and assembly, and extends equipment life. It also replaces metal-to-metal bearings to reduce the coefficient of friction.

By making a mold of a high-precision part, a high-precision mating surface is created. This is the basis of bearing replication. Various bearing replicant-materials

contain teflon, steel or aluminum fillers, depending on stiffness and friction requirements. The bearing replicant-material also comes in putty form, a no drip solution for overhead and vertical surfaces, and an injectable form to fill pockets.

An abbreviated description of the replication process is as follows

- A high-precision master part is machined to provide the molding surface. It is preferred to have a ground surface finish as any errors will be duplicated in the replication process. This part is coated with a release agent, usually a spray wax, that provides final bearing clearance.
- Sandblasting a loosely toleranced part provides a large adhesion surface area.
- The adhesion surface part and molding surface part are placed in a fixture so that the bearing surfaces are properly aligned. Bearing replicant is then injected/poured between the mating parts and allowed to cure.

Minimizing the amount of bearing replicant maintains bearing stiffness and avoids polymerization thermal affects (part deformation). A typical compressive modulus of elasticity, according to (ASTM D-695) (1/2" Cube) value is 60,000 kg/cm^3 or 8.5 $\times$ 10 ^{5} psi.

Putty bearing replicant was initially tried on prototype 1 but it was difficult to apply due to poor machine-assembly design, the putty was squeezed out while assembling the machine. Designing an injectable bearing replication system for both prototypes is quite feasible and should be implemented in future work.

More information on replicants can be found from Devitt Machinery Company [3] and Philadelphia Resins [10].

Chapter 4

Prototype 1

4.1 Exact Constraint Theory Applied

The kinematic bearing system shown in Figure 4-1 eliminates five degrees of freedom as only inboard-outboard motion is needed. A side view of the cutting head, perpendicular to the inboard-outboard direction (see Figure 4-2), shows the round-shaft bearing constraining vertical and horizontal motion. The rectangular-shaft bearing constrains rotation about the round bearing, therefore three degrees-of-freedom are constrained.

To prevent the linear bearing system from yawing or pitching, the bearing-pad spacing-ratio should be 2:1 or higher, length to width. Length is along the direction of motion [12]. To achieve this ratio, a split-bearing "catamaran" configuration is employed as shown in Figure 4-3. Each bearing pad has a 1:1 minimum surface area, length to width. They are spaced 3:1, length to width. This exactly constrains two rotational degrees-of-freedom, leaving only inboard-outboard motion free.

Although placing a round shaft through a hole overconstrains the round shaft bearing, it is chosen because the shaft parts (bushings and shafting) are "off the shelf" and can be purchased at low cost in high quantities. Thomson Nyliner bearing pads and Thomson rails comprise the round-shaft bearing system. Production-run manufacturing of the catamaran bracket can be a cost effective extrusion with secondary machining to "clean up" the loose tolerances inherent to the extrusion process

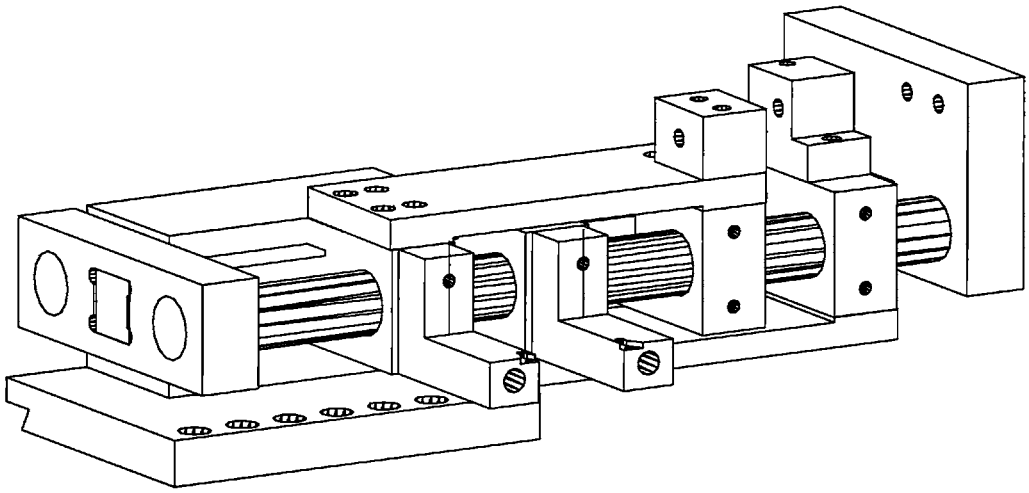

Figure 4-1: Prototype 1: assembly of the first cutting-head prototype

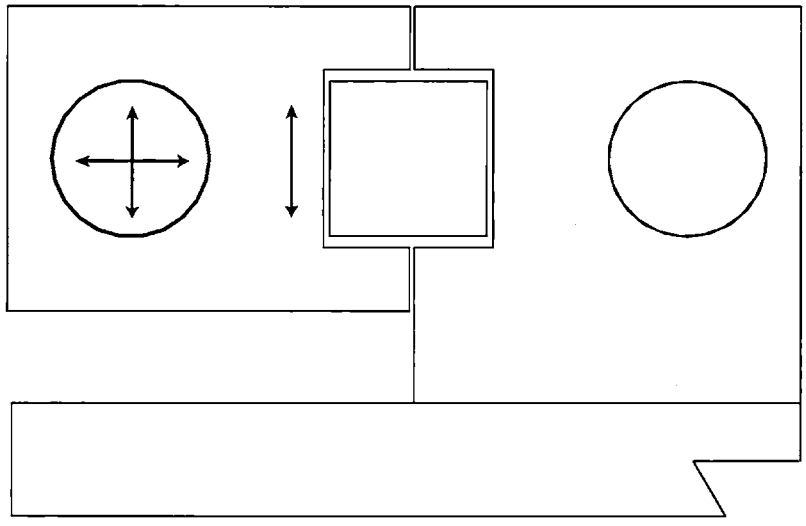

Figure 4-2: Prototype 1: side view showing kinematic constraints on catamaran slider

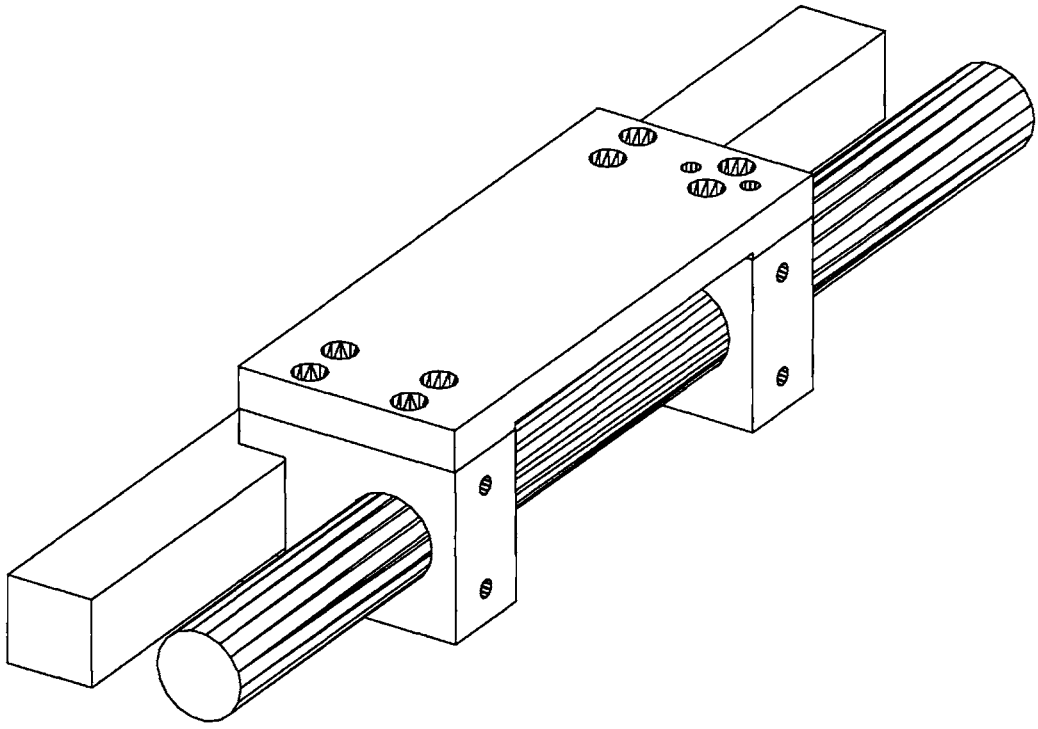

Figure 4-3: Prototype 1: view of catamaran bearing system

(usually ± 0.02" per inch along the length of the part).

For the rectangular bearing, the catamarans ride on bearing pads made of Nylon sheets 0.015" thick, backed by aluminum shims. Nylon acts as a soft elastic polymer pad that embeds any asperities of the square-bearing shaft or metal particles generated during the lathe operation. Thus it prevents the bearing surface from being damaged. The aluminum shim provides stiff backing for the Nylon and provides proper spacing for 6 lbs minimum preload.

C-1002, a high-performance vibration isolation/damping material by E-A-R [4], is placed between the aluminum shim and the catamaran bearing as shown in Figure 4-4, thus providing bearing preload. The preloaded level was set based on feel; the sliders are movable by hand with some effort, and easily placed via lead screws.

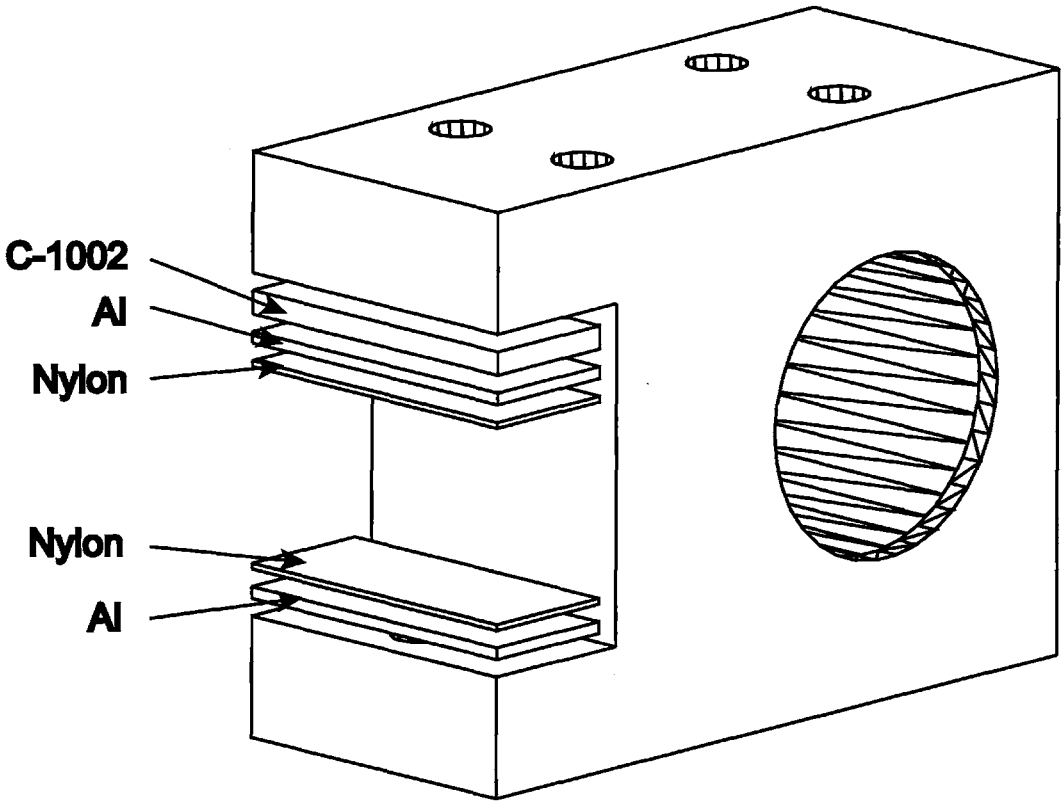

Figure 4-4: Prototype 1: view showing catamaran bearing preload mechanism

4.2 Mockup Testing

4.2.1 Goals

A mockup was built to determine the dynamic response of the machine while cutting and to measure the prototype's surface-finish capabilities. Simulation is a very powerful and useful tool but it is only as good as the model. It is difficult to accurately model all bearing surface interactions and the cutting forces under our time constraint. Therefore, a mockup was built because it gives accurate results in a minimal amount of time.

4.2.2 Methods

After bolting the lathe to a rotor, a dial indicator is used to measure the displacement between the cutting head and the rotor's brake surface (lateral run-out). Screws between the brake lathe and hub compensate for misalignment, which are adjusted so that lateral run-out is less than 0.003". This ensures alignment between the cutters' feed direction and the rotor's surface.

The rotor is rotated to cutting speed and the cutting tips are moved into cutting position. A micrometer measures rotor thickness before and after cutting and their values are subtracted and divided in half to estimate each side's depth of cut.

A tri-axial accelerometer, PCB corporation model number 356B08 [8], is mounted to the inboard cutting tip and the power spectrum is collected. Also, modal tests are performed to match the mode-shapes' frequencies to the power-spectrum-data frequencies. Due to the lack of fixtures, the lathe is tested in the outboard position only. This is not the ideal testing situation because the lathe is "retracted" and is more "stiff" than in the fully inboard position, and it is best to test the system in the "worst case scenario" to determine its full capabilities.

4.2.3 Results

Based on visual inspection, light-cut lathe operations produce a smoother and a more non-directional surface finish than the current cutting head. A profilometer measures smoothness of 50 μ-inches on average, where the manual cutting head outputs 75-80 μ-inches on average. A light cut is defined as a depth of cut less than .007" on each side.

Depth of cut greater than .007" on each side causes the system to vibrate wildly. By visual inspection, chattering cutting tips produce an extremely rough surface finish as shown in Figure 4-5. The patterned surface finish indicates that the cutting tips are moving periodically; i.e., the system is excited at a resonant mode. It is not clear, based solely on the power spectrum data as shown in Figure 4-6, which mode is being excited at 150 Hz but it is certain that the mode comes from either the bearing shafts bending or play between the catamaran bearings and the round shafts. The catamaran bearings are not preloaded on the round shafts and we believe this is the culprit.

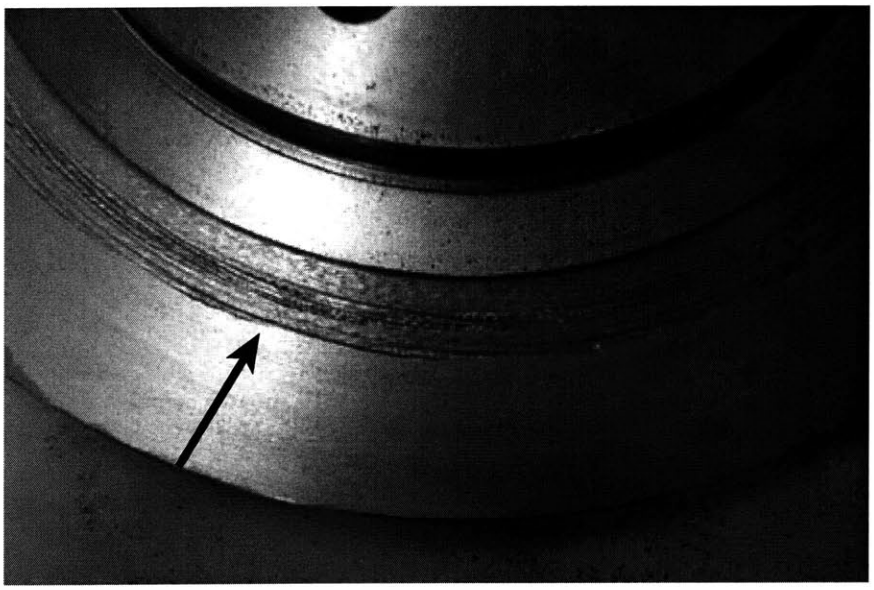

Figure 4-5: Prototype 1: output rotor finish, chatter highly visible as indicated by the arrow

Modal analysis determines the mode shape at 150 Hz, which can be seen in Figure 4-8. The bearing shafts bend up and down about the x-axis and there is minimal

differential motion between the catamaran bearing and the shaft bearings, indicating that the bearing pads are adequately preloaded. An extra bearing with significant preload is added in an attempt to reduce the vibration problem. Comparing the power spectra of the light and deep cuts for the system without the extra bearing and the system with an extra bearing (Figures 4-6 and 4-7), it is clear that the system still has a resonance at 150 Hz. The extra bearing pad does not solve the problem.

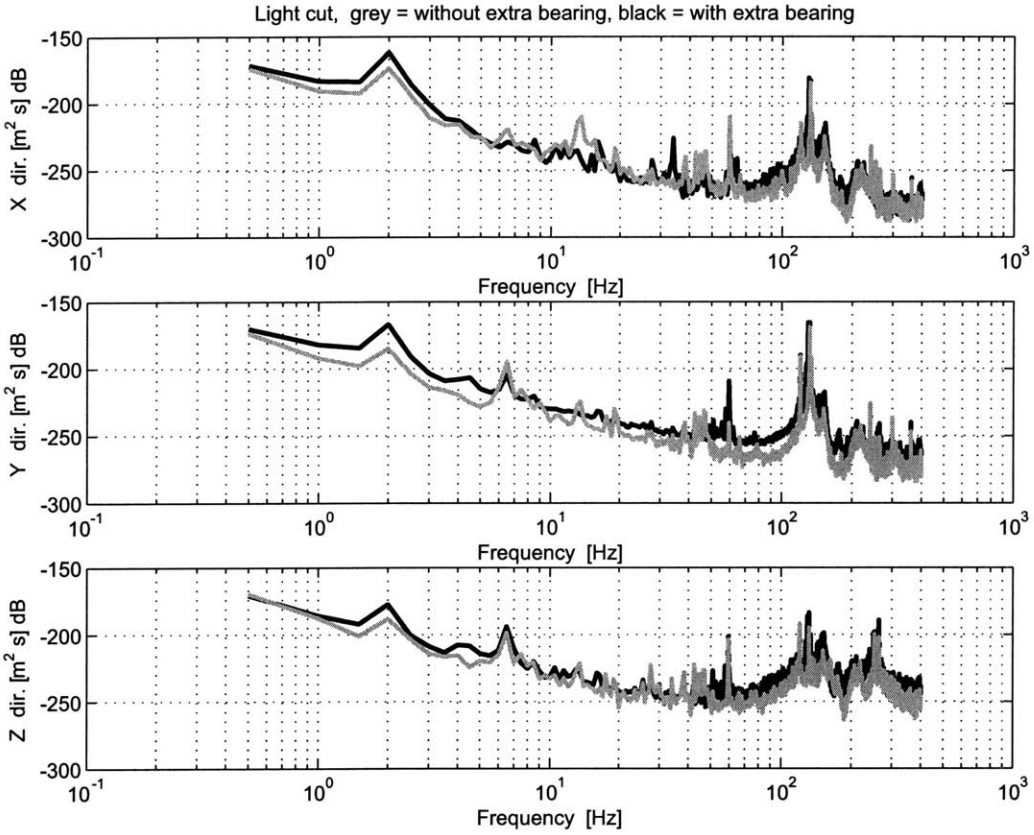

Figure 4-6: Prototype 1: light cut power spectrum data from outboard cutting tip. X-direction is the inboard-outboard direction, Y-direction is the feed direction and the Z-direction is along the vertical plane

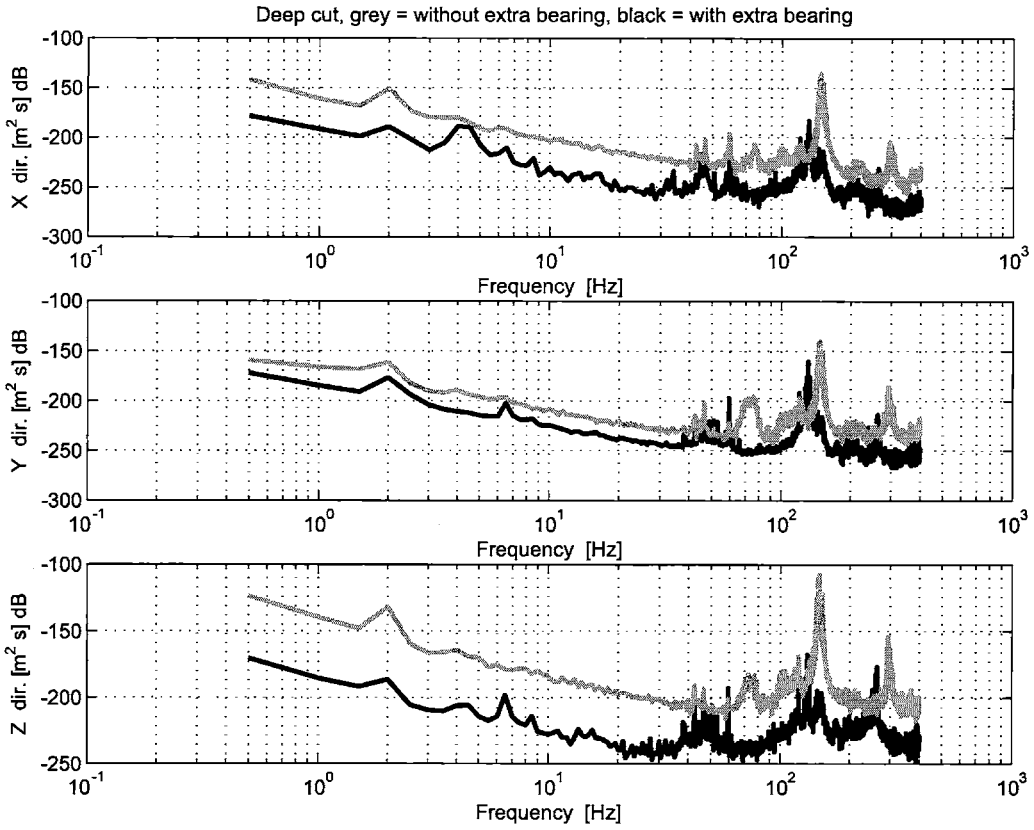

Figure 4-7: Prototype 1: deep cut power spectrum data from outboard cutting tip

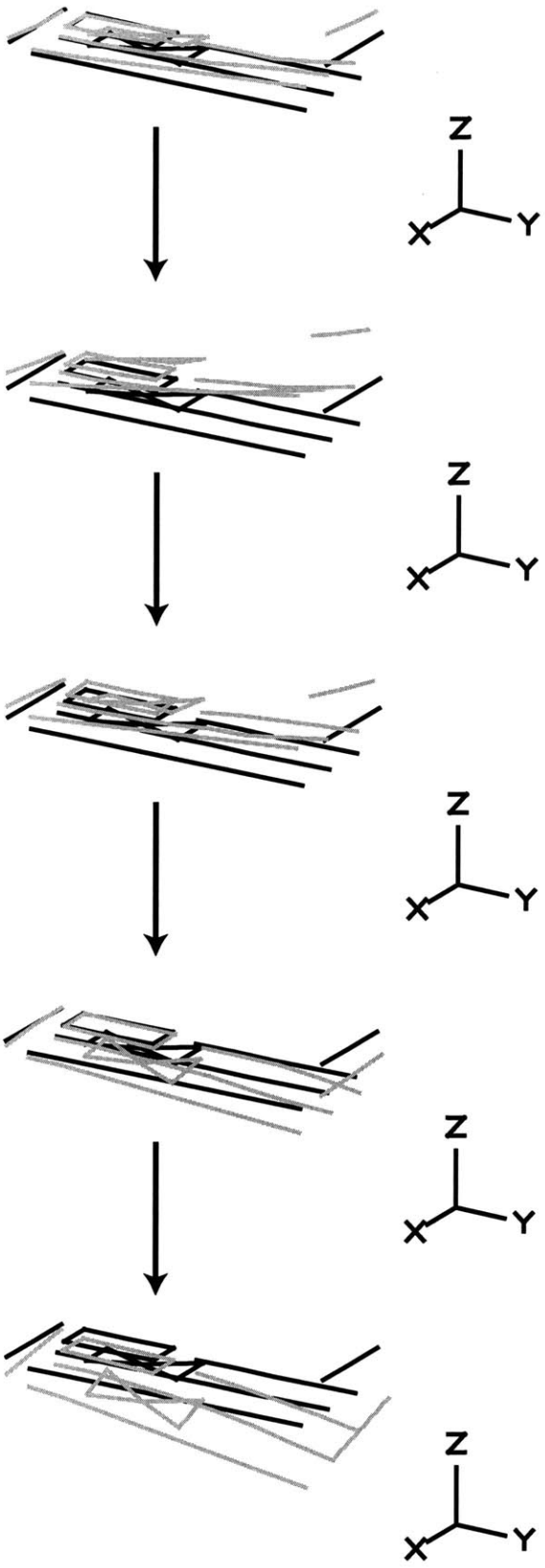

Figure 4-8: Prototype 1: first bending mode. The system bends about the X-axis. The gray line represents the deformed system and the black line represents the undeformed system

4.2.4 Conclusions

The floating bearing design with two round shafts and one square shaft is far too compliant for this application. Fluctuating cutting forces excite the cutting head at its resonant frequency and cause chatter; an investigation of stiffer inboard-outboard bearing designs is needed.

Chapter 5

Prototype 2

5.1 Goals

The main stumbling block in developing an on-car brake lathe that meets the length-of-travel requirements is designing a linear motion system that travels the cutting envelope range, yet is inexpensive and "stiff enough." We consider three approaches to the design and manufacture of the linear bearings: (1) bolt together "off-the-shelf" modular linear bearing slides, (2) design an extrusion and tighten tolerances with a secondary machining process, or (3) design an extrusion with a flexure that preloads the bearings and allows for loose tolerances of extruded parts.

The use of modular linear bearings is a quick and easy solution. In this design we "piggy back" two slides, thus achieving the range of travel depicted in Figure 1-2. The bottom slide bolts to the feed mechanism on the brake lathe while a plate—with cutting tips and a fine-linear motion system—bolts to the back-side of the first slide. The disadvantage is high cost. A size-35 linear ball bearing slide with 12" travel costs $435. Two of these are needed, putting the price at $870. This puts the project well over budget and therefore is not a viable option.

An aluminum extrusion along with a secondary machining operation to tighten the tolerances is a less expensive approach. Aluminum extrusions cost roughly $1 per pound, which is equivalent to $5 per inboard-outboard bearing. The use of a grinding process to tighten up tolerances would increase the price to roughly $75 per

inboard-outboard slide system. While not overly inexpensive, this design can be made "stiff enough" by carefully designing the slide geometry. An extrusion with a built-in flexure to account for loose tolerances is risky, but would result in a lucrative cost reduction. This idea is discussed in Chapter 6, but because of time constraints, we decided to take the middle road and design an extrusion with a secondary grinding operation to obtain the desired tolerances on the linear slide.

5.2 Description of Redesign

The second prototype's assembly and exploded drawings can be seen in Figures 5-1 and 5-2 respectively. The new inboard-outboard bearing is redesigned as an oddly shaped beam where the sliders are kinematically constrained as shown in Figure 5-3. The kinematic constraints are similar to the first prototype's constraints; the sliders are constrained in the vertical direction by sides 1 and 3 and constrained in the feed direction by sides 2 and 4. Constraining sides 5 and 6 prevents rotation about the front bearing. Making each bearing a catamaran-style bearing system constrains the other two rotational degrees of freedom as previously discussed. Coarse inboard-outboard motion need not be highly repeatable or accurate, thus the inboard-outboard bearing is comprised of a loosely toleranced dovetail. The inboard-outboard bearing beam has a large thickness to stiffen it in the vertical direction.

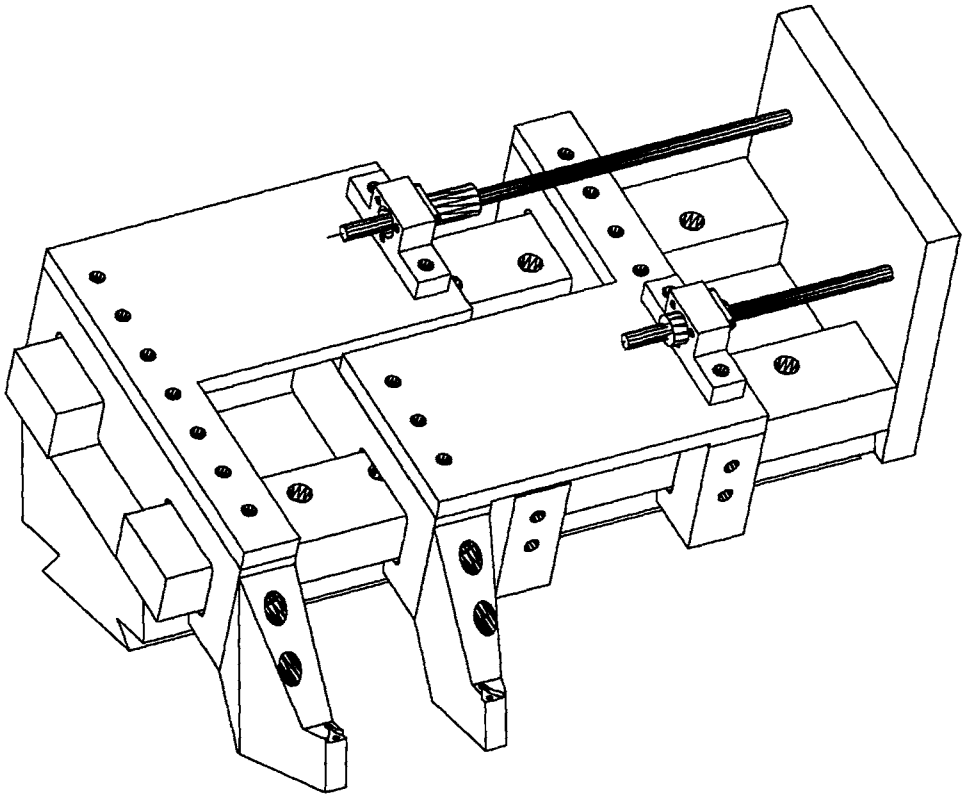

Figure 5-1: Prototype 2: assembly view

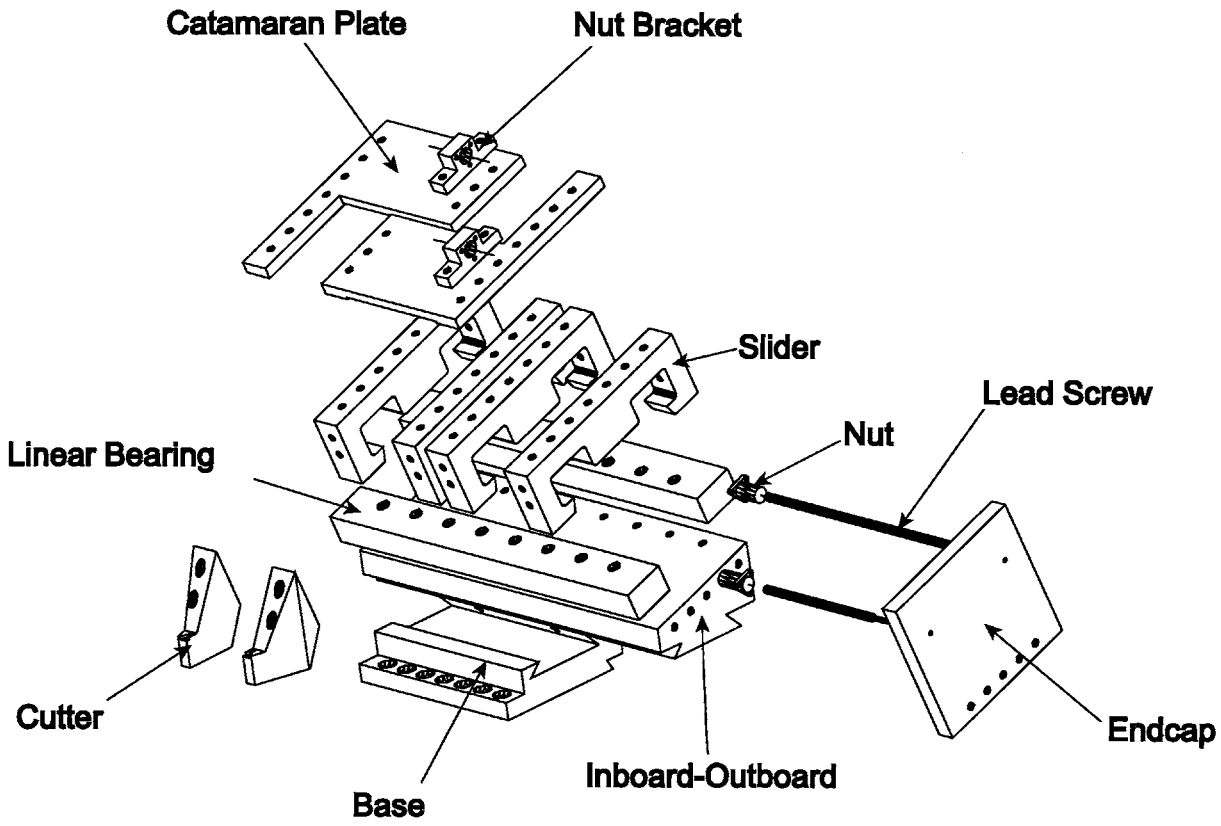

Figure 5-2: Prototype 2: exploded view

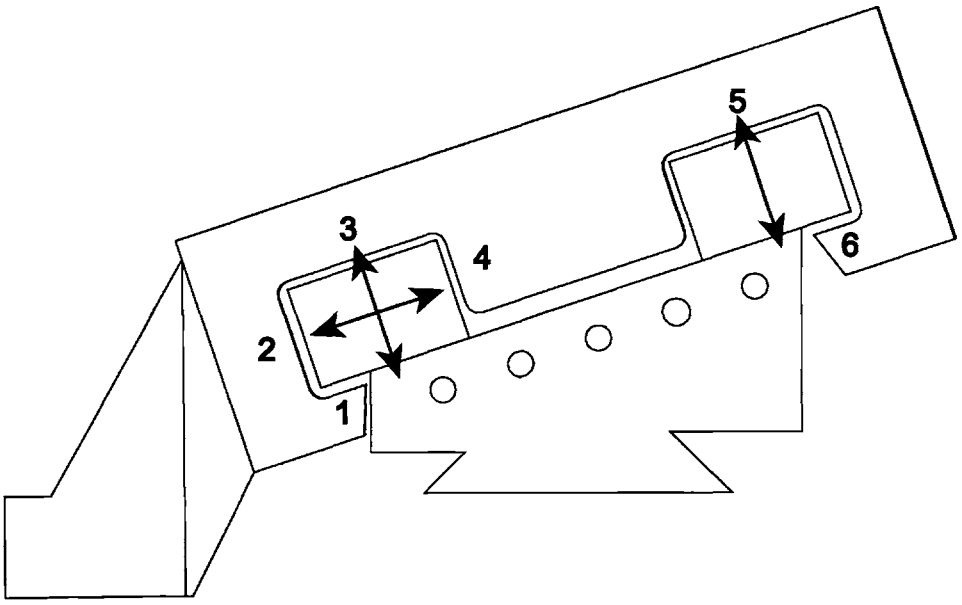

Figure 5-3: Prototype 2: side view showing kinematically constrained catamaran bearing

5.3 Results

Preliminary cutting tests show poor results. The rotor's surface finish has a pattern due to cutting tip chatter, see Figure 5-5. Modal data from the catamarans (Figure 5-6), was difficult to process due to several modes in the 140 Hz frequency range. Power spectrum data from the outboard cutting tip can be seen as the black line in Figure 5-4. The peak response at 140 Hz concurs with the modal data.

The use of C-1002 damping material to preload the bearings on this system is difficult because lubricant from the linear bearings in conjunction with vibration cause the pads to creep out. Therefore the C-1002 was removed and aluminum-backed Nylon pads are preloaded via setscrews. This allows for more accurate bearing preload and is easier to adjust.

Inboard-cutter power spectrum data can be seen in Figure 5-8. The black line represents the C-1002-preloaded system and the gray line represents the setscrew-preloaded system. The setscrew-preloaded system slightly shifts the resonant frequency from 140 Hz to 150 Hz, but the overall magnitudes and general machine behavior are the same.

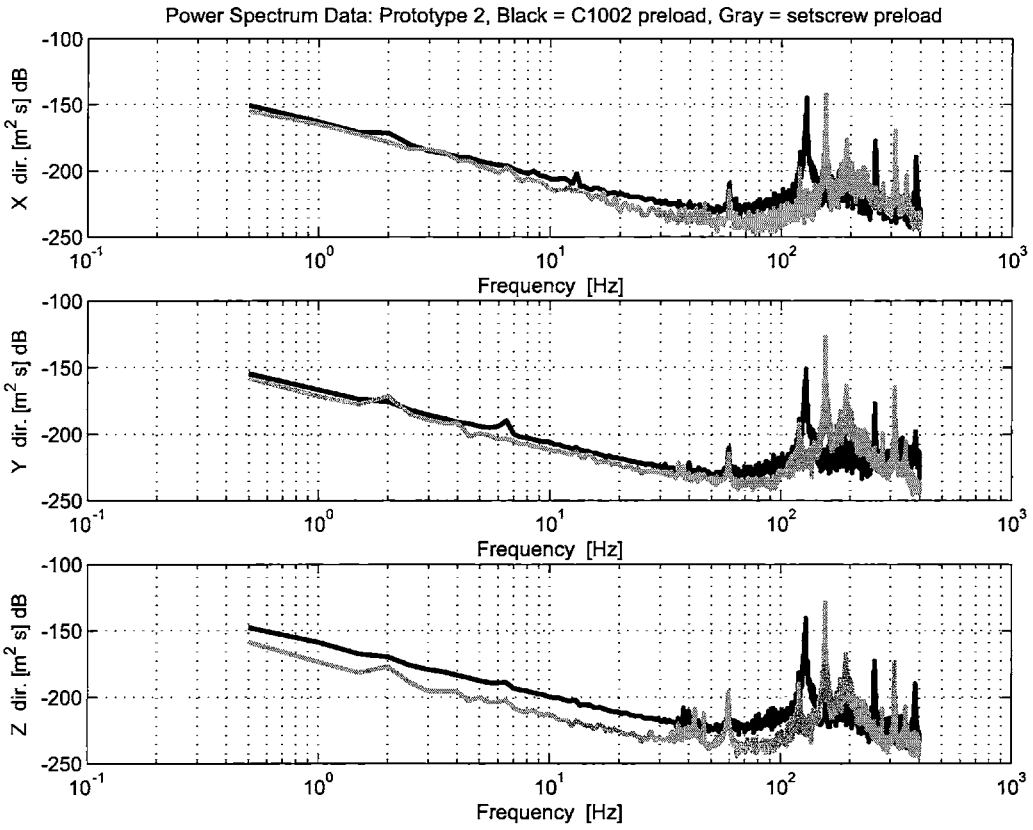

Figure 5-4: Prototype 2: power spectrum of outboard cutter comparing C-1002 preload to setscrew preload. X-direction is in the inboard-outboard direction. Y-direction is in the feed direction. Z-direction is in the vertical plane.

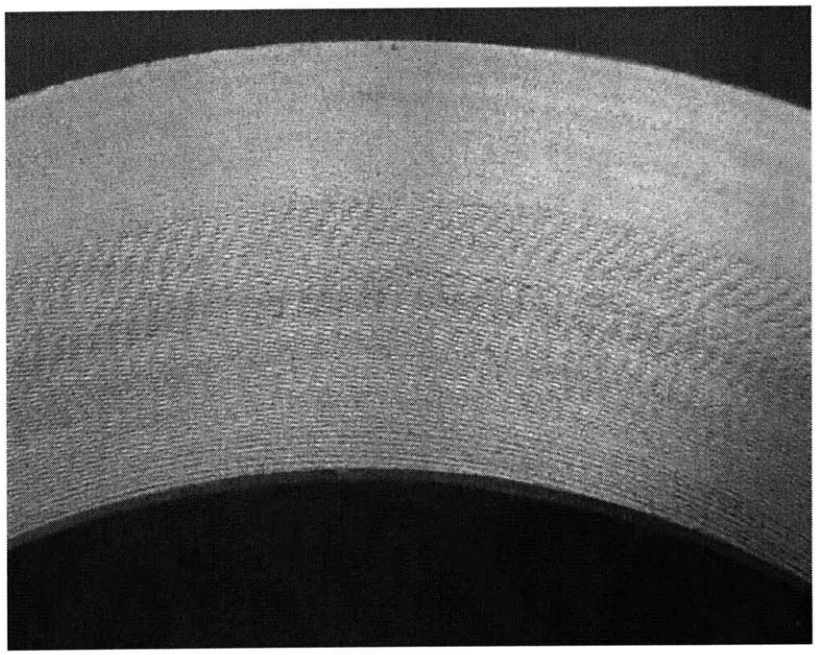

Figure 5-5: Prototype 2: chatter output surface finish, 0.015" depth of cut on each side

Adding a stiffener plate as shown in Figure 5-7 to the inboard catamaran bearing dramatically improves rotor surface finish and reduces chatter as shown in Figure 5-9. Power spectrum data comparing the C-1002-preloaded system to the setscrew-preloaded catamaran-stiffened system shows that stiffening the catamaran plate dramatically reduces the magnitude at resonant frequency (see Figure 5-8).

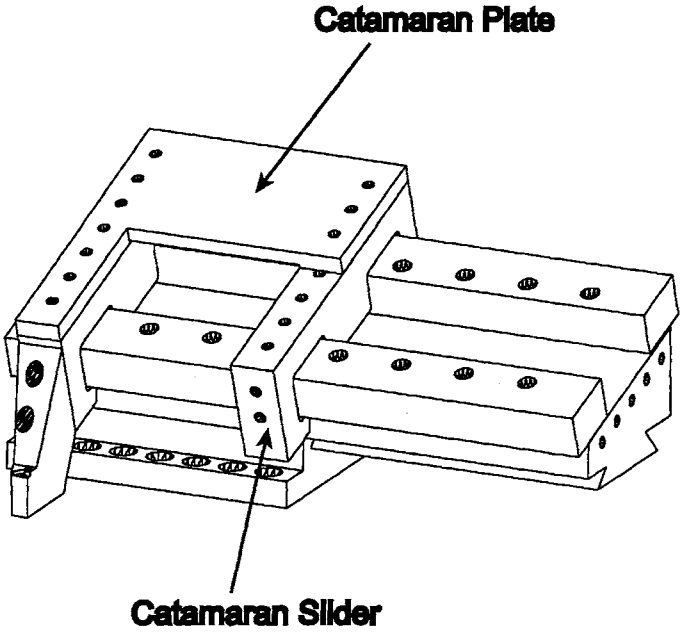

Figure 5-6: Prototype 2: view of catamaran bearing system

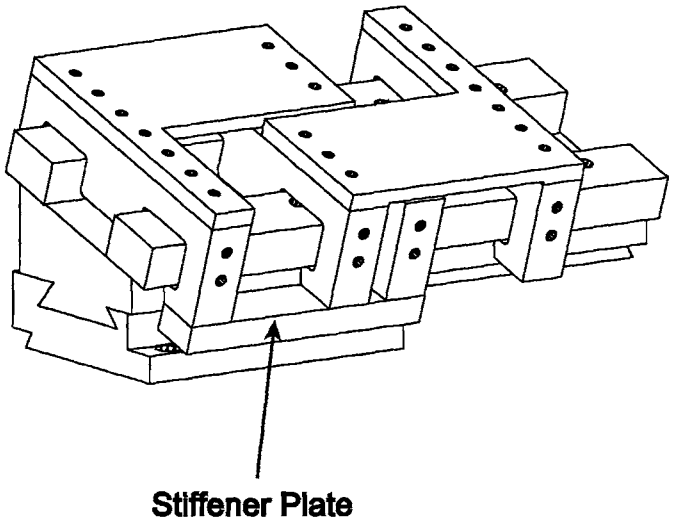

Figure 5-7: Prototype 2: view of stiffener plate

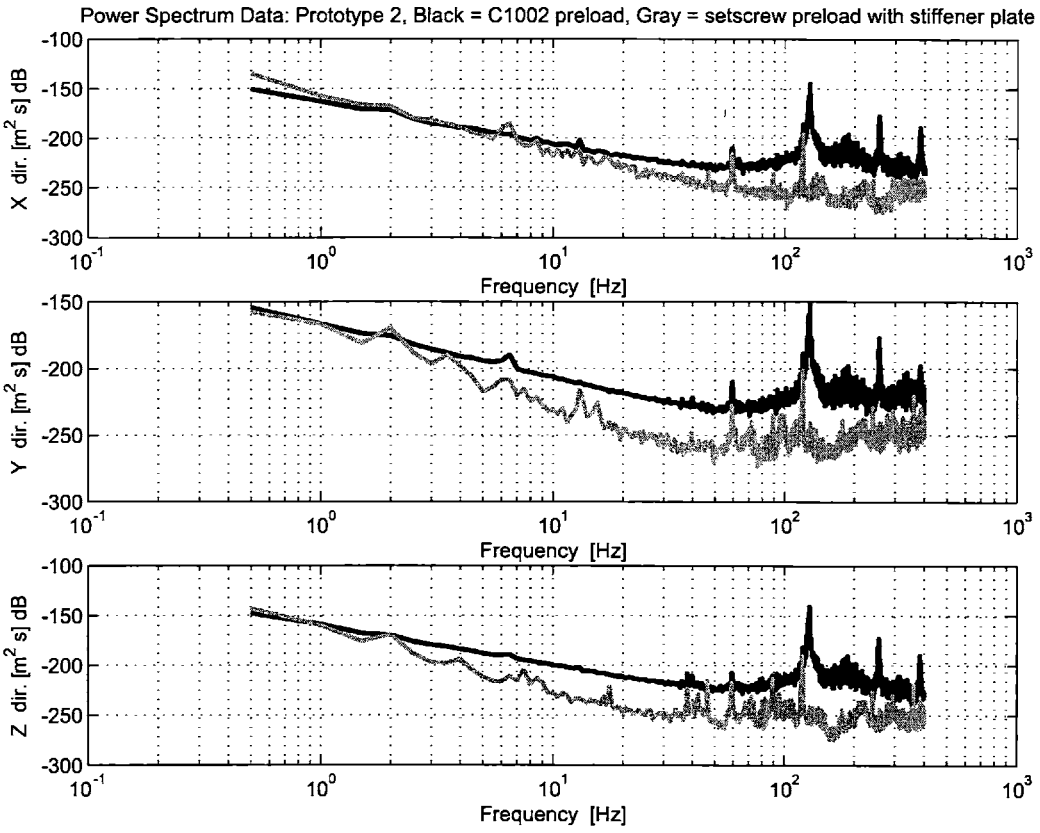

Figure 5-8: Prototype 2: power spectrum; setscrew preload with stiffener plate compared to C-1002 preload

Figure 5-9: Prototype 2: output 50 μ-inch surface finish at 0.010" depth of cut per side

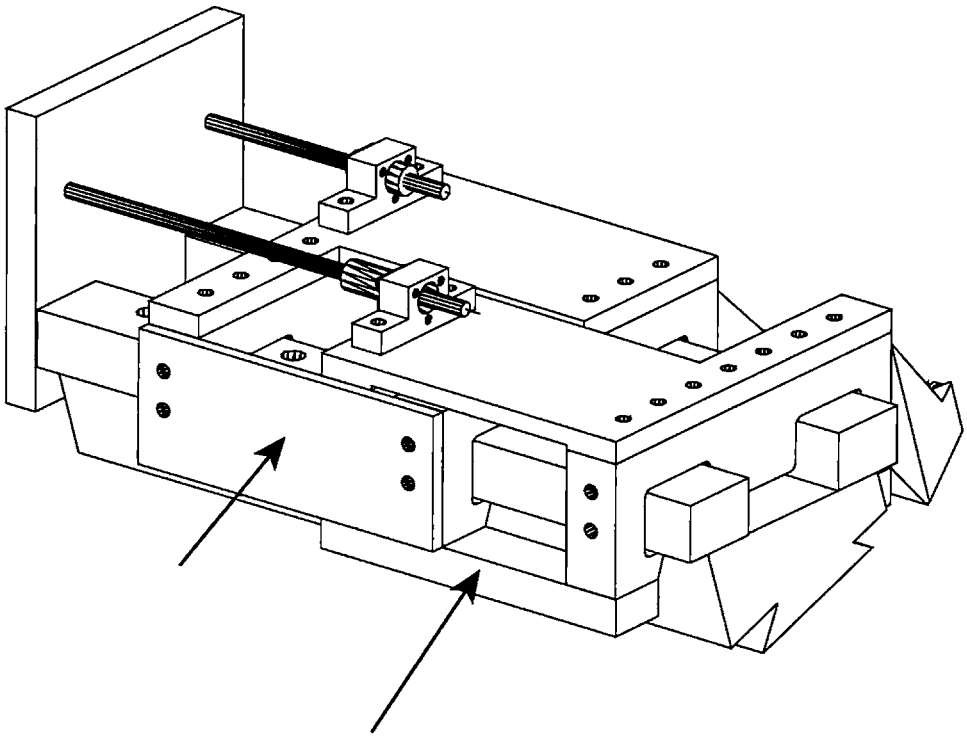

Figure 5-10: Prototype 2: view showing added stiffener plates

To increase the catamarans' stiffness two more stiffening plates were added (see Figure 5-10). The power spectrum at the inboard cutting tip in this new configuration can be seen in Figure 5-11. The rotor's surface finish is measured as 70-80 μ-inch at a 0.015" depth of cut per side (see Figure 5.3). The 70-80 μ-inch surface finish is acceptable, but a slight chatter pattern forms.

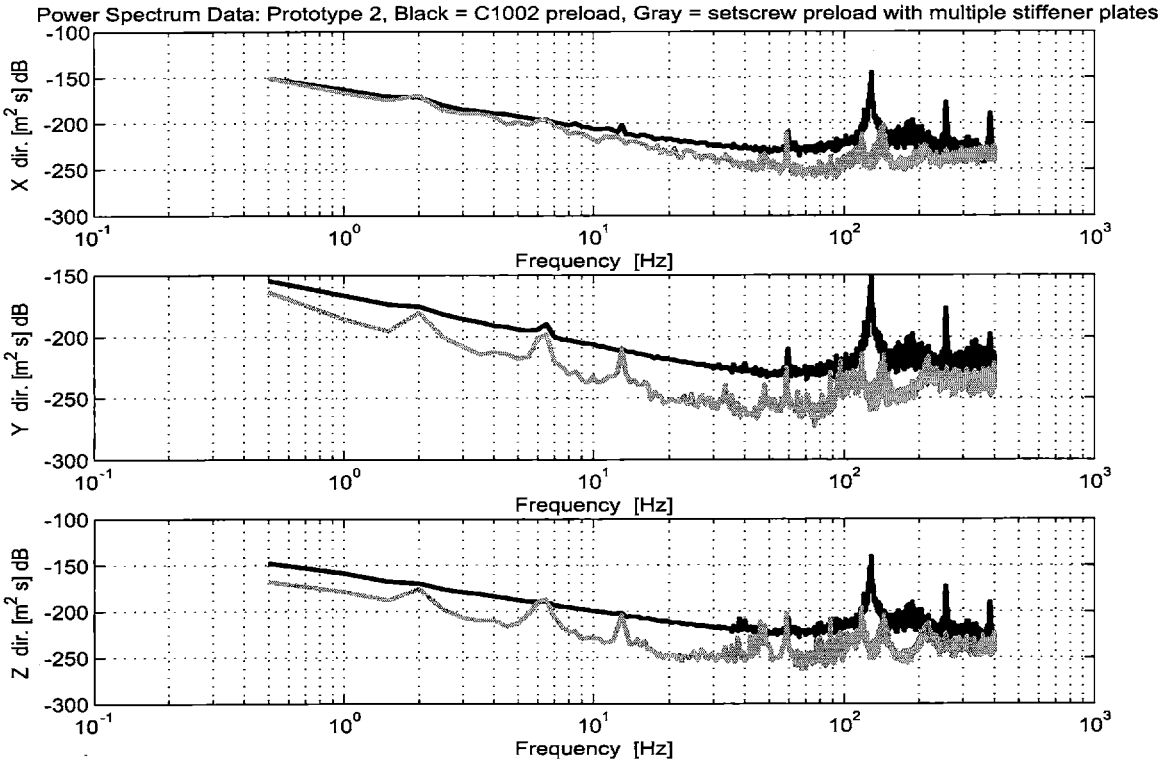

Figure 5-11: Prototype 2: power spectrum; setscrew preload with multiple stiffener plates to C-1002 preloaded system

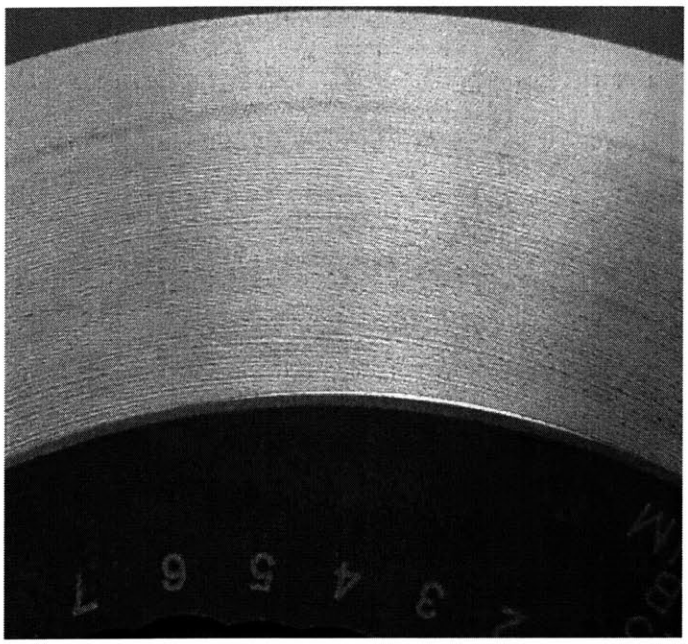

Figure 5-12: Prototype 2: output 70 μ-inch surface finish at 0.015" depth of cut per side

Resonances occur at 60 Hz, 135 Hz, 150 Hz and 225 Hz as can be seen from the power spectrum data shown in Figure 5-11. The mode shapes at these frequencies must be determined in order to "stiffen" the structure at those resonances.

Numerous unsuccessful modal data collection attempts revealed that the test stand has several modes in the frequency range of interest. These mask the cutting head dynamics, making cutting head modal analysis difficult. To eliminate the unwanted test-stand dynamics, the brake lathe was suspended by surgical tubing. The brake lathe is roughly 100 lbs and the surgical tubing acts as a very light spring, thus any resonances due to the suspension will be less than 2 Hz, well below the frequency range of interest.

For the suspended brake-lathe setup, the first mode is at 118 Hz and its mode shape is shown in Figure 5-13. Therefore we conclude that the 60 Hz spike in Figure 5-11 is most likely an artifact of the AC current supplied to the motor. The 118 Hz mode appears to be primarily rigid body rotation about the y-axis, but it is physically impossible for this to happen; as previously stated, all rigid body modes are less than 2 Hz. Thus another part of the machine, such as the brake lathe's motor interface, must have strain energy developing. It is not likely that this mode is the source of chatter because it is far enough below 135 Hz.

The second mode, at 143 Hz, can be seen in Figure 5-14. This top-down view shows differential motion between the entire cutting head assembly and the brake lathe. The linear bearings and catamarans are rotating about the z-axis slightly more than the gear box. The third mode, at 161 Hz, can be seen in Figure 5-15. Again, this front view shows differential motion between the cutting head assembly and the brake lathe about the x-axis. The fourth mode, at 177 Hz, can be seen in Figure 5-16. This mode shape is very similar to the third mode in that the cutting head is deflecting about the x-axis with respect to the gear box. The gear box also deflects in this case.

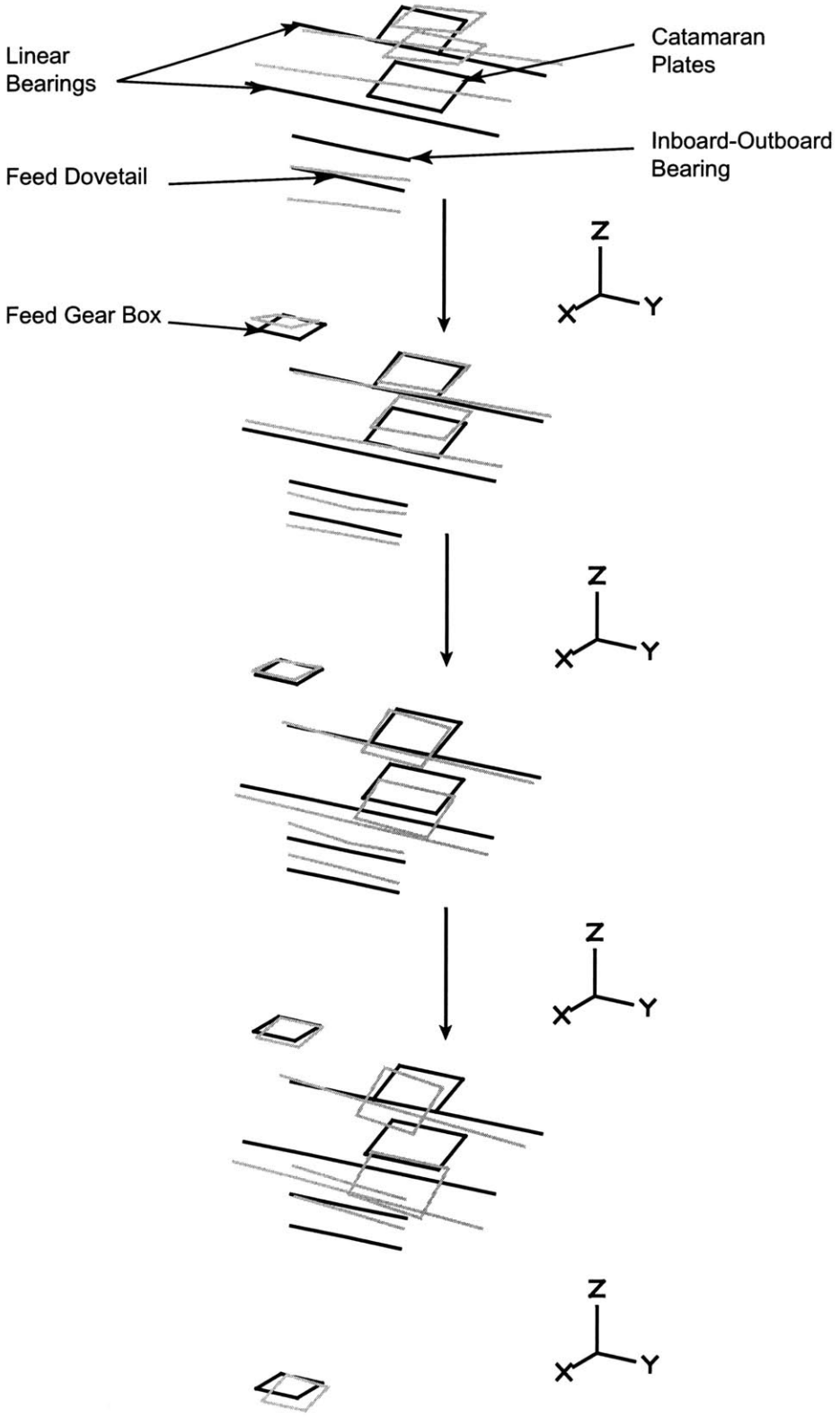

Figure 5-13: Prototype 2: first mode at 118 Hz. The grey lines are the deflected cutting head, the black lines are the un-deflected cutting head.

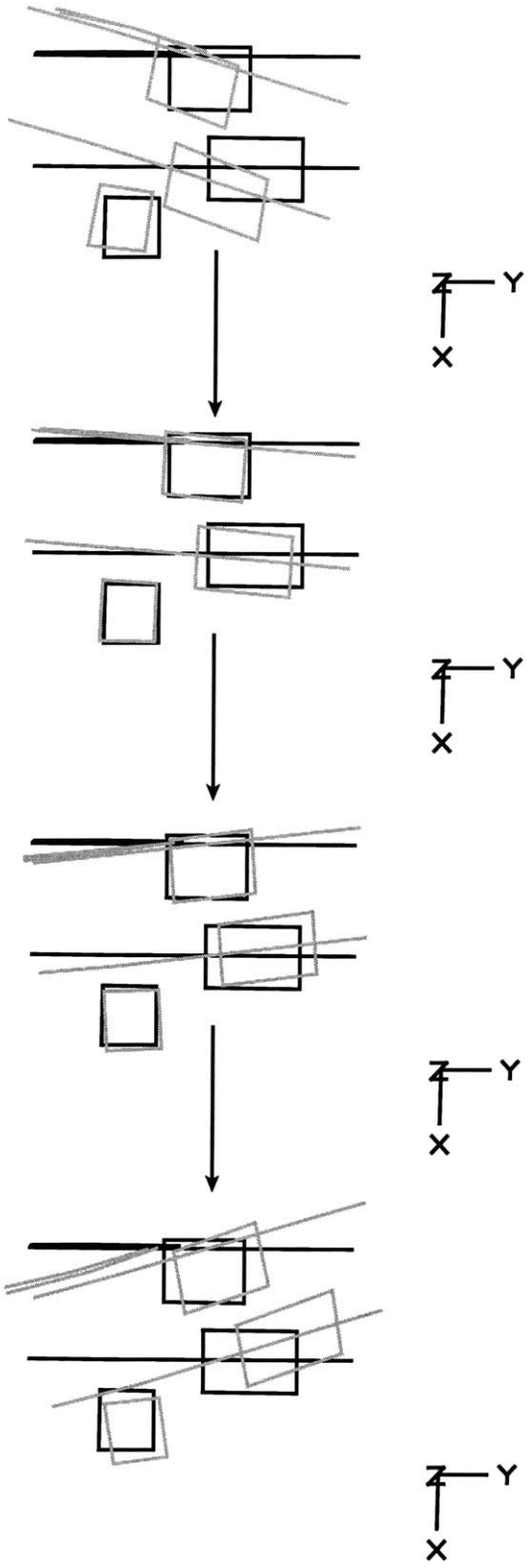

Figure 5-14: Prototype 2: second mode at 143 Hz. Top-down view. The grey lines are the deflected cutting head, the black lines are the un-deflected cutting head.

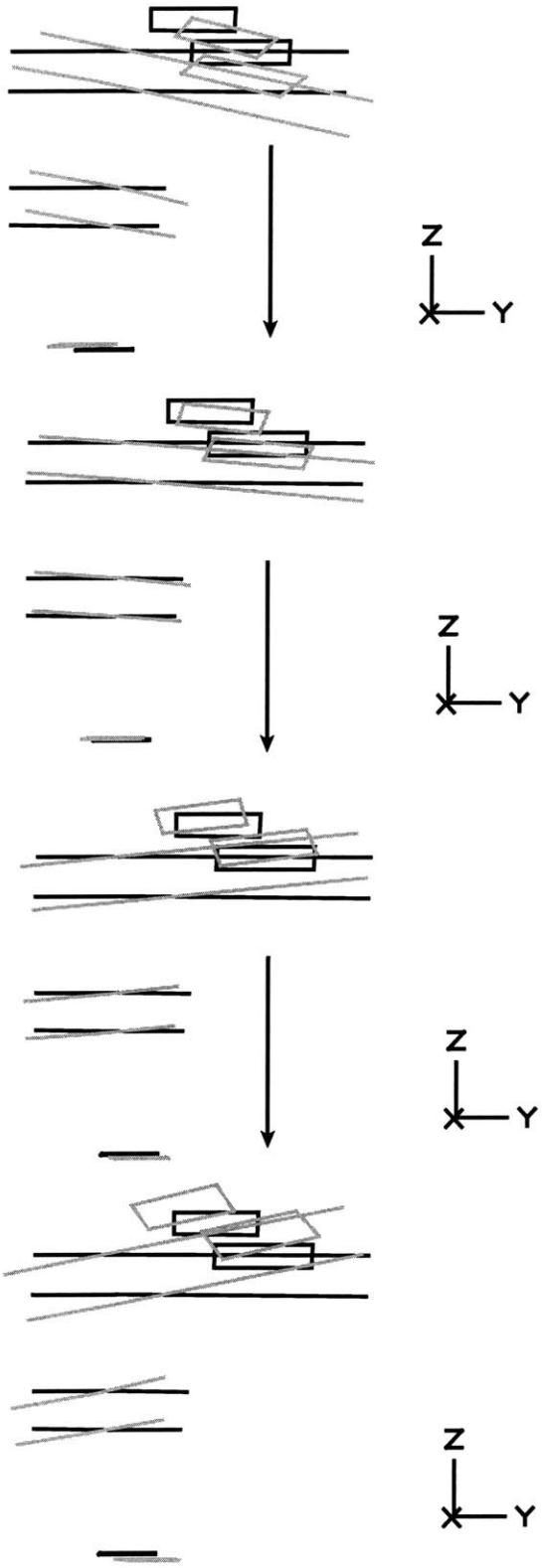

Figure 5-15: Prototype 2: third mode at 161 Hz. Front view. The grey lines are the deflected cutting head, the black lines are the un-deflected cutting head.

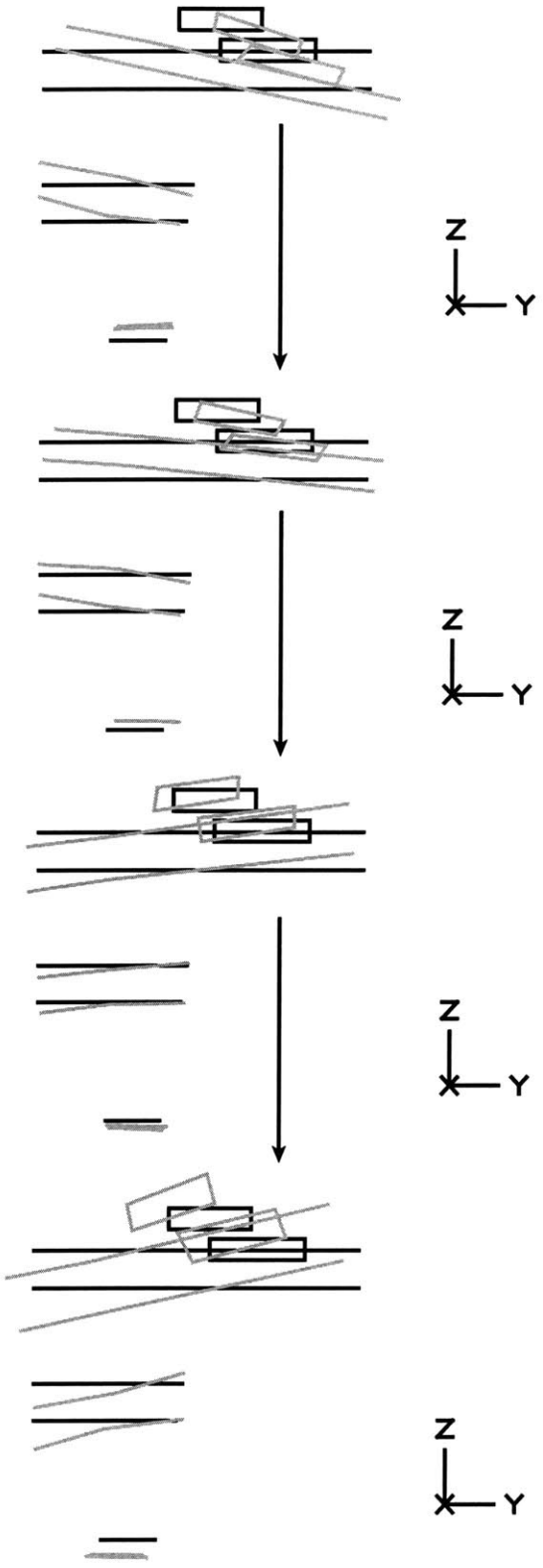

Figure 5-16: Prototype 2: fourth mode at 177 Hz. Front view. The grey lines are the deflected cutting head, the black lines are the un-deflected cutting head.

5.4 Conclusions

The new cutting head with the stiffener plates is extremely stiff, and meets the cutting specifications. However, the feed dovetail bearing is now the most compliant element of the machine and therefore is the source of slight pattern that occurs at full depth of cut. Therefore to improve this design, (1) the cutting head should be lightened, (2) the catamarans should be stiffened and damped, and (3) the feed dovetail should be stiffened to improve this design.

Chapter 6

Non-Linear Flexure Design

6.1 Desired Characteristics

An extrusion process yields loosely toleranced parts; the tightest being ±0.010 " per foot on the specified dimension along the length of the part. For example, an extruded 1" square profile may have profile dimensions 1.010" or 0.990" at the opposite end if it is 1' long.

For a preloaded linear bearing with stiff bearing pads, 0.020" tolerance is impractical. To maintain bearing pad contact, bearing preload must exceed the sum of the tolerance dimensions of the two mating parts. Specifically, the opposing bearing pads must be preloaded 0.040" to account for the 0.020" variance of dimensions on the slide and the catamarans. This ensures bearing contact along the entire length of bearing and preserves stiffness afforded by full contact of the bearing pad. A light preload is desired in order to maintain low friction and low torque requirements from the actuator. Therefore preload force should be between six and ten pounds.

Using the specifications above, and assuming that elements in the preload path have a linear stiffness k, it is found that k must be 50 lbs/in. The initial preload must be 0.12" and the maximum displacement is 0.2", which is very large and is difficult to design for with our size constraints. Thus a regressive preload device is needed, i.e., one in which the nesting force dies out as displacement increases.

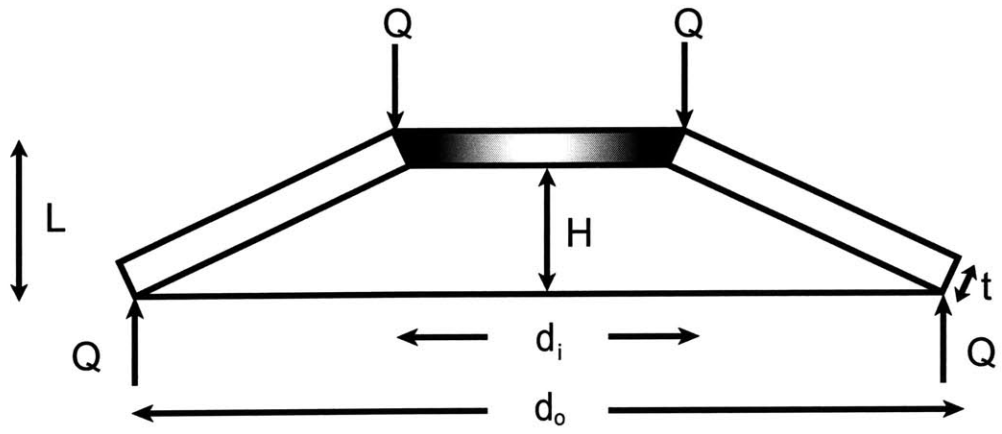

Figure 6-1: Belleville washer geometry

6.2 Belleville Washer

Coned disk springs, also known as Belleville washers, are conical dishes of rectangular or trapezoidal cross-section. They can provide linear, progressive and regressive loading deflection behavior by changing characteristic dimensions and stacking the springs in parallel and series. Their regressive loading deflection characteristics makes them ideal for preloading the inboard-outboard bearing. A significant initial preload is needed but as part tolerances vary slightly, preload force must not significantly increase. The regressive nature of a Belleville washer allows for the stiffness curve to decrease at increasing displacements. Using a properly designed Belleville washer for bearing preload, the preload will be small at loads above minimum preload, so that preload force becomes insensitive to dimension variation as required.

6.2.1 Belleville Geometry

The cross section of a standard Belleville washer can be seen in Figure 6-1. Its geometry is defined by the outer diameter d_o, inside diameter d_i, the thickness t, and the height L. A load Q is distributed uniformly over the circumference of the inner and outer edges flattening the washer, reducing its free camber H [6].

6.2.2 Theory and Limitations

The most widely used model for calculating forces and stress on Belleville washers is the *Elastic Coned Disk* [1]. Its basic assumptions are:

- The washer has a small initial cone angle so that small angle mathematical simplifications apply.
- It has rectangular cross-section over the entire range of deflection.
- It does not have stresses in radial direction.
- Load application is on the edges of the spring (see Figure 6-1).
- The Belleville behaves Linearly elastically.

This approach gives good results for values of $D = d_o/d_i$, ranging from 1.3 to 2.5 and values of H/t up to 1.5. Deviations from theory are that measured initial loads are smaller than theoretical loads, and loads at deflections of more than 80% of full deflection will be higher than predicted [6].

6.2.3 Formulae for designing Belleville Washers with rectangular cross-section

The following formulae are derived by Almen [1]. These equations determine loading characteristics and stress characteristics of Belleville washers.

$$Q = \frac{E}{1-v^2}\left(\frac{H}{1/2 D_o}\right)^2\left(\frac{t^2}{\frac{H}{t}}\right)\left(\frac{z}{m}\right)\left[1+(1-z)\left(1-\frac{z}{2}\right)\left(\frac{H}{t}\right)^2\right] \tag{6.1}$$

$$\sigma_{\max} = \frac{E}{1-v^2}\left(\frac{H}{t}\right)^2 z\frac{\left(1+\frac{p}{o}\right)\left(1-\frac{z}{2}\right)\left(\frac{H}{t}\right)^2}{p\left(\frac{H}{t}\right)} \tag{6.2}$$

$$z = \frac{\delta}{H} \tag{6.3}$$

$$p = \frac{2(D-1)}{D^2} \tag{6.4}$$

$$o = \frac{(D-1)^2}{D^2\left[\left(\frac{D-1}{\ln(D)}\right)-1\right]} \tag{6.5}$$

$$m = \frac{(D-1)^2}{\pi D^2\left[\left(\frac{D+1}{D-1}\right)-\frac{2}{\ln(D)}\right]} \tag{6.6}$$

$$D = \frac{d_o}{d_i} \tag{6.7}$$

where

Q = applied distributed load

d_o = Belleville washer outside diameter (see Figure 6-1)

d_i = Belleville washer inside diameter (see Figure 6-1)

σ_{max} = maximum stress

δ = deflection

In order to simplify spring design, the preceding equations are non-dimensionalized. Setting $z = 1$ and solving for Q gives $Q_{1.0}$. The ratio of any force Q to $Q_{1.0}$ can be found as:

$$\frac{Q}{Q_{1.0}} = z\left[1+(1-z)\left(1-\frac{z}{2}\right)\left(\frac{H}{t}\right)^2\right] \tag{6.8}$$

Equation 6.8 is known as the load-deflection line and the ratio H/t determines the shape of this line. Figure 6-2 shows a range of load-deflection lines where H/t ranges from 0 to 2, $Q/Q_{1.0} = 1$ and z =1. When $H/t = \sqrt{2}$ the load-deflection line becomes horizontal about the point (1.0,1.0). Theoretically, it is possible to design a Belleville washer with constant force at preload deflection even though the preload deflection varies slightly. As can easily be seen, as the ratio H/t increases, the load-deflection line rises and dies out more quickly. Once the disk is loaded past the "flattened" position, the disk will "snap through" (flip inside out at point (1.0,1.0)) and requires a loading force in the opposite direction to "pop" it back to the original state.

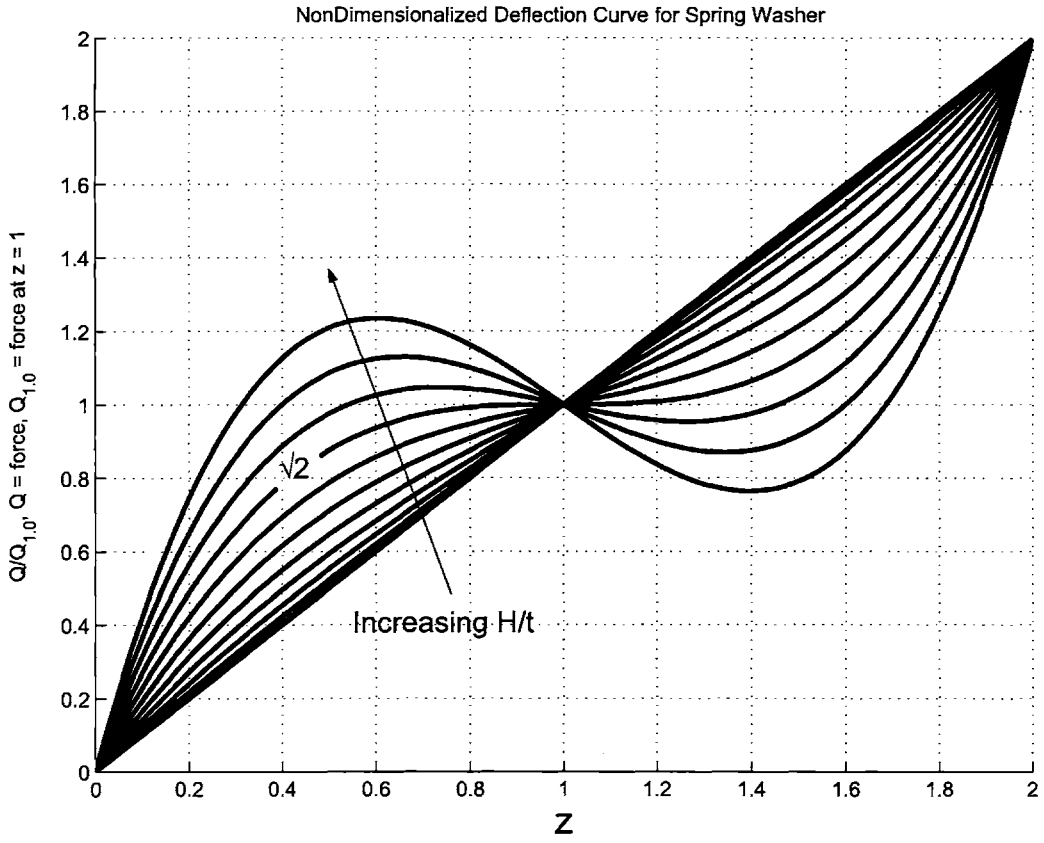

Figure 6-2: Belleville Load-Deflection Curve

6.2.4 Belleville Design

The tightest tolerances on extruded parts are ±0.010." When mating two extruded parts together, a tolerance deviation, $\delta_{tolerance}$, of 0.040" must be accounted for.

$$\delta_{tolerance} = 0.040" \tag{6.9}$$

Therefore the minimum preload deflection, $\delta_{preload}$, should be 0.050" yielding a minimum δ_{total} of 0.010" and a maximum δ_{total} of 0.090". The relationship between these displacements can be seen in Equation 6.10.

$$\delta_{total} = \delta_{preload} \pm \delta_{tolerance} \tag{6.10}$$

The desired Belleville washer gives 6 lbs at the minimum deflection of 0.010", and no more than 10 lbs at the maximum deflection of 0.090", Equations 6.11 and 6.12 respectively.

$$Q|_{\delta=0.010"} = 6lbs \tag{6.11}$$

$$Q|_{\delta=0.090"} \leqslant 10lbs \tag{6.12}$$

Bearing pad size constraints on require d_o to be 1" or less (Equation 6.13).

$$d_o \leqslant 1" \tag{6.13}$$

The spring must not to invert because it is not possible to reverse this without disassembling the machine. Therefore δ_{total} must be slightly less than the height H (Equation 6.14).

$$\delta_{total} < H \tag{6.14}$$

$$z < 1 \tag{6.15}$$

As previously stated, H/t must be $\sqrt{2}$ so that the Belleville washer is insensitive to tolerance deviations.

$$\frac{H}{t} \geqslant \sqrt{2} \tag{6.16}$$

The upper limit of z is set to 0.95, to prevent washer inversion. An initial guess of the lower limit of z is 0.35, thus the Belleville travels from 35% compression to 95% compression. These z values correspond to minimum and maximum δ values, therefore we can obtain H and t as shown in table (6.1).

Table 6.1: Belleville Washer Design Parameters

δ_{min}	δ_{max}	t	H
0.047"	0.127"	0.094"	0.133"

To obtain load values constrained by Equations 6.11 and 6.12, m, from Equation 6.6, must be on the order of 1500. Looking at Figure 6-3, it is impossible for $m = 1500$. A belleville washer cannot meet all constraints specified by Equations 6.16 through 6.15.

6.3 Regressive Flexure

In a simplistic explanation, Belleville washers behave like a hinged spring. The definition of a hinged spring for the purposes of this paper can be seen in Figure 6-4; it has stiffness K along the axial direction, see Equation 6.21, and zero rotary stiffness about the simple support. Because the spring is at an initial angle θ, the reactive force in the vertical direction, F_y is given by

$$F_y = P_{axial} \sin\theta \tag{6.17}$$

The vertical displacement, δ_y, is of main concern. It is related to the axial displacement of the spring by

$$\delta_y = \delta_{axial} \sin\theta \tag{6.18}$$

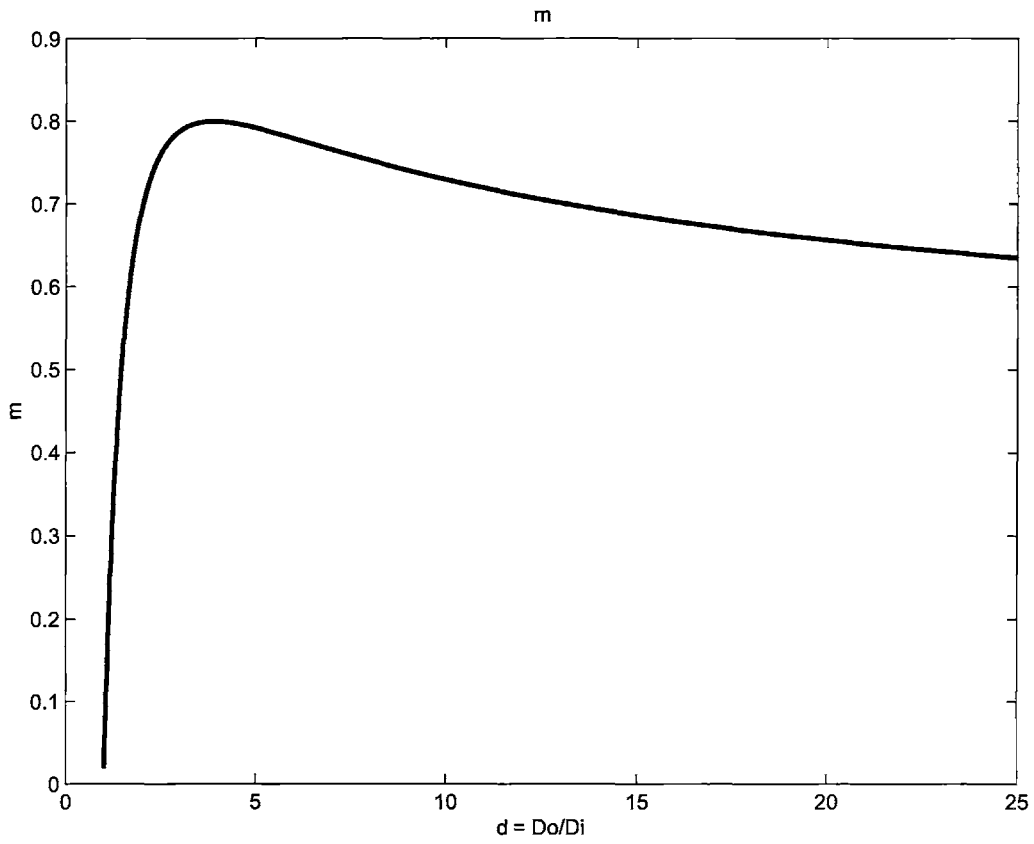

Figure 6-3: Belleville washer parameter m

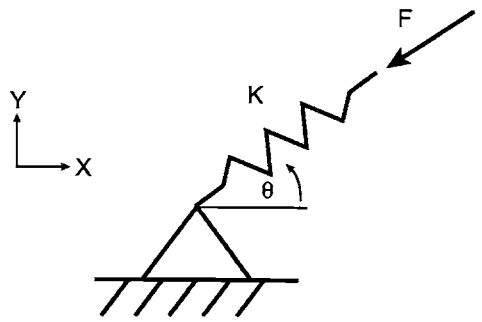

Figure 6-4: Hinged spring

Combining Equations 6.17 and 6.18, a relationship between F_y and δ_y is:

$$F_y = K\delta_y \sin^2\theta \tag{6.19}$$

where K is the axial stiffness of the spring.

As can be seen from Figure 6-5, the effective spring rate decreases as the load increases, thus mimicking the general behavior of the Belleville washer. A flexure designed as a hinged spring can give the desired stiffness characteristic. A discussion of beam deflections is a prerequisite for flexure designs.

Beam Deflections

In axial loading, assuming the beam material follows Hooke's law (see Equation 6.20), deflection is proportional to the applied axial load according to Equation 6.21.

$$\sigma_{axial} = E\varepsilon_{axial} \tag{6.20}$$

$$P_{axial} = \frac{EA}{L}\delta_{axial} \tag{6.21}$$

where

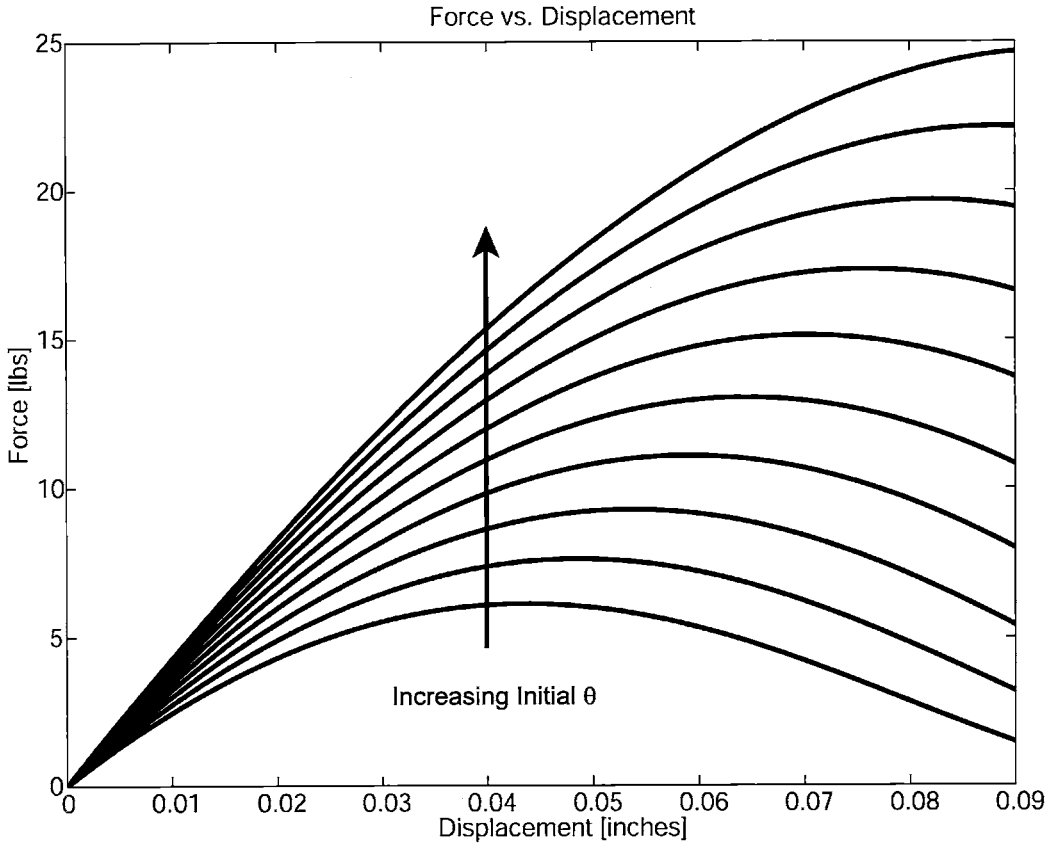

Figure 6-5: Hinged spring: load-deflection curve, where deflection is on the same order as the spring length

P = applied axial load

E = Young's modulus

ε_{axial} = δ/L

σ_{axial} = P/A

A = cross-sectional area of the prismatic beam

L = length of the beam

δ = axial deflection of the beam

In beam bending, deflections are governed by differential equations who's derivations are found in any undergraduate level text book on mechanics of materials. The results are as follows

$$EI\frac{d^2v}{dx^2} = M \tag{6.22}$$

$$EI\frac{d^3v}{dx^3} = V \tag{6.23}$$

$$EI\frac{d^4v}{dx^4} = -q \tag{6.24}$$

where

I = moment of inertia of the beam

v = deflection of the beam

M = bending moment applied to the beam

V = shear applied to the beam

q = distributed load applied to the beam

The assumptions used in deriving Equations 6.22 through 6.24 are that the beam is prismatic, the material follows Hooke's law, the slopes of the deflected beam are small so that small-angle simplifications apply, and all deformations are due to pure bending.

For a cantilever beam supporting load P at its free end, by applying the boundary conditions and integrating the differential Equations 6.22 through 6.24, we obtain

$$P = \frac{3EI}{L^3}\delta \tag{6.25}$$

$$P = \frac{2EI}{L^2}\theta \tag{6.26}$$

where

δ = lateral deflection of the free end

θ = angular displacement of the free end

6.4 Finite Elements

We can write the governing beam equations and boundary conditions but due to geometry, simple analytical solutions are not easily obtained for systems of beams. Finite-element analysis, *FEA*, produces approximate solutions to such problems. Taking the results for beam deflections, a finite-beam element can be created. A typical beam element is shown in the Figure 6-6. Forces *Fx*, *Fy* and M, as well as corresponding displacements u, v and θ are applied at nodes 1 and 2. The following assumptions are made

- The beam is assumed to have a uniform cross-section A, modulus of elasticity E and mass moment of inertia I, therefore it behaves in a linear manner.
- The beam has a uniform flexural stiffness EI over its length L and uniform axial stiffness EA over its length L.
- Plane cross-sections remain plane after deformation, a slender beam approximation.

Separating displacement states for which known results are available, we can derive a stiffness matrix relating the forces and moments to displacements and slopes.

State 1: Compression in the axial direction:

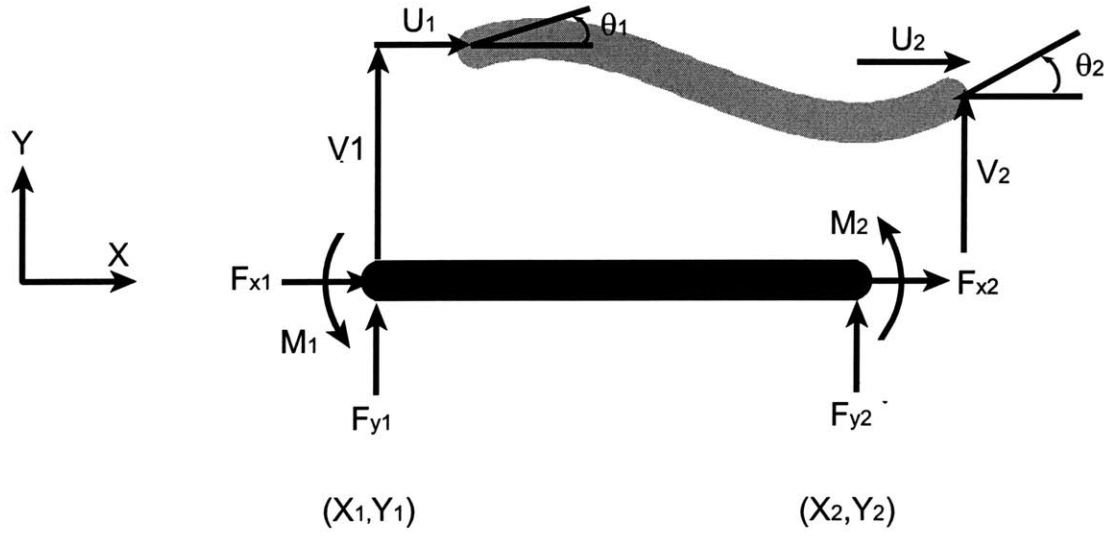

Figure 6-6: Beam element

The Beam is loaded axially by a force F_{x2} and the beam displacements are constrained so that $v_1 = \theta_1 = v_2 = \theta_2 = u_1 = 0$. The axial displacement is given by

$$u_2 = \frac{F_{x2}L}{AE} \tag{6.27}$$

Likewise the displacement u_1 caused by F_{x1} is as follows

$$u_1 = \frac{F_{x1}L}{AE} \tag{6.28}$$

which can be written in matrix form as

$$\begin{bmatrix} F_{x1} \\ F_{x2} \end{bmatrix} = \begin{bmatrix} \frac{AE}{L} & 0 \\ 0 & \frac{AE}{L} \end{bmatrix} \times \begin{bmatrix} u_1 \\ u_2 \end{bmatrix} = K \times \begin{bmatrix} u_1 \\ u_2 \end{bmatrix} \tag{6.29}$$

State 2: Cantilever beam at node 1:

The force F_{y2} = constant, moment M_2 = constant and the displacement constraints are $v_1 = \theta_1 = 0$. According to beam theory, the displacements v_2 and θ_2 are

given in terms of loads F_{y2} and M_2 as

$$\begin{aligned} \upsilon_2 &= \frac{F_{y2}L^3}{3EI} + \frac{M_2L^2}{2EI} \\ \theta_2 &= \frac{F_{y2}L^2}{2EI} + \frac{M_2L}{EI} \end{aligned} \tag{6.30}$$

which can be rewritten as

$$\begin{bmatrix} F_{y2} \\ M_2 \end{bmatrix} = EI \begin{bmatrix} \frac{12}{L^3} & -\frac{6}{L^2} \\ -\frac{6}{L^2} & \frac{4}{L} \end{bmatrix} \times \begin{bmatrix} \upsilon_2 \\ \theta_2 \end{bmatrix} = K_{22} \times \begin{bmatrix} \upsilon_2 \\ \theta_2 \end{bmatrix} \tag{6.31}$$

The reacting forces at node 1 can be calculated by applying Newton's law

$$\sum F_y = F_{y1} + F_{y2} = 0 \tag{6.32}$$

$$\sum M_2 = F_{y1}L + M_1 + M_2 = 0 \tag{6.33}$$

which can be written as

$$\begin{bmatrix} F_{y1} \\ M_1 \end{bmatrix} = \begin{bmatrix} -1 & 0 \\ -L & -1 \end{bmatrix} \times \begin{bmatrix} F_{y2} \\ M_2 \end{bmatrix} = A \times \begin{bmatrix} F_{y2} \\ M_2 \end{bmatrix} \tag{6.34}$$

Substituting Equation 6.31 into Equation 6.34 we obtain

$$\begin{bmatrix} F_{y1} \\ M_1 \end{bmatrix} = AK_{22} \times \begin{bmatrix} \upsilon_1 \\ \theta_1 \end{bmatrix} = EI \begin{bmatrix} -\frac{12}{L^3} & \frac{6}{L^2} \\ -\frac{6}{L^2} & \frac{2}{L} \end{bmatrix} \times \begin{bmatrix} \upsilon_2 \\ \theta_2 \end{bmatrix} = K_{12} \times \begin{bmatrix} \upsilon_2 \\ \theta_2 \end{bmatrix} \tag{6.35}$$

State 3: Cantilevered beam constraints at node 2:

The node force F_{y1} = constant, M_1 = constant and constraints are $\upsilon_2 = \theta_2 = 0$. The results are the same for state one except for signs. Therefore

$$\begin{aligned} \begin{bmatrix} F_{y1} \\ M_1 \end{bmatrix} &= K_{11} \times \begin{bmatrix} \upsilon_1 \\ \theta_1 \end{bmatrix} \\ K_{11} &= EI \begin{bmatrix} \frac{12}{L^3} & \frac{6}{L^2} \\ \frac{6}{L^2} & \frac{4}{L} \end{bmatrix} \end{aligned} \tag{6.36}$$

$$\begin{bmatrix} F_{y2} \\ M_2 \end{bmatrix} = K_{21} \times \begin{bmatrix} v_1 \\ \theta_1 \end{bmatrix}$$
$$K_{21} = EI \begin{bmatrix} -\frac{12}{L^3} & -\frac{6}{L^2} \\ \frac{6}{L^2} & \frac{2}{L} \end{bmatrix} \tag{6.37}$$

Collecting the Equations 6.31, 6.35, 6.36, and 6.37 into a single matrix equation gives

$$\begin{bmatrix} F_{y1} \\ M_1 \\ F_{y2} \\ M_2 \end{bmatrix} = \begin{bmatrix} K_{11} & K_{21}^T \\ K_{21} & K_{22} \end{bmatrix} \times \begin{bmatrix} v_1 \\ \theta_1 \\ v_2 \\ \theta_2 \end{bmatrix} \tag{6.38}$$

An element stiffness matrix can be formed by combining Equations 6.29 and 6.38 to get

$$\begin{bmatrix} F_{x1} \\ F_{y1} \\ M_1 \\ F_{x2} \\ F_{y2} \\ M_2 \end{bmatrix} = \begin{bmatrix} \frac{AE}{L} & 0 & 0 & 0 & 0 & 0 \\ 0 & \frac{EI12}{L^3} & \frac{EI6}{L^2} & 0 & -\frac{EI12}{L^3} & \frac{EI6}{L^2} \\ 0 & \frac{EI6}{L^2} & \frac{EI4}{L} & 0 & -\frac{EI6}{L^2} & \frac{EI2}{L} \\ 0 & 0 & 0 & \frac{AE}{L} & 0 & 0 \\ 0 & -\frac{EI12}{L^3} & -\frac{EI6}{L^2} & 0 & \frac{EI12}{L^3} & -\frac{EI6}{L^2} \\ 0 & \frac{EI6}{L^2} & \frac{EI2}{L} & 0 & -\frac{EI6}{L^2} & \frac{EI4}{L} \end{bmatrix} \times \begin{bmatrix} u_1 \\ v_1 \\ \theta_1 \\ u_2 \\ v_2 \\ \theta_2 \end{bmatrix} \tag{6.39}$$

The bending beam element's stiffness matrix has now been established for the local coordinate system. It must be transformed to the global coordinate system before each element can be combined to determine the system's load-displacement characteristics.

Element matrix equations, Equation 6.39, have the following form

$$[F_L] = [K_L][\delta_L] \tag{6.40}$$

where

F_L = local applied forces.

K_L = local stiffness matrix.

δ_L = local displacements.

From geometry, local displacements, $[\delta_L]$, can be transformed to the global displacements, $[\delta]$, via the transformation matrix $[R]$.

$$[\delta_L] = [R] \times [\delta] \tag{6.41}$$

Because the element's total potential energy, $\Pi^{(e)}$ is independent of the coordinate systems, conservation of potential energy is used to derive the transformation equations as follows

$$\Pi^{(e)} = \tfrac{1}{2}[\delta_L][K_L][\delta_L] - [\delta_L][F_L] \tag{6.42}$$

Making use of the transformation Equation 6.41 we obtain

$$\Pi^{(e)} = \tfrac{1}{2}[\delta][R]^T[K_L][R][\delta] - [\delta][R]^T[F_L] \tag{6.43}$$

The total potential energy in global coordinates can be written as

$$\Pi^{(e)} = \tfrac{1}{2}[\delta][K][\delta] - [\delta][F] \tag{6.44}$$

The element transformation equations are

$$[K]^{(e)} = [R]^T[K_L]^{(e)}[R] \tag{6.45}$$

and

$$[F]^{(e)} = [R]^T[F_L]^{(e)} \tag{6.46}$$

For the beam elements, the rotation matrix $[R]$ can be found. The element displacements are given in Figure 6-7. It is easily seen that the local displacements can be projected upon the global axes to obtain their global components. Thus we may

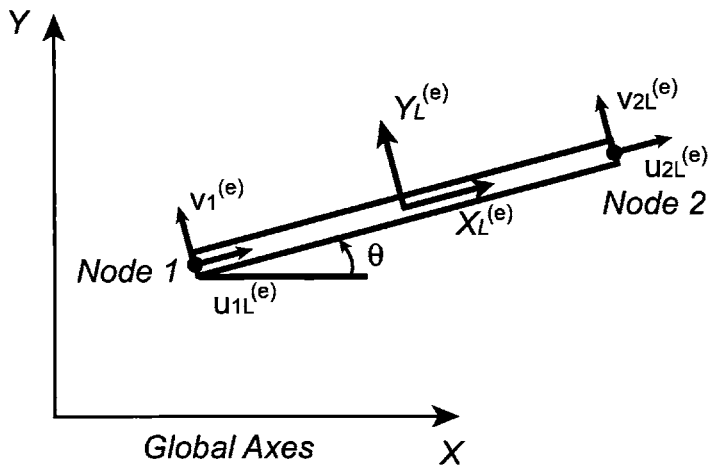

Figure 6-7: Beam element displacements for transformation matrix derivation

write Equation 6.41 as

$$\begin{bmatrix} u_{1L} \\ v_{1L} \\ \theta_{1L} \\ u_{2L} \\ v_{2L} \\ \theta_{2L} \end{bmatrix}^{(e)} = \begin{bmatrix} \cos\theta & \sin\theta & 0 & 0 & 0 & 0 \\ -\sin\theta & \cos\theta & 0 & 0 & 0 & 0 \\ 0 & 0 & 1 & 0 & 0 & 0 \\ 0 & 0 & 0 & \cos\theta & \sin\theta & 0 \\ 0 & 0 & 0 & -\sin\theta & \cos\theta & 0 \\ 0 & 0 & 0 & 0 & 0 & 1 \end{bmatrix} \times \begin{bmatrix} u_1 \\ v_1 \\ \theta_1 \\ u_2 \\ v_2 \\ \theta_2 \end{bmatrix}^{(e)} = [R] \times \begin{bmatrix} u_1 \\ v_1 \\ \theta_1 \\ u_2 \\ v_2 \\ \theta_2 \end{bmatrix}^{(e)} \tag{6.47}$$

The next step is to combine all of the elements to form a complete set governing the composite of elements. Compatibility at the element nodes is the assembly procedure basis. Nodal variables (displacements and forces) are the same for all elements connected at that node. Thus, summing element stiffness matrices in a manner that compatibility is satisfied, generates a global stiffness matrix [7].

In summary, the finite element analysis is performed as follows

- Create $n \times n$ and $n \times 1$ null matrices where n is the number of nodes.
- Transform the local element equations to the global equations for each element.
- Add these global terms into the $n \times n$ and $n \times 1$ matrices so that compatibility is satisfied.

Repeating the last two steps for the entire set of elements gives

$$\overset{n\times n}{[K]} \times \overset{n\times 1}{[\delta]} = \overset{n\times 1}{[F]} \tag{6.48}$$

Equation 6.48 is not yet ready to be solved because matrix $[K]$ is singular. That is, there are infinite solutions to the set of equations described. To find a unique solution, boundary conditions are introduced. There are many ways to introduce boundary conditions, but we would like to make use of the banded matrix $[K]$ so matrix restructuring will be avoided. Three methods will be discussed: Matrix Partitioning, Penalty and Ones-on-diagonal [9].

In the Matrix Partitioning method, the global stiffness matrix is partitioned as described by Equation 6.49:

$$\begin{bmatrix} K_{11} & K_{12} \\ K_{21} & K_{22} \end{bmatrix} \begin{bmatrix} \delta_k \\ \delta_u \end{bmatrix} = \begin{bmatrix} F_u \\ F_k \end{bmatrix} \tag{6.49}$$

where

δ_k = vector containing known displacements

δ_u = vector of unknown displacements

F_u = vector of unknown forces

F_k = vector containing known forces

Partitioning $[K]$ into the form of Equation 6.49 can destroy its diagonal dominance and other "nice matrix" properties, but is completely doable. It should be noted that K_{11}, K_{12}, K_{21}, and K_{22} are not necessarily those of Equation 6.38.

Solving the bottom row for the unknown displacements gives

$$[\delta_u] = [K_{22}]^{-1}\{[F_k] - [K_{21}][\delta_k]\} \tag{6.50}$$

Substituting Equation 6.50 back into the top row of 6.49 the unknown forces can be found as follows

$$[F_u] = [K_{11}][\delta_k] + [K_{12}][\delta_u] \tag{6.51}$$

The penalty method is the easiest to apply, but is highly prone to mathematical errors. A boundary condition at the ith node determines $\delta_i = a$. The K_{ii} value is multiplied by a very large number that is many orders of magnitude larger than the largest number in the $[K]$ matrix giving K^*_{ii}. The F_i value is replaced with the value of $a \times K^*_{ii}$.

For example, our basic equations are

$$[K][\delta] = [F] = \begin{bmatrix} a & b \\ c & d \end{bmatrix} \begin{bmatrix} x \\ y \end{bmatrix} = \begin{bmatrix} f_1 \\ f_2 \end{bmatrix} \tag{6.52}$$

We have a constraint x = constant, accordingly $K_{11} = 10^6 \times x$

$$\begin{bmatrix} a \times 10^6 & b \\ c & d \end{bmatrix} \begin{bmatrix} x \\ y \end{bmatrix} = \begin{bmatrix} a \times 10^6 \times x \\ f_2 \end{bmatrix} \tag{6.53}$$

By inspection, using Gauss elimination to solve Equation 6.53, the displacements will be very close to those from the Partitioning method, but the displacements are sensitive to numerical errors.

Or finally applying the ones-on-diagonal method, we want the constraint $\delta_i = a$, then: (1) all terms in Row i of the stiffness matrix are set to zero, (2) K_{ii} is set to unity, and (3) F_i is set to a. For example, using Equation 6.52, applying a constraint x = const, gives

$$\begin{bmatrix} 1 & 0 \\ c & d \end{bmatrix} \begin{bmatrix} x \\ y \end{bmatrix} = \begin{bmatrix} a \\ f_2 \end{bmatrix} \tag{6.54}$$

It is easy to see the mechanics of ones-on-diagonal method.

6.4.1 Non-linear FEA

The non-linear force-displacement relationship is solely based on geometry. The hinged spring is a linear element, but as geometric constraints cause spring rotation, the vertical reaction-force to vertical-displacement relationship is non-linear. To obtain this result via FEA

- Zero elemental forces.
- Displace desired elements by a small increment δ.
- Record reaction forces found by solving the Finite Element Model.
- Taking displaced shape found by the previous solve and create a new FEM.
- Repeat these steps until the desired displacement is reached.

6.5 Flexure

An extruded part's wall thickness can be as thin as 0.075". This may be thin enough for flexure actuated preloading bearing-pad. Attempting to mimic a hinged spring, the flexure shape depicted in Figure 6-8 was designed. It behaves more like the spring system shown in Figure 6-9. Beam 1 and the Beam Set are analogous to K_1 and K_2 respectively.

We model this configuration using FEA. Boundary conditions at the base node are set to zero displacement in all degrees-of-freedom, Figure 6-10. The loading node is constrained in the x-direction and theta-direction. The loading node's y-component is displaced at 0.006" decrements according to the non-linear FEA technique.

FEM results show high flexure stiffness and minimal non-linear behavior (see Figure 6-11). High stiffness is a function of part thickness and part depth into the page. The non-linear behavior is minimal due to the flexure's bending stiffness, the Beam 1 and the Beam set are clearly curling as shown in Figure 6-12, thus exerting a moment. The hinged spring has zero bending stiffness and therefore does not exert a restoring moment. Greatly reducing the flexure wall-thickness at the Beam 1 to Beam Set connection and freeing the Loading Node's theta constraint, allows the system to behave similar to the hinged spring as shown in Figures 6-13 and 6-14. Unfortunately, a flexure with the desired force characteristics and size constraints isn't possible with the extrusion process alone. Therefore this approach left for future work.

Modifying the extrusion process to obtain thinner walled parts is beyond the

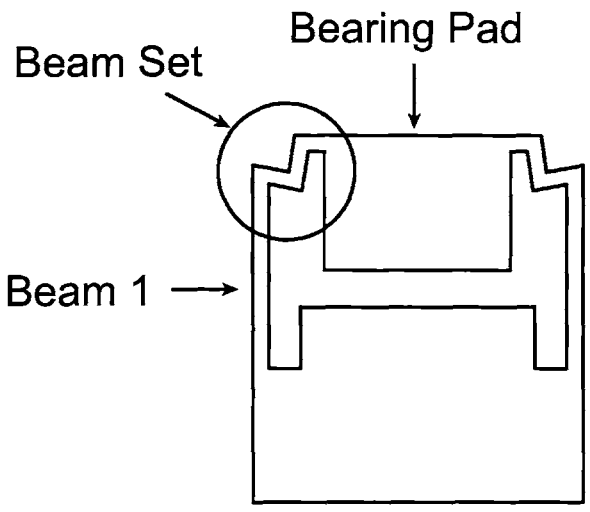

Figure 6-8: Flexure Design

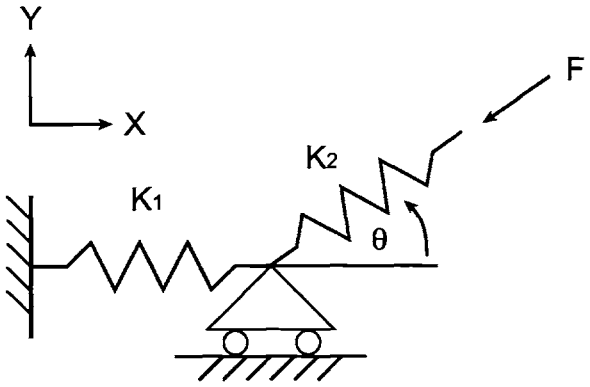

Figure 6-9: Modified hinged spring

scope of this thesis. Making the part depth thinner is possible but requires a second machining operation, which defeats the purpose of designing a non-linear flexure.

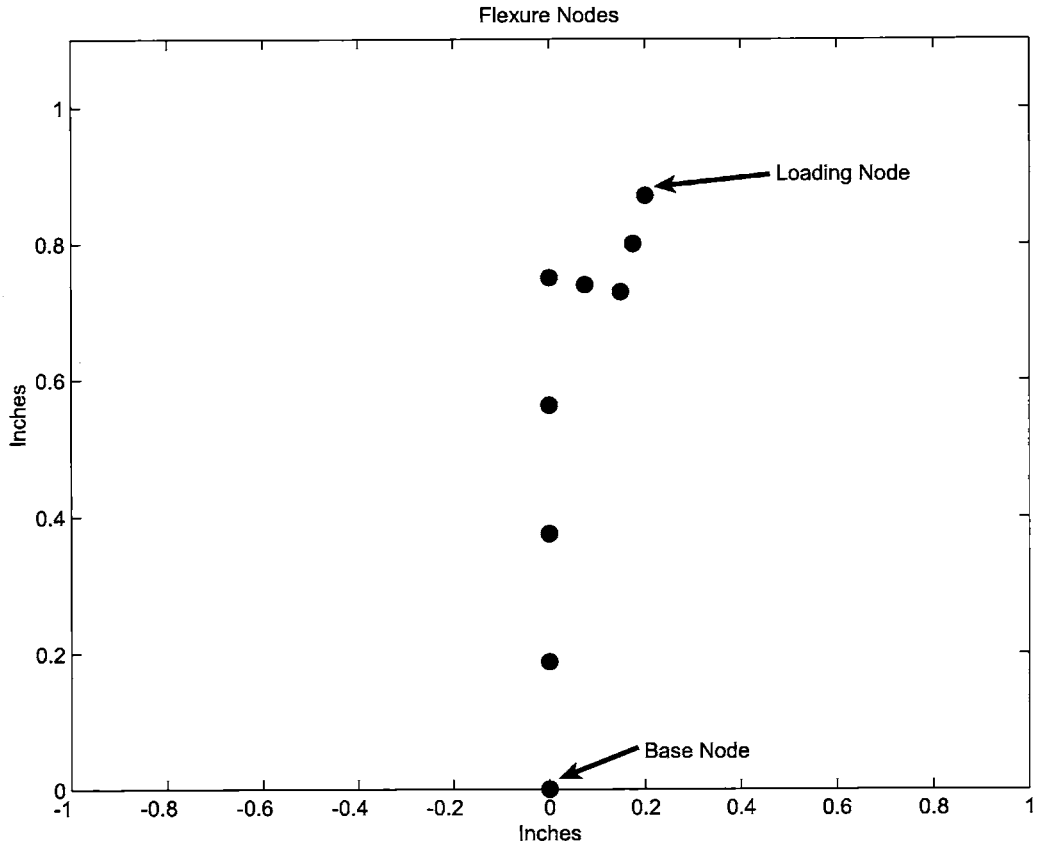

Figure 6-10: FEM Nodes

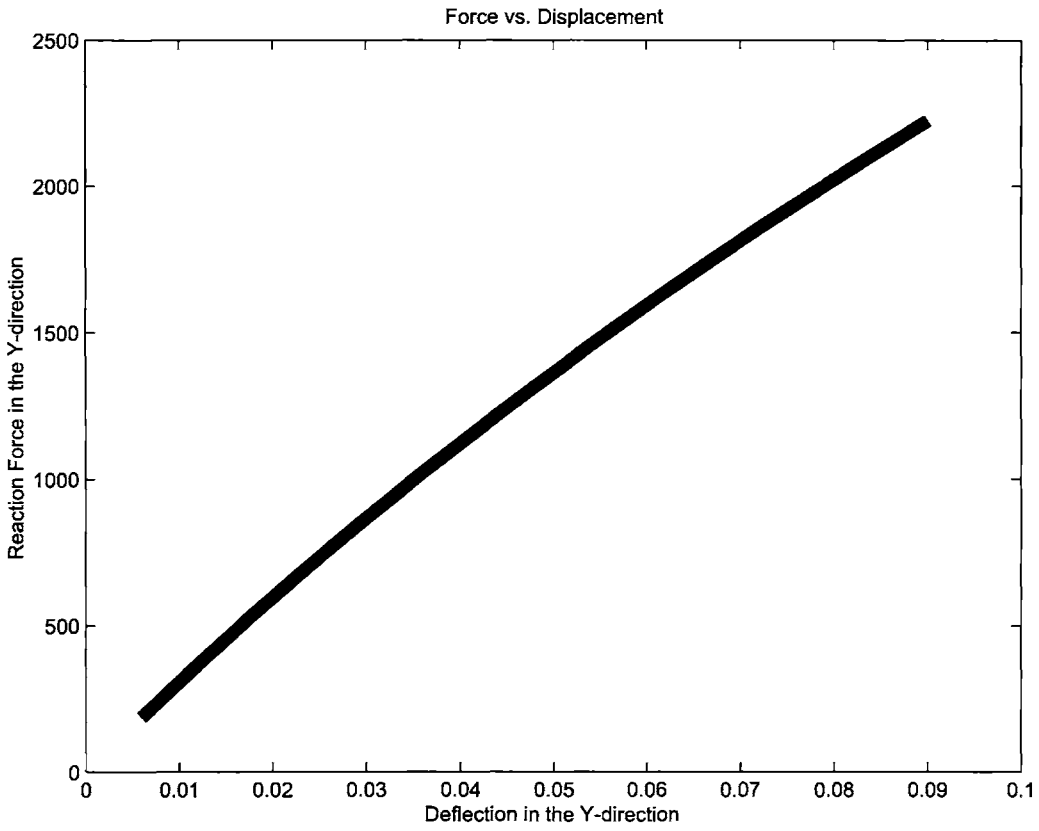

Figure 6-11: Non-linear flexure load-deflection curve

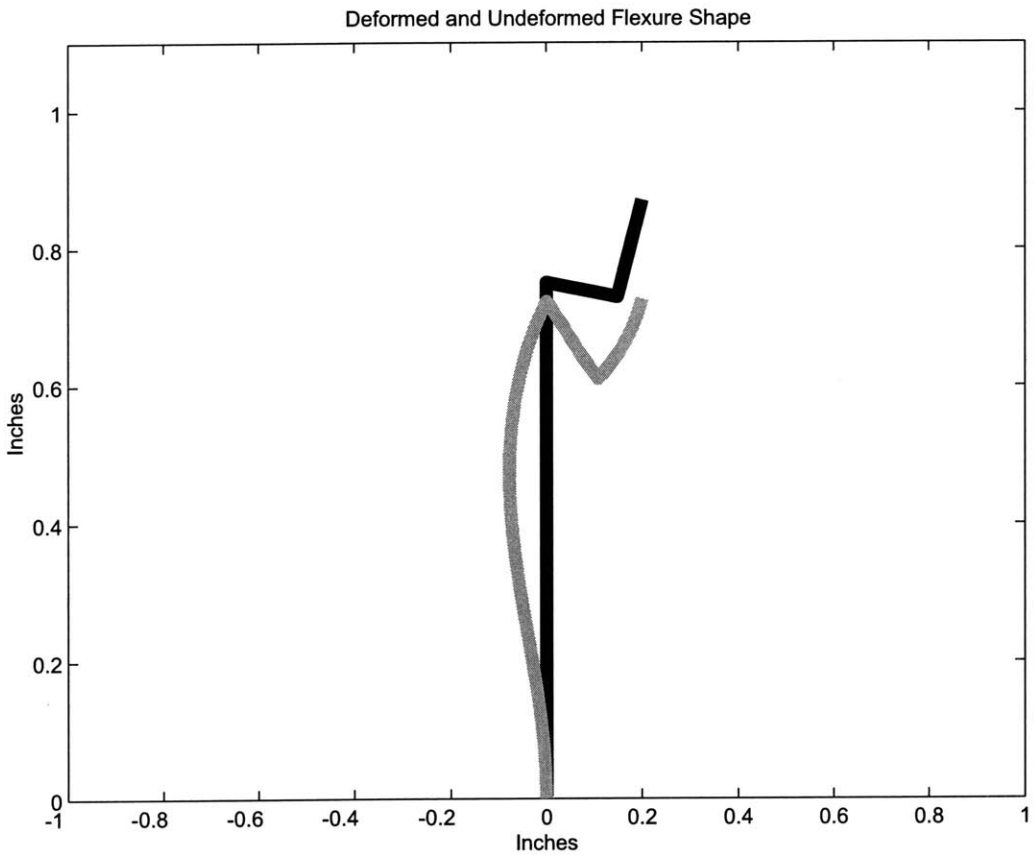

Figure 6-12: Non-linear flexure deformation: base node is constrained in all directions and load node is constrained in the x-direction and rotation

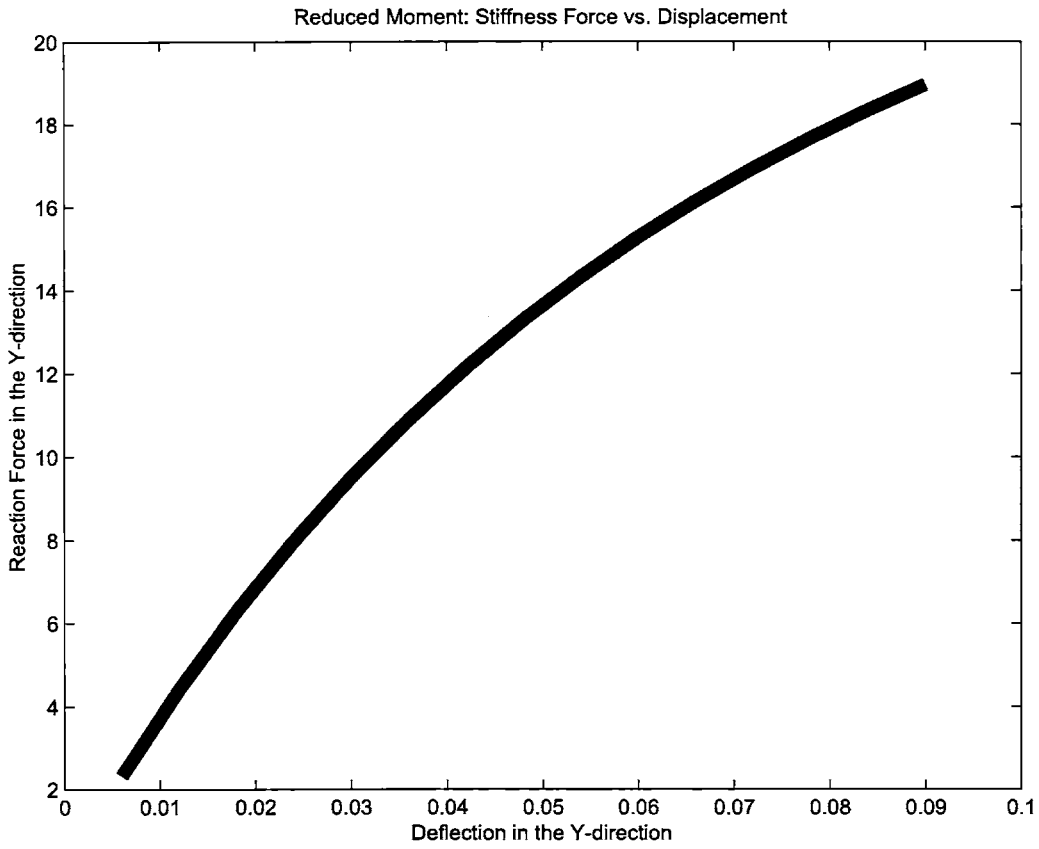

Figure 6-13: Non-linear flexure reduced moment stiffness load-deflection curve

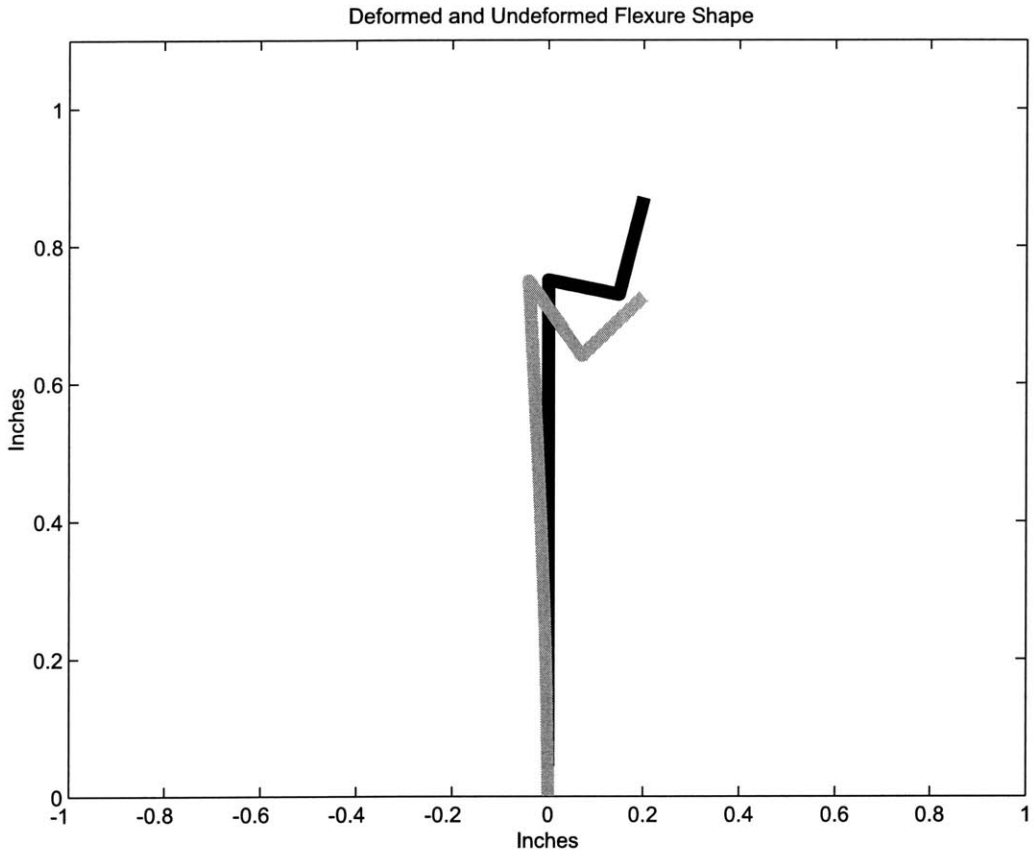

Figure 6-14: Non-linear flexure reduced moment stiffness deformation: The base node is constrained in all directions and the load node is constrained only in the x-direction. A very thin element is placed between Beam 1 and the Beam Set to reduce moment stiffness

Chapter 7

Conclusion

The first prototype's inboard-outboard bearing system is extremely light and compliant. The floating-beam bearing design is easy to manufacture and assemble at low cost, but is far too compliant to serve as a precision machine tool bearing system. Fluctuating cutting forces cause the cutting head to resonate, producing unacceptable chatter.

The second prototype's inboard-outboard bearing system is sufficiently stiff, but rather bulky. Stiffening the catamaran plates, this design works well. The cutting head's high weight and the low stiffness of the feed dovetail bearing causes the system to have a hint of chatter at full depth of cut (0.015"). To improve on this design, the catamaran plates need to be stiffened and damped, perhaps by a shear damping technique, and the inboard-outboard bearing needs to be lightened.

In order to rapidly produce this prototype, it was assembled from a number of plates using bolted joints. These joints lead to a rather bulky design and also contribute to its compliance. However, we anticipate that in production, the bearing set will be manufactured by extrusion, thus eliminating much of the weight and size of the prototype.

7.1 Future Work

The final design must combine the stiffness of prototype 2 and the light-weight of prototype 1. Hollowing out prototype 2's inboard-outboard bearing greatly increases the stiffness to mass ratio, and production of the carriages from an extrusion as outlined above will yield a stiffer and lighter design. These changes will increase the fundamental frequency and damping of the device decreases its peak response, thus creating a more "well behaved" precision bearing system.

Although we have designed the servo mechanism, automated operation was not tested due to time constraints. Designing, building, and analyzing prototype 1 unexpectedly usurped large amounts of time due to changing specifications and miscommunication between the sponsor and MIT. Fully redesigning, building, and analyzing prototype 2 received the remainder of the allotted time.

Designing a feasible linear bearing with large travel was the most technically challenging project task. Designing a controller for this machine is a trivial task in concept, but lengthy in implementation time because designing a user interface is subjective and requires interaction between many different people.

Bibliography

[1] Laslo Almen. *The Uniform-Section Disk Spring.* Trans. ASME, 1936.

[2] Douglass L. Blanding. *Exact Constraint: Machine Design Using Kinematic Principles.* ASME Press, New York, New York, 1999.

[3] Bruce Campbell and Drew Devitt. *Machine Tool Way Rebuilding.* http://www.moglice.com, 1999.

[4] EAR Corporation. 7911 Zionsville Road, Indianapolis, Indiana 46268.

[5] John J. Craig. *Introduction to Robotics Mechanics and Control, Second Edition.* Addison-WesleyPublishing Co., Reading, MA, 1989.

[6] Siegfried Gross. *Calculation and Design of Metal Springs.* Willmer Brothers Ltd., 1966.

[7] Thornton Huebner and Byrom. *The Finite Element Method For Engineers, third edition.* Wiley-Interscience, 1995.

[8] PCB Piezotronics Inc. http://pcb.com, Depew, New York.

[9] Steven M. Lepi. *Practical Guide to Finite Elements.* Marcel Dekker, Inc., New York, New York, 1998.

[10] Philadelphia Resins. http://www.philadelphiaresins.com, Aston, Pennsylvania.

[11] James G. Skakoon. *Detailed Mechanical Design: A Practical Guide.* ASME Press, New York, New York, 2000.

[12] Alexander H. Slocum. *Precision Machine Design.* Prentice Hall, Englewood Cliffs, New Jersey, 1992.

[13] G. Temple and W.G Bickley. *Rayleigh's principle and its applications to Engineering.* Dover Publications Inc., USA, 1956.

Appendix A

Prototype 1 Drawings

Part List:

1. Bearing Endcap
2. Catamaran Bearing
3. Catamaran Plate
4. Left Cutter
5. Right Cutter
6. Lead Screw Bracket Short
7. Lead Screw Bracket Tall
8. Base Plate
9. Base Bracket
10. Bearing End Cap Motor
11. Thomson Shaft: Class L solid 316 stainless steel 60 Case LinearRace, part number 1 L SS316, 14.6" Length: Qty 2
12. Thomson Nyliner Polymer Bearing: part number 16L16: Qty 5

13. Ground Steel Shaft: McMaster Carr part number 9517K281 cut to 14.6": Qty 1

14. 1" Wide .015" Thick Black MDS-Filled Nylon 6/6 Strip: McMaster Carr part number 8751K12: Qty 1

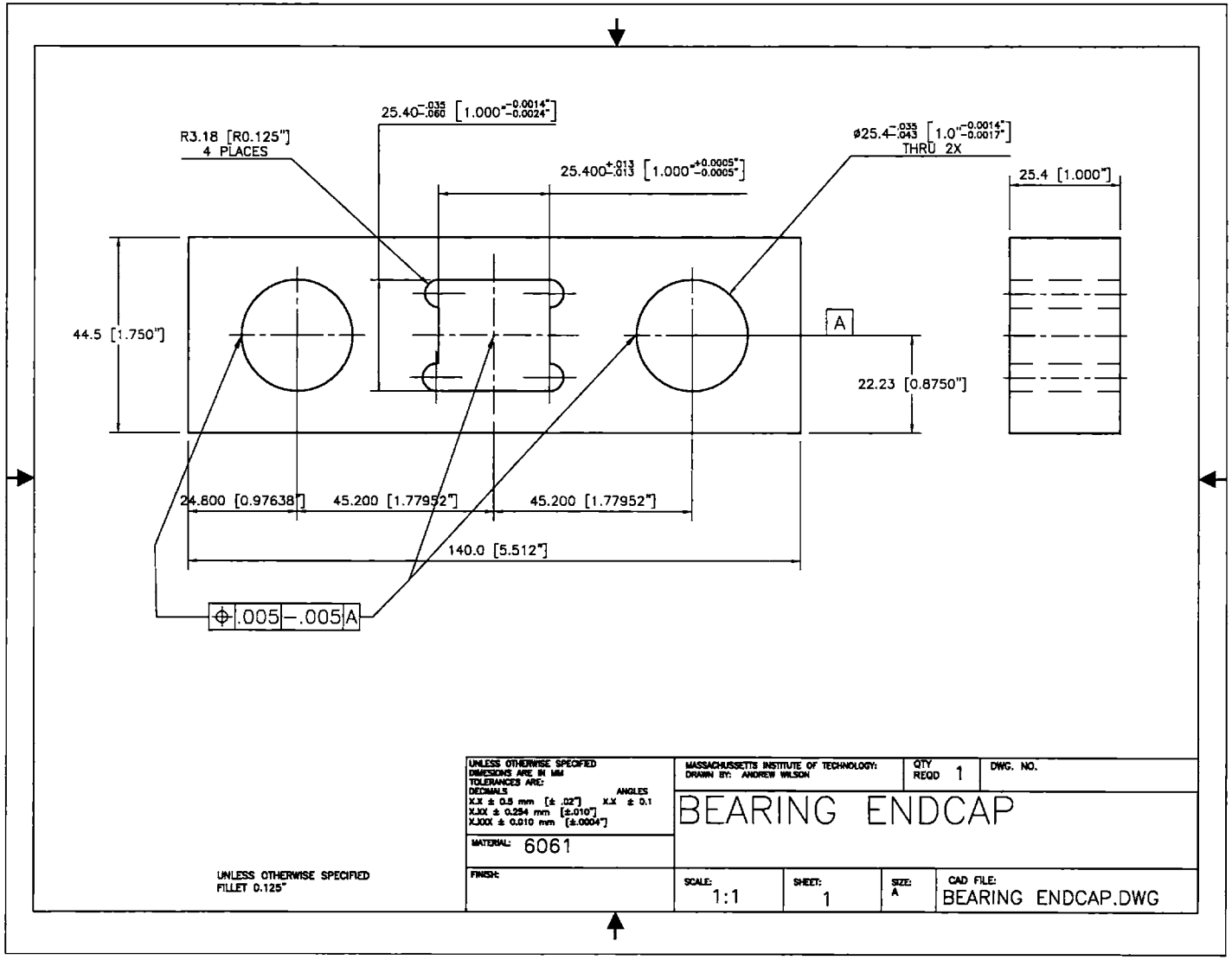
R3.18 [R0.125"]
4 PLACES
25.40 -.035 -.060 [1.000 +-0.0014 -0.0024]
25.400 +.013 -.013 [1.000 +-0.0005 -0.0005]
ø25.4 -.035 -.043 [1.0 +-0.0014 -0.0017]
THRU 2X
25.4 [1.000"]
44.5 [1.750"]
A
22.23 [0.8750"]
24.800 [0.97638"]
45.200 [1.77952"]
45.200 [1.77952"]
140.0 [5.512"]
.005 -.005 A
UNLESS OTHERWISE SPECIFIED
DIMENSIONS ARE IN MM
TOLERANCES ARE:
DECIMALS
ANGLES
X.X ± 0.5 mm [± .02"]
X.XX ± 0.1
X.XX ± 0.254 mm [±.010"]
X.XXX ± 0.010 mm [±.0004"]
MATERIAL: 6061
FINISH:
UNLESS OTHERWISE SPECIFIED
FILLET 0.125"
MASSACHUSSETTS INSTITUTE OF TECHNOLOGY:
DRAWN BY: ANDREW WILSON
QTY REQD 1
DWG. NO.
BEARING ENDCAP
SCALE: 1:1
SHEET: 1
SIZE: A
CAD FILE: BEARING ENDCAP.DWG

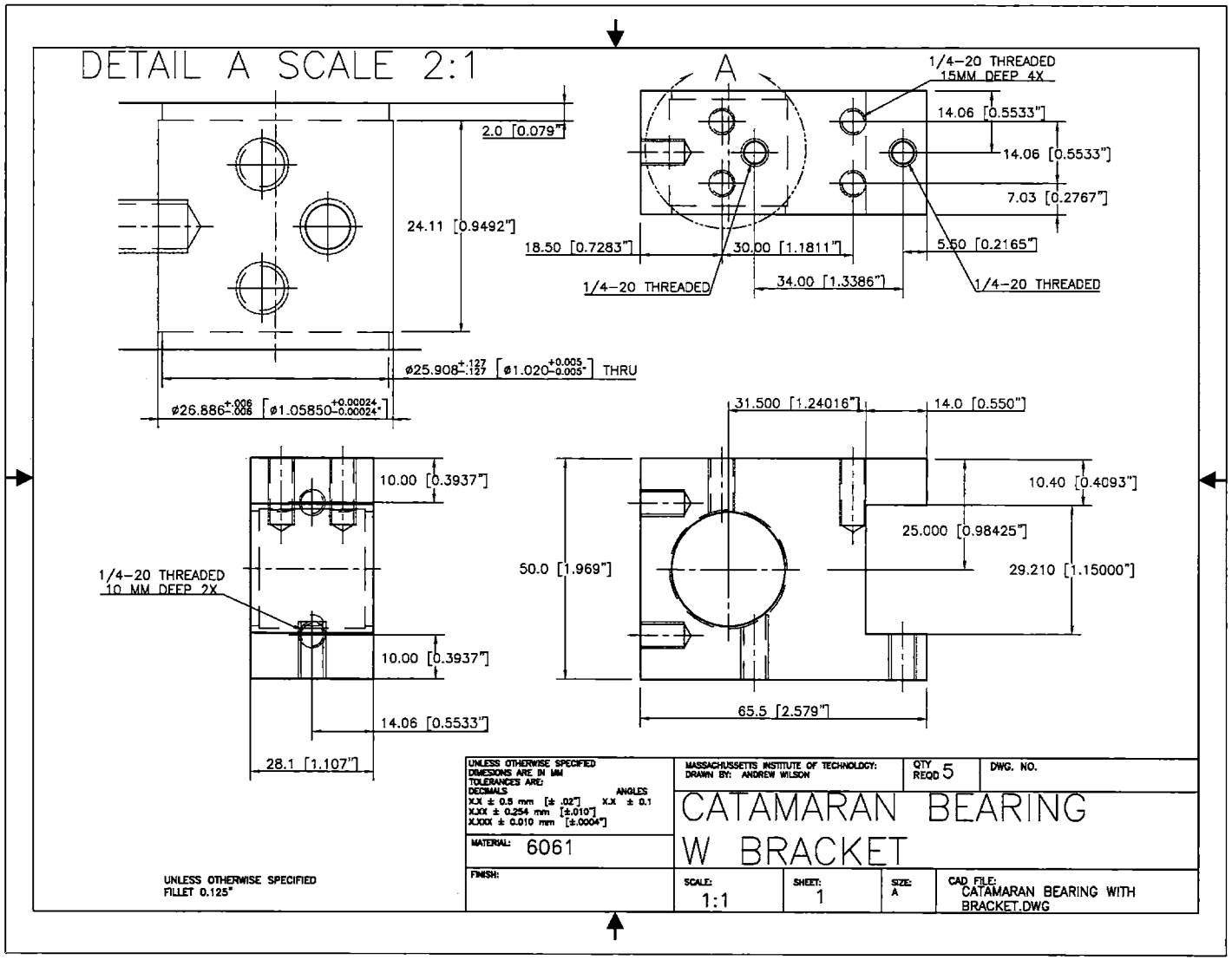
DETAIL A SCALE 2:1
A
1/4–20 THREADED
15MM DEEP 4X
14.06 [0.5533"]
14.06 [0.5533"]
7.03 [0.2767"]
5.50 [0.2165"]
18.50 [0.7283"]
30.00 [1.1811"]
34.00 [1.3386"]
1/4–20 THREADED
1/4–20 THREADED
2.0 [0.079"]
24.11 [0.9492"]
ø25.908 +.127 -.127 [ø1.020 +0.005 -0.005] THRU
ø26.886 +.006 -.006 [ø1.05850 +0.00024 -0.00024]
31.500 [1.24016"]
14.0 [0.550"]
10.40 [0.4093"]
25.000 [0.98425"]
29.210 [1.15000"]
50.0 [1.969"]
65.5 [2.579"]
10.00 [0.3937"]
1/4–20 THREADED
10 MM DEEP 2X
10.00 [0.3937"]
14.06 [0.5533"]
28.1 [1.107"]
UNLESS OTHERWISE SPECIFIED
FILLET 0.125"
UNLESS OTHERWISE SPECIFIED
DIMESIONS ARE IN MM
TOLERANCES ARE:
DECIMALS
ANGLES
X.X ± 0.5 mm [± .02"]
X.X ± 0.1
X.XX ± 0.254 mm [±.010"]
X.XXX ± 0.010 mm [±.0004"]
MATERIAL: 6061
FINISH:
MASSACHUSSETTS INSTITUTE OF TECHNOLOGY:
DRAWN BY: ANDREW WILSON
QTY REQD 5
DWG. NO.
CATAMARAN BEARING W BRACKET
SCALE: 1:1
SHEET: 1
SIZE: A
CAD FILE: CATAMARAN BEARING WITH BRACKET.DWG

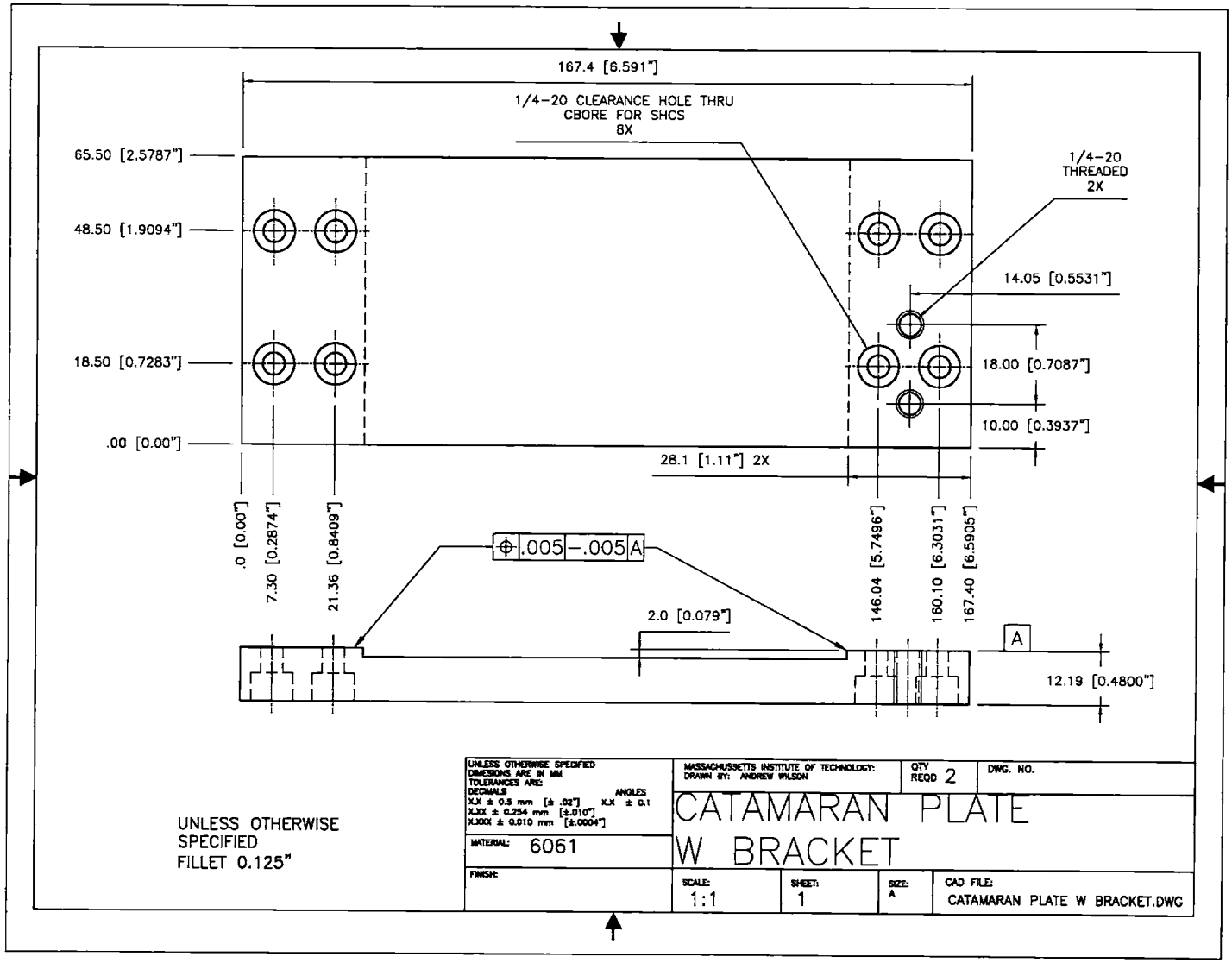
167.4 [6.591"]
1/4-20 CLEARANCE HOLE THRU
CBORE FOR SHCS
8X
65.50 [2.5787"]
48.50 [1.9094"]
18.50 [0.7283"]
.00 [0.00"]
1/4-20
THREADED
2X
14.05 [0.5531"]
18.00 [0.7087"]
10.00 [0.3937"]
28.1 [1.11"] 2X
.0 [0.00"]
7.30 [0.2874"]
21.36 [0.8409"]
.005 -.005 A
2.0 [0.079"]
146.04 [5.7496"]
160.10 [6.3031"]
167.40 [6.5905"]
A
12.19 [0.4800"]
UNLESS OTHERWISE
SPECIFIED
FILLET 0.125"
UNLESS OTHERWISE SPECIFIED
DIMENSIONS ARE IN MM
TOLERANCES ARE:
DECIMALS ANGLES
X.X ± 0.5 mm [± .02"] X.X ± 0.1
X.XX ± 0.254 mm [±.010"]
X.XXX ± 0.010 mm [±.0004"]
MATERIAL: 6061
FINISH:
MASSACHUSSETTS INSTITUTE OF TECHNOLOGY:
DRAWN BY: ANDREW WILSON
QTY REQD 2
DWG. NO.
CATAMARAN PLATE
W BRACKET
SCALE: 1:1
SHEET: 1
SIZE: A
CAD FILE:
CATAMARAN PLATE W BRACKET.DWG

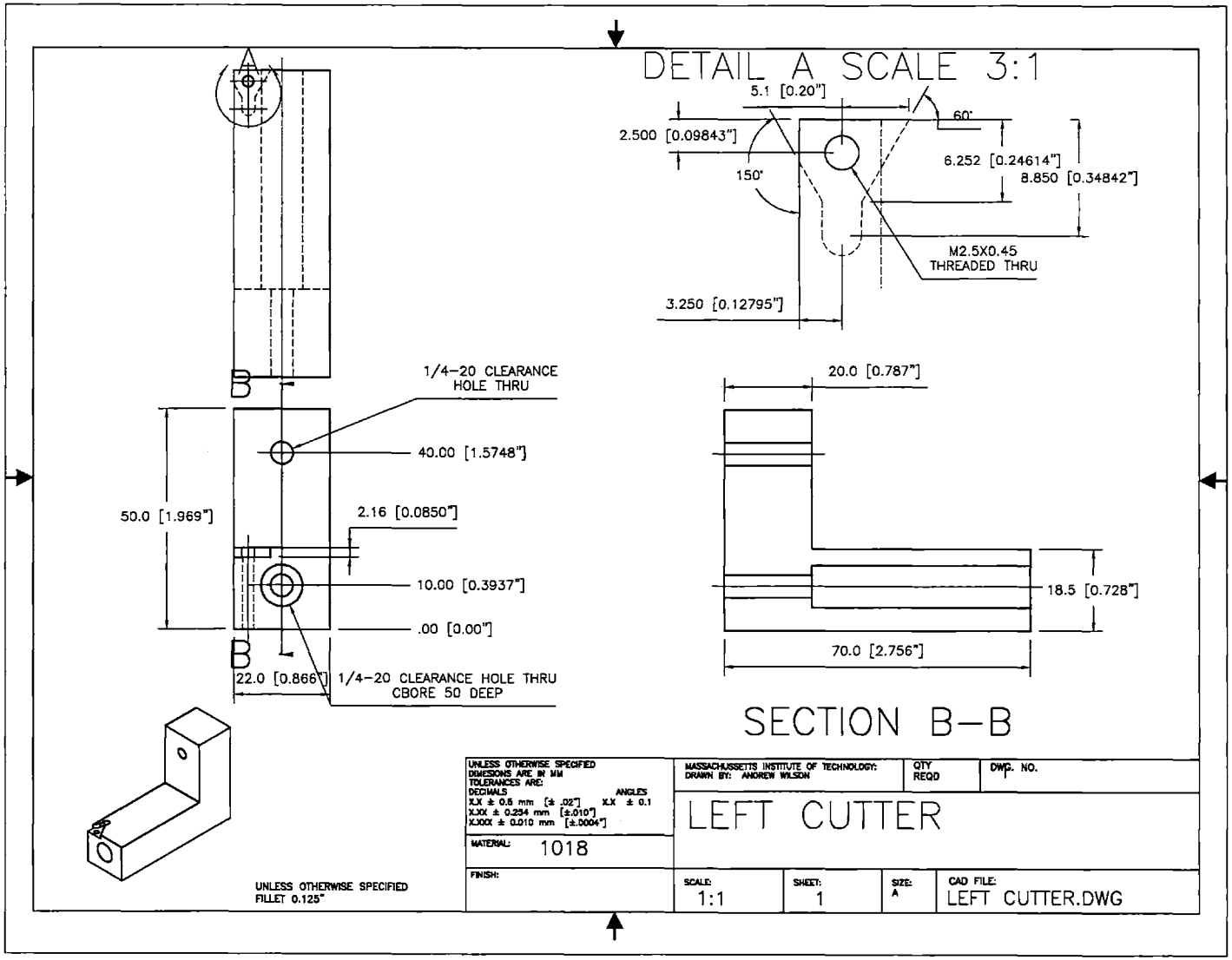
DETAIL A SCALE 3:1
5.1 [0.20"]
60°
2.500 [0.09843"]
150°
6.252 [0.24614"]
8.850 [0.34842"]
M2.5X0.45
THREADED THRU
3.250 [0.12795"]
1/4-20 CLEARANCE
HOLE THRU
40.00 [1.5748"]
50.0 [1.969"]
2.16 [0.0850"]
10.00 [0.3937"]
.00 [0.00"]
22.0 [0.866"]
1/4-20 CLEARANCE HOLE THRU
CBORE 50 DEEP
20.0 [0.787"]
18.5 [0.728"]
70.0 [2.756"]
SECTION B-B
UNLESS OTHERWISE SPECIFIED
FILLET 0.125"
UNLESS OTHERWISE SPECIFIED
DIMESIONS ARE IN MM
TOLERANCES ARE:
DECIMALS
ANGLES
X.X ± 0.5 mm [± .02"]
X.X ± 0.1
X.XX ± 0.254 mm [±.010"]
X.XXX ± 0.010 mm [±.0004"]
MATERIAL: 1018
FINISH:
MASSACHUSSETTS INSTITUTE OF TECHNOLOGY:
DRAWN BY: ANDREW WILSON
QTY REQD
DWG. NO.
LEFT CUTTER
SCALE: 1:1
SHEET: 1
SIZE: A
CAD FILE: LEFT CUTTER.DWG

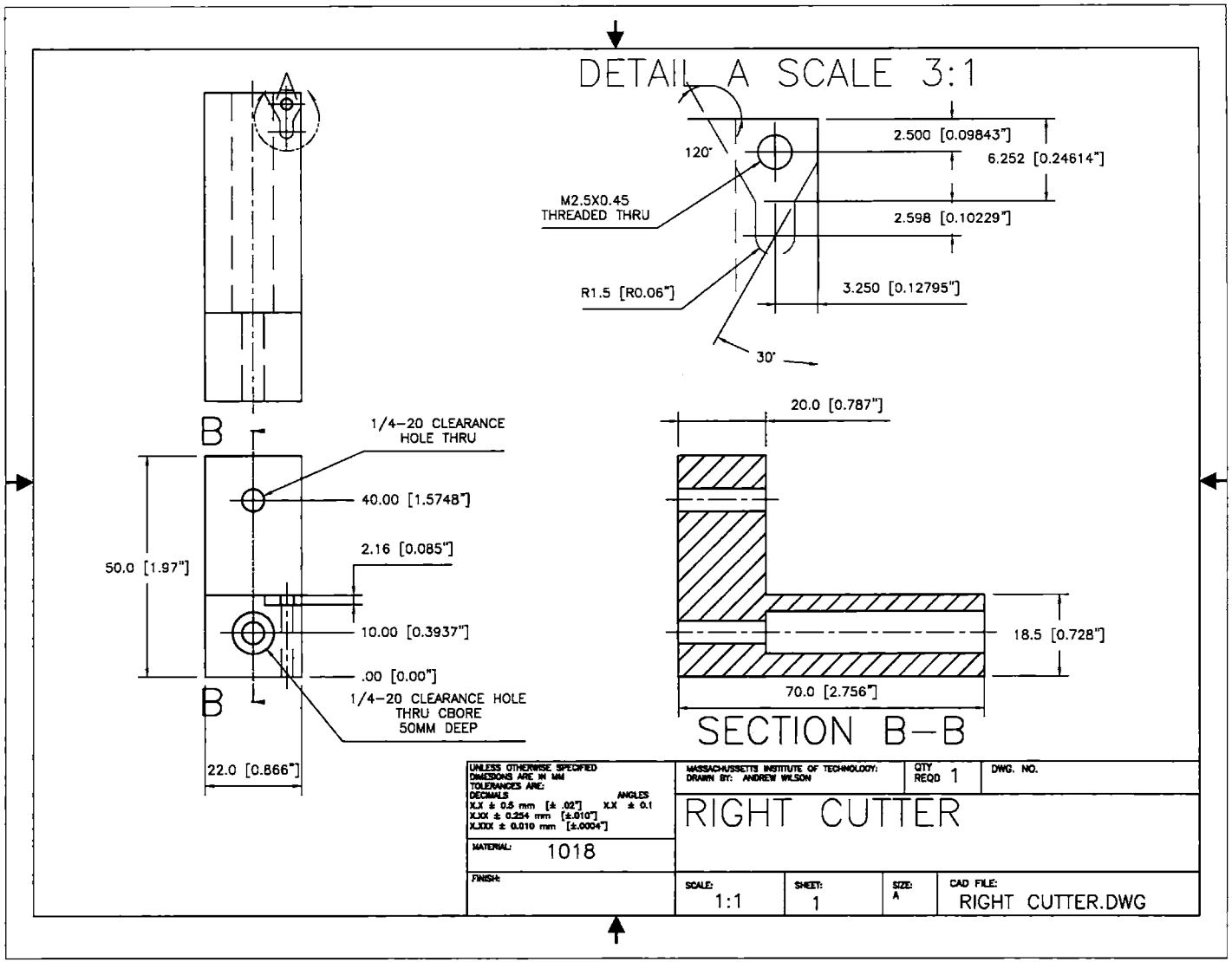
DETAIL A SCALE 3:1
120°
2.500 [0.09843"]
6.252 [0.24614"]
M2.5X0.45
THREADED THRU
2.598 [0.10229"]
R1.5 [R0.06"]
3.250 [0.12795"]
30°
B
1/4-20 CLEARANCE
HOLE THRU
40.00 [1.5748"]
2.16 [0.085"]
50.0 [1.97"]
10.00 [0.3937"]
.00 [0.00"]
B
1/4-20 CLEARANCE HOLE
THRU CBORE
50MM DEEP
22.0 [0.866"]
20.0 [0.787"]
18.5 [0.728"]
70.0 [2.756"]
SECTION B-B
UNLESS OTHERWISE SPECIFIED
DIMESIONS ARE IN MM
TOLERANCES ARE:
DECIMALS
X.X ± 0.5 mm [± .02"]
X.XX ± 0.254 mm [±.010"]
X.XXX ± 0.010 mm [±.0004"]
ANGLES
X.X ± 0.1
MATERIAL: 1018
FINISH:
MASSACHUSSETTS INSTITUTE OF TECHNOLOGY:
DRAWN BY: ANDREW WILSON
QTY REQD 1
DWG. NO.
RIGHT CUTTER
SCALE: 1:1
SHEET: 1
SIZE: A
CAD FILE: RIGHT CUTTER.DWG

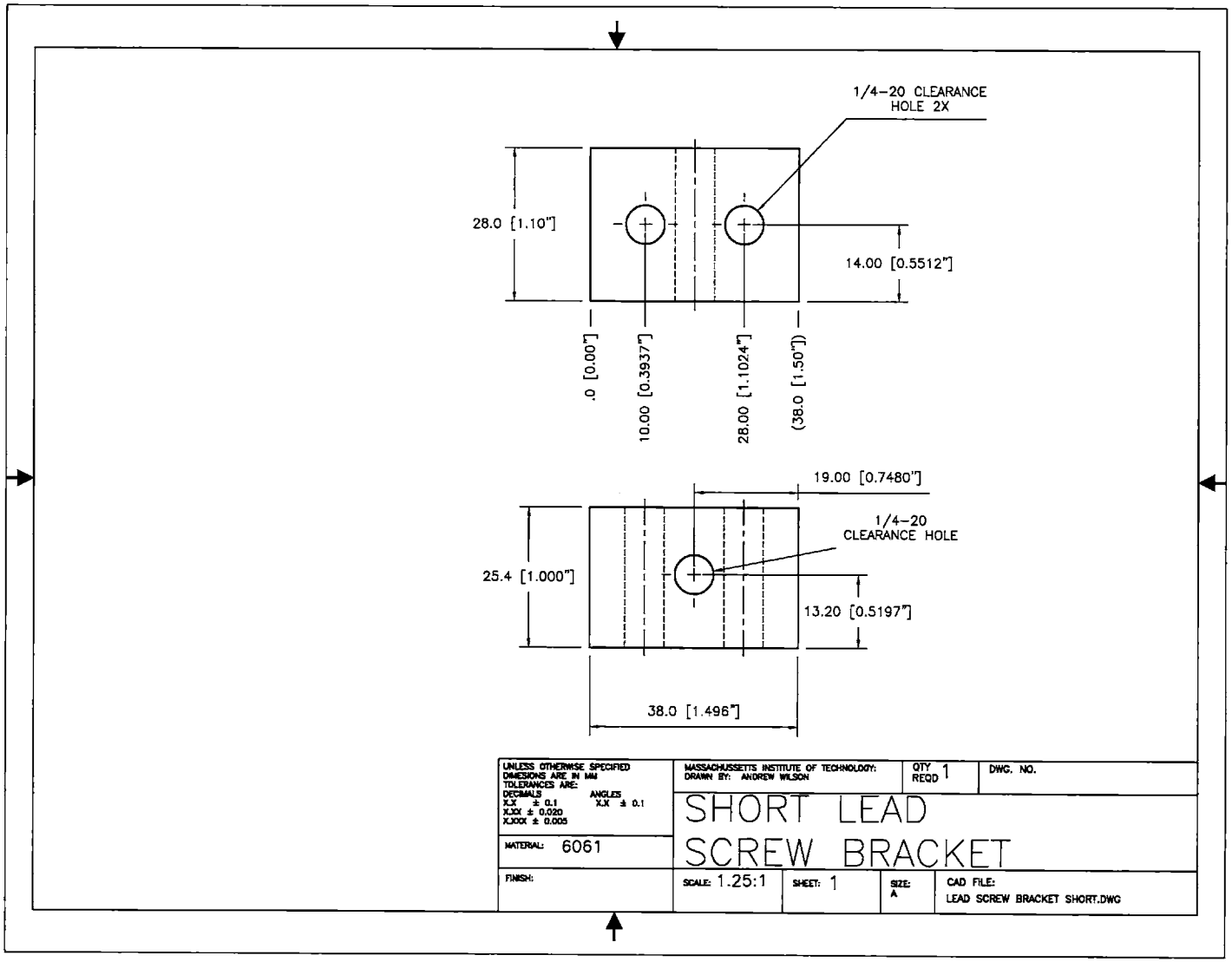
1/4–20 CLEARANCE
HOLE 2X
28.0 [1.10"]
14.00 [0.5512"]
.0 [0.00"]
10.00 [0.3937"]
28.00 [1.1024"]
(38.0 [1.50"])
19.00 [0.7480"]
1/4–20
CLEARANCE HOLE
25.4 [1.000"]
13.20 [0.5197"]
38.0 [1.496"]
UNLESS OTHERWISE SPECIFIED
DIMESIONS ARE IN MM
TOLERANCES ARE:
DECIMALS
X.X ± 0.1
X.XX ± 0.020
X.XXX ± 0.005
ANGLES
X.X ± 0.1
MASSACHUSSETTS INSTITUTE OF TECHNOLOGY:
DRAWN BY: ANDREW WILSON
QTY REQD 1
DWG. NO.
SHORT LEAD
SCREW BRACKET
MATERIAL: 6061
FINISH:
SCALE: 1.25:1
SHEET: 1
SIZE: A
CAD FILE:
LEAD SCREW BRACKET SHORT.DWG

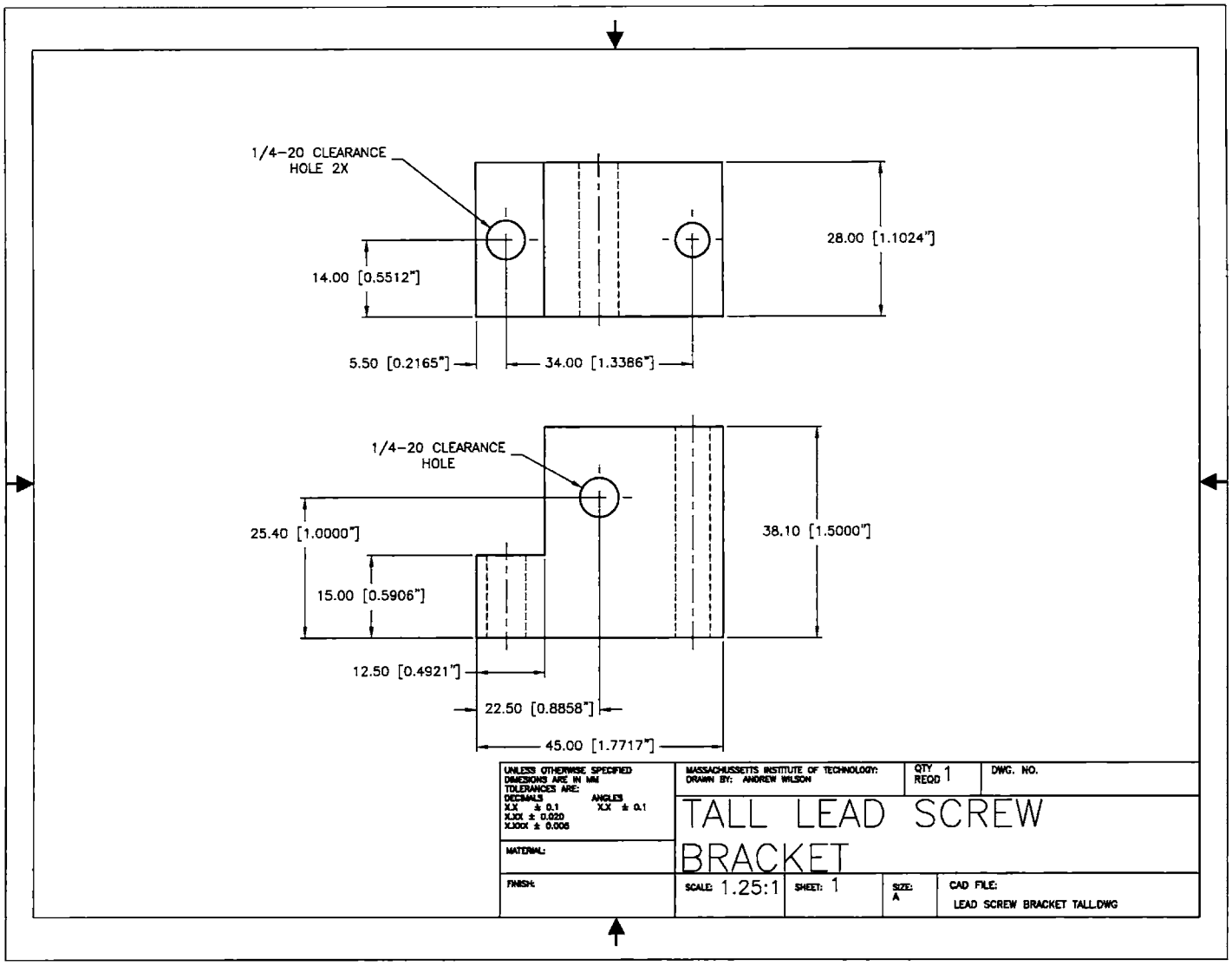
1/4-20 CLEARANCE HOLE 2X
28.00 [1.1024"]
14.00 [0.5512"]
5.50 [0.2165"]
34.00 [1.3386"]
1/4-20 CLEARANCE HOLE
38.10 [1.5000"]
25.40 [1.0000"]
15.00 [0.5906"]
12.50 [0.4921"]
22.50 [0.8858"]
45.00 [1.7717"]
UNLESS OTHERWISE SPECIFIED DIMENSIONS ARE IN MM
TOLERANCES ARE:
DECIMALS
X.X ± 0.1
X.XX ± 0.020
X.XXX ± 0.005
ANGLES
XX ± 0.1
MATERIAL:
FINISH:
MASSACHUSSETTS INSTITUTE OF TECHNOLOGY:
DRAWN BY: ANDREW WILSON
QTY REQD 1
DWG. NO.
TALL LEAD SCREW BRACKET
SCALE: 1.25:1
SHEET: 1
SIZE: A
CAD FILE:
LEAD SCREW BRACKET TALL.DWG

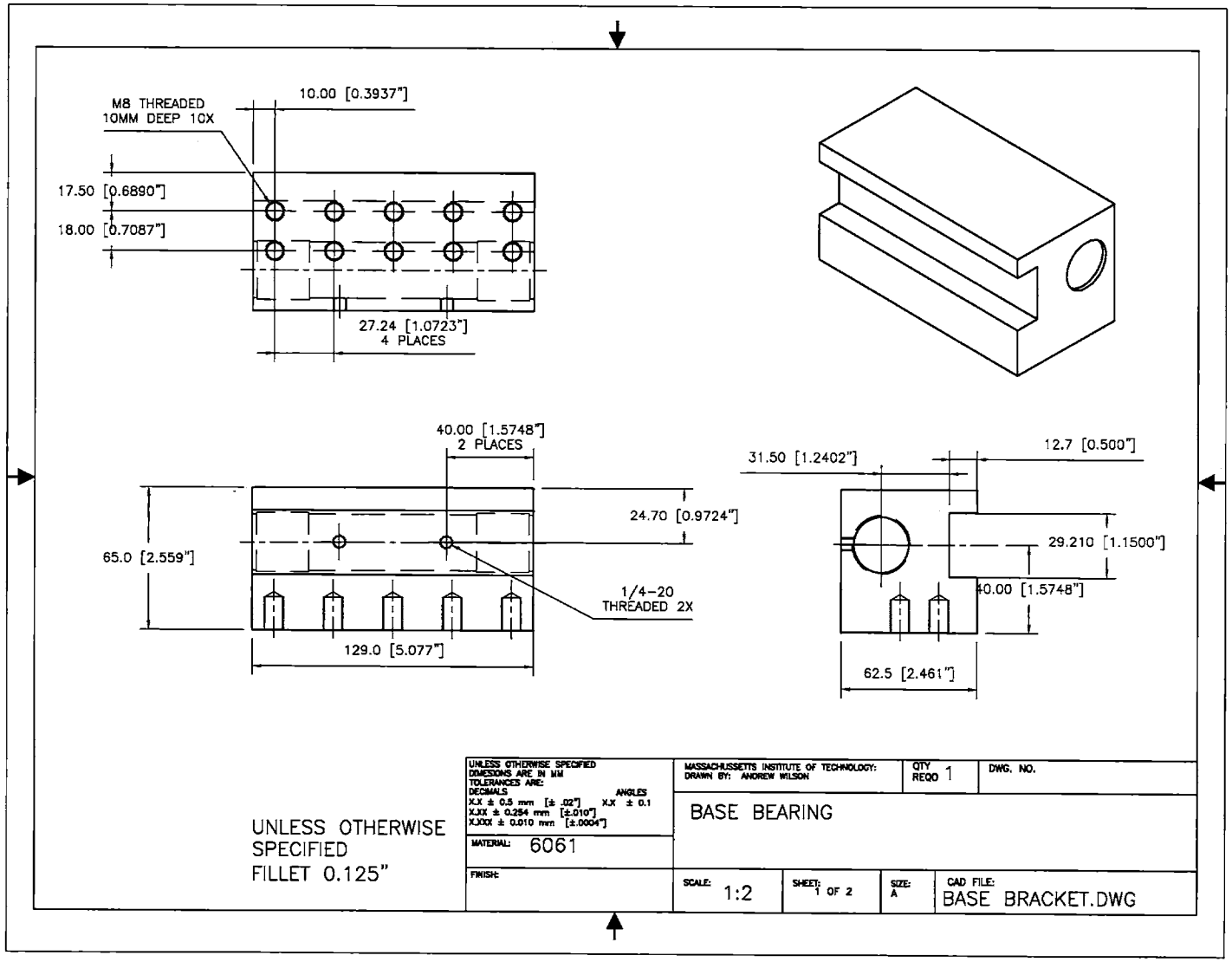
M8 THREADED
10MM DEEP 10X
10.00 [0.3937"]
17.50 [0.6890"]
18.00 [0.7087"]
27.24 [1.0723"]
4 PLACES
40.00 [1.5748"]
2 PLACES
65.0 [2.559"]
24.70 [0.9724"]
1/4-20
THREADED 2X
129.0 [5.077"]
31.50 [1.2402"]
12.7 [0.500"]
29.210 [1.1500"]
40.00 [1.5748"]
62.5 [2.461"]
UNLESS OTHERWISE
SPECIFIED
FILLET 0.125"
UNLESS OTHERWISE SPECIFIED
DIMESIONS ARE IN MM
TOLERANCES ARE:
DECIMALS ANGLES
X.X ± 0.5 mm [± .02"] X.X ± 0.1
X.XX ± 0.254 mm [±.010"]
X.XXX ± 0.010 mm [±.0004"]
MATERIAL: 6061
FINISH:
MASSACHUSSETTS INSTITUTE OF TECHNOLOGY:
DRAWN BY: ANDREW WILSON
QTY REQD 1
DWG. NO.
BASE BEARING
SCALE: 1:2
SHEET: 1 OF 2
SIZE: A
CAD FILE:
BASE BRACKET.DWG

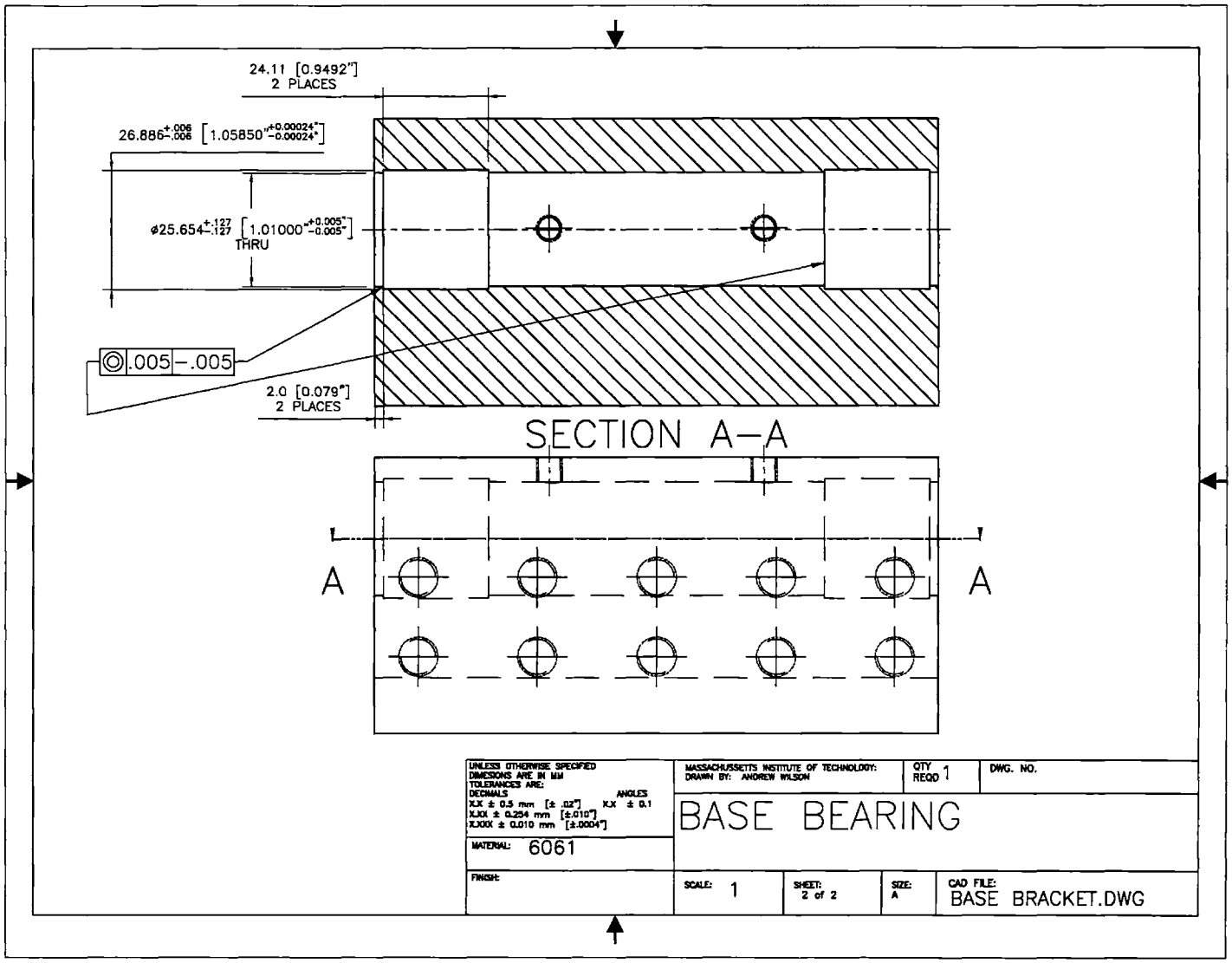
24.11 [0.9492"]
2 PLACES
26.886 +.006 -.006 [1.05850" +0.00024 -0.00024]
ø25.654 ±.127 [1.01000" +0.005 -0.005]
THRU
.005 -.005
2.0 [0.079"]
2 PLACES
SECTION A–A
A
A
UNLESS OTHERWISE SPECIFIED
DIMENSIONS ARE IN MM
TOLERANCES ARE:
DECIMALS ANGLES
X.X ± 0.5 mm [± .02"] X.X ± 0.1
X.XX ± 0.254 mm [±.010"]
X.XXX ± 0.010 mm [±.0004"]
MATERIAL: 6061
FINISH:
MASSACHUSSETTS INSTITUTE OF TECHNOLOGY:
DRAWN BY: ANDREW WILSON
QTY REQD 1
DWG. NO.
BASE BEARING
SCALE: 1
SHEET: 2 of 2
SIZE: A
CAD FILE: BASE BRACKET.DWG

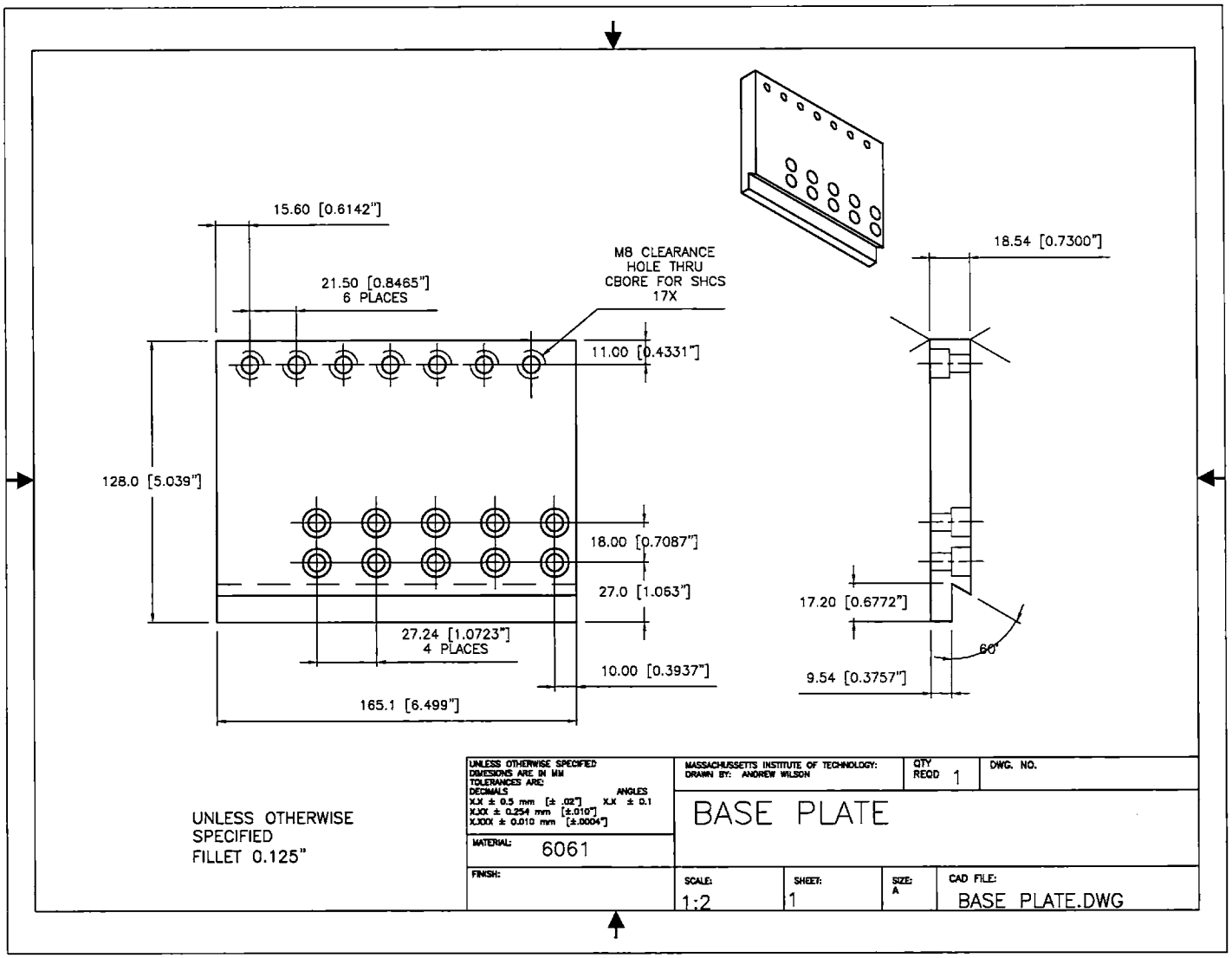
15.60 [0.6142"]
21.50 [0.8465"]
6 PLACES
M8 CLEARANCE
HOLE THRU
CBORE FOR SHCS
17X
11.00 [0.4331"]
128.0 [5.039"]
18.00 [0.7087"]
27.0 [1.063"]
27.24 [1.0723"]
4 PLACES
10.00 [0.3937"]
165.1 [6.499"]
18.54 [0.7300"]
17.20 [0.6772"]
60°
9.54 [0.3757"]
UNLESS OTHERWISE
SPECIFIED
FILLET 0.125"
UNLESS OTHERWISE SPECIFIED
DIMESIONS ARE IN MM
TOLERANCES ARE:
DECIMALS ANGLES
X.X ± 0.5 mm [± .02"] X.X ± 0.1
X.XX ± 0.254 mm [±.010"]
X.XXX ± 0.010 mm [±.0004"]
MATERIAL: 6061
FINISH:
MASSACHUSSETTS INSTITUTE OF TECHNOLOGY:
DRAWN BY: ANDREW WILSON
QTY REQD 1
DWG. NO.
BASE PLATE
SCALE: 1:2
SHEET: 1
SIZE: A
CAD FILE: BASE PLATE.DWG

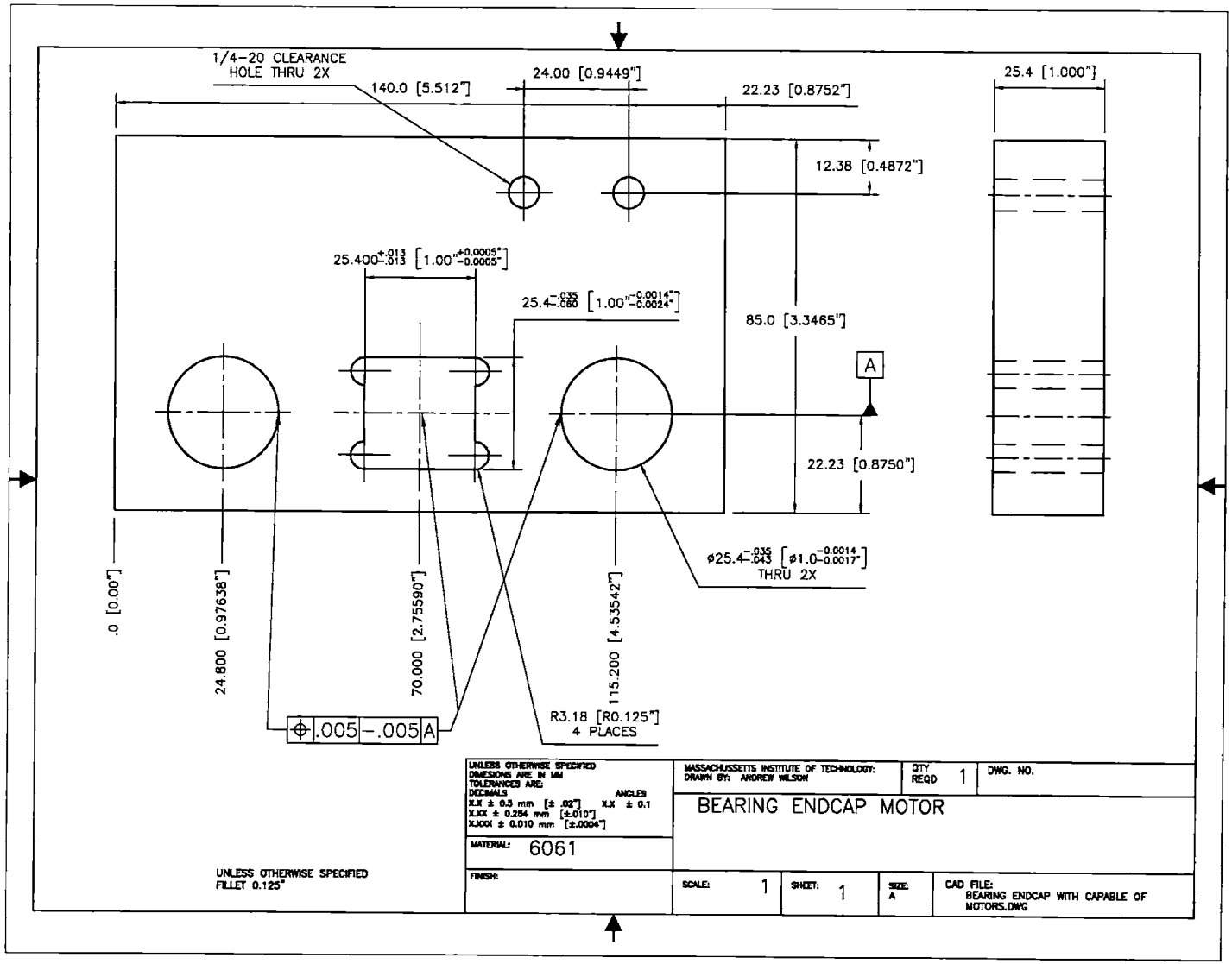
1/4-20 CLEARANCE
HOLE THRU 2X
140.0 [5.512"]
24.00 [0.9449"]
22.23 [0.8752"]
25.4 [1.000"]
12.38 [0.4872"]
25.400 +.013 -.013 [1.00" +0.0005" -0.0005"]
25.4 -.035 -.060 [1.00" -0.0014" -0.0024"]
85.0 [3.3465"]
A
22.23 [0.8750"]
ø25.4 -.035 -.043 [ø1.0 -0.0014 -0.0017"]
THRU 2X
.0 [0.00"]
24.800 [0.97638"]
70.000 [2.75590"]
115.200 [4.53542"]
.005 -.005 A
R3.18 [R0.125"]
4 PLACES
UNLESS OTHERWISE SPECIFIED
FILLET 0.125"
UNLESS OTHERWISE SPECIFIED
DIMESIONS ARE IN MM
TOLERANCES ARE:
DECIMALS ANGLES
X.X ± 0.5 mm [± .02"] X.X ± 0.1
X.XX ± 0.254 mm [±.010"]
X.XXX ± 0.010 mm [±.0004"]
MATERIAL: 6061
FINISH:
MASSACHUSSETTS INSTITUTE OF TECHNOLOGY:
DRAWN BY: ANDREW WILSON
QTY REQD 1
DWG. NO.
BEARING ENDCAP MOTOR
SCALE: 1
SHEET: 1
SIZE: A
CAD FILE:
BEARING ENDCAP WITH CAPABLE OF MOTORS.DWG

Appendix B

Prototype 2 Drawings

Part List:

1. Base Plate
2. Inboard-Outboard
3. Slider
4. Slider Plate
5. Left Cutter
6. Right Cutter
7. Bearing Endcap
8. Nut Bracket
9. Linear Bearing
10. Stiffener 1
11. Stiffener 2
12. 2 Lead Screws
13. 1" Wide .015" Thick Black MDS-Filled Nylon 6/6 Strip: McMaster Carr part number 8751K12: Qty 1

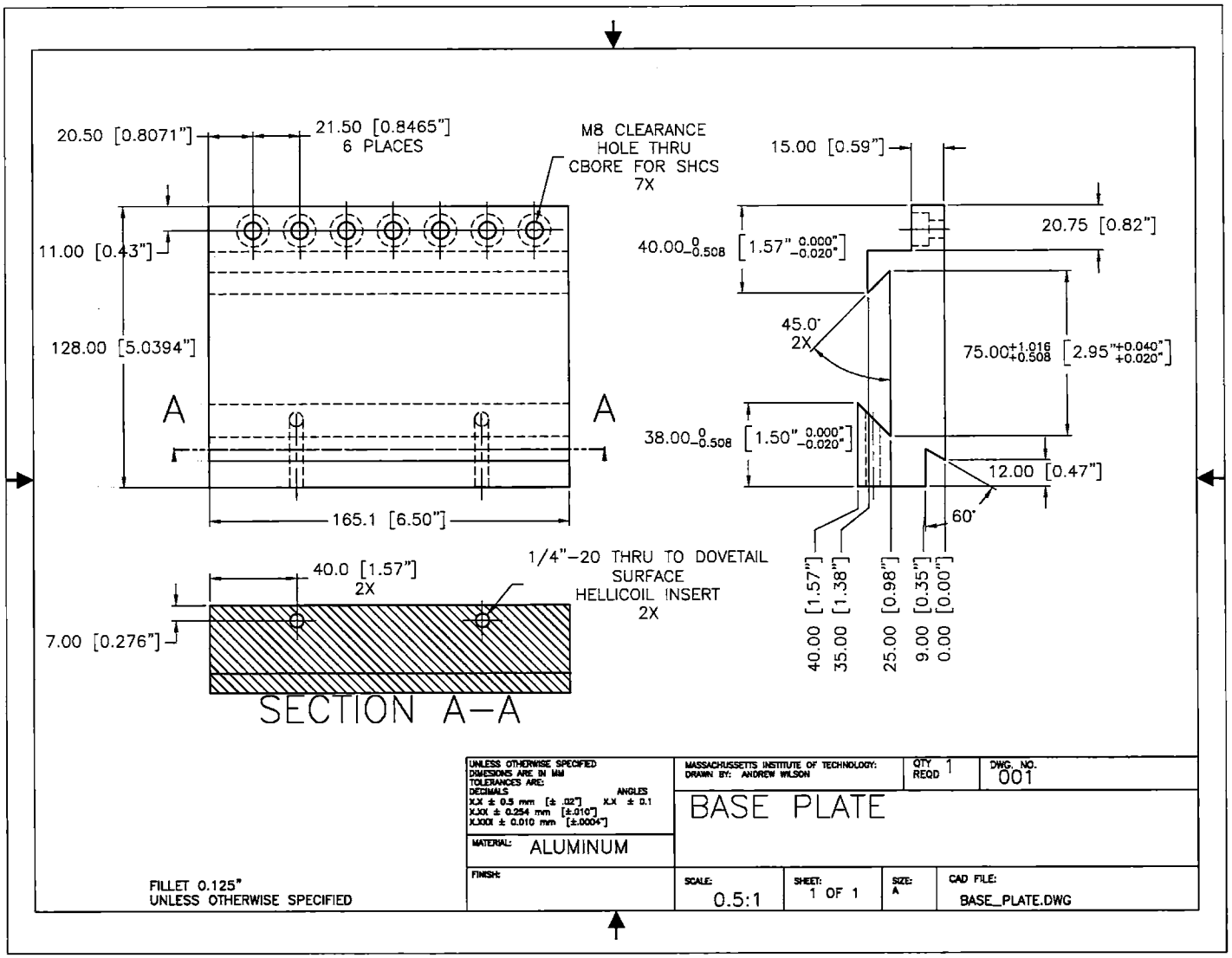
20.50 [0.8071"]
21.50 [0.8465"]
6 PLACES
M8 CLEARANCE
HOLE THRU
CBORE FOR SHCS
7X
11.00 [0.43"]
128.00 [5.0394"]
A
A
165.1 [6.50"]
15.00 [0.59"]
20.75 [0.82"]
40.00 0 -0.508 [1.57" 0.000" -0.020"]
45.0°
2X
75.00 +1.016 +0.508 [2.95" +0.040" +0.020"]
38.00 0 -0.508 [1.50" 0.000" -0.020"]
12.00 [0.47"]
60°
40.00 [1.57"]
35.00 [1.38"]
25.00 [0.98"]
9.00 [0.35"]
0.00 [0.00"]
40.0 [1.57"]
2X
1/4"-20 THRU TO DOVETAIL
SURFACE
HELLICOIL INSERT
2X
7.00 [0.276"]
SECTION A-A
FILLET 0.125"
UNLESS OTHERWISE SPECIFIED
UNLESS OTHERWISE SPECIFIED
DIMESIONS ARE IN MM
TOLERANCES ARE:
DECIMALS
ANGLES
X.X ± 0.5 mm [± .02"]
X.X ± 0.1
X.XX ± 0.254 mm [±.010"]
X.XXX ± 0.010 mm [±.0004"]
MATERIAL: ALUMINUM
FINISH:
MASSACHUSSETTS INSTITUTE OF TECHNOLOGY:
DRAWN BY: ANDREW WILSON
QTY. REQD 1
DWG. NO. 001
BASE PLATE
SCALE: 0.5:1
SHEET: 1 OF 1
SIZE: A
CAD FILE: BASE_PLATE.DWG

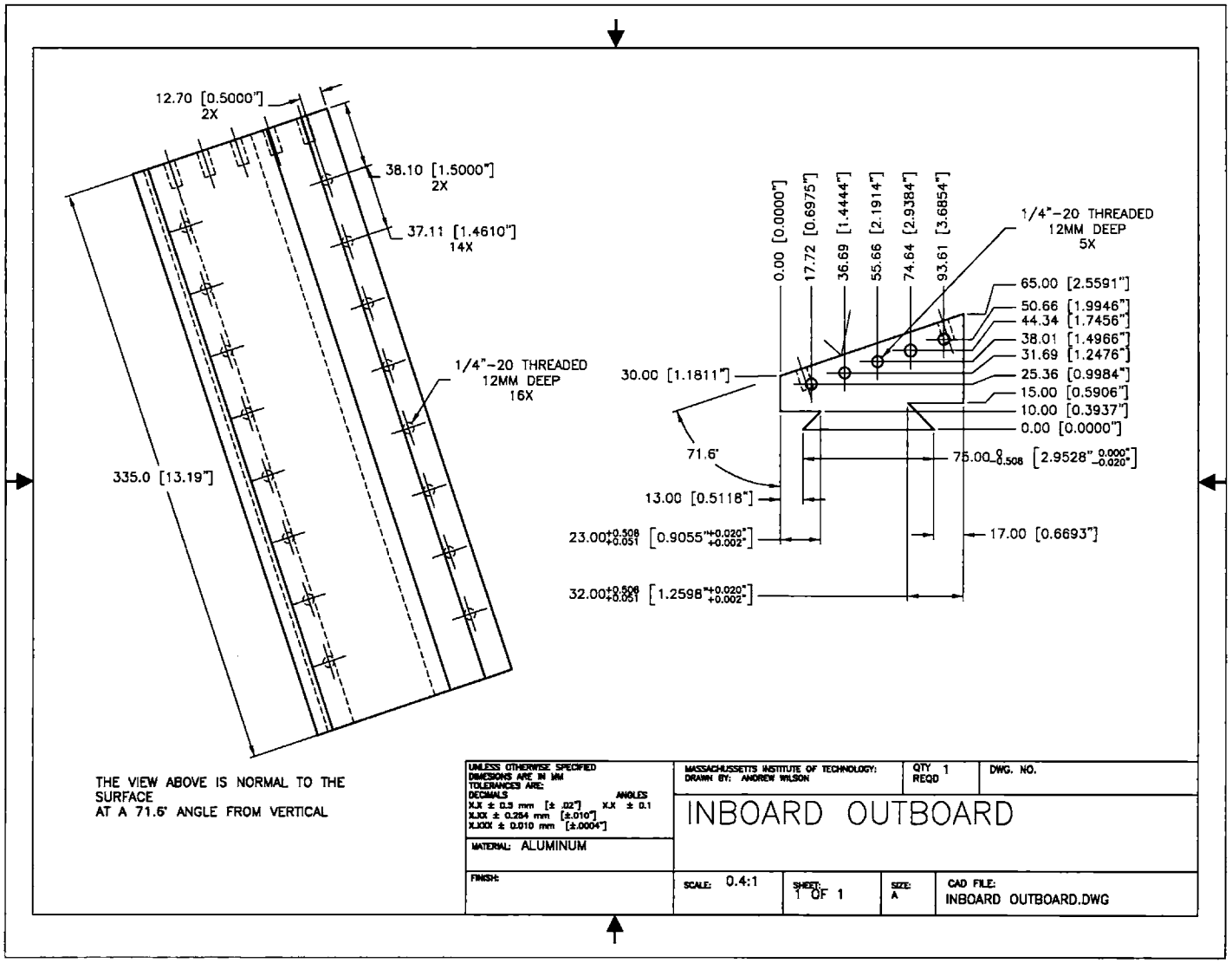
12.70 [0.5000"]
2X
38.10 [1.5000"]
2X
37.11 [1.4610"]
14X
1/4"-20 THREADED
12MM DEEP
16X
335.0 [13.19"]
THE VIEW ABOVE IS NORMAL TO THE SURFACE
AT A 71.5° ANGLE FROM VERTICAL
0.00 [0.0000"]
17.72 [0.6975"]
36.69 [1.4444"]
55.66 [2.1914"]
74.64 [2.9384"]
93.61 [3.6854"]
1/4"-20 THREADED
12MM DEEP
5X
65.00 [2.5591"]
50.66 [1.9946"]
44.34 [1.7456"]
38.01 [1.4966"]
31.69 [1.2476"]
25.36 [0.9984"]
15.00 [0.5906"]
10.00 [0.3937"]
0.00 [0.0000"]
30.00 [1.1811"]
71.6°
75.00 [2.9528"]
13.00 [0.5118"]
23.00 [0.9055"]
17.00 [0.6693"]
32.00 [1.2598"]
UNLESS OTHERWISE SPECIFIED
DIMENSIONS ARE IN MM
TOLERANCES ARE:
DECIMALS
X.X ± 0.3 mm [± .02"]
X.XX ± 0.254 mm [±.010"]
X.XXX ± 0.010 mm [±.0004"]
ANGLES
X.X ± 0.1
MASSACHUSSETTS INSTITUTE OF TECHNOLOGY:
DRAWN BY: ANDREW WILSON
QTY REQD 1
DWG. NO.
INBOARD OUTBOARD
MATERIAL: ALUMINUM
FINISH:
SCALE: 0.4:1
SHEET: 1 OF 1
SIZE: A
CAD FILE:
INBOARD OUTBOARD.DWG

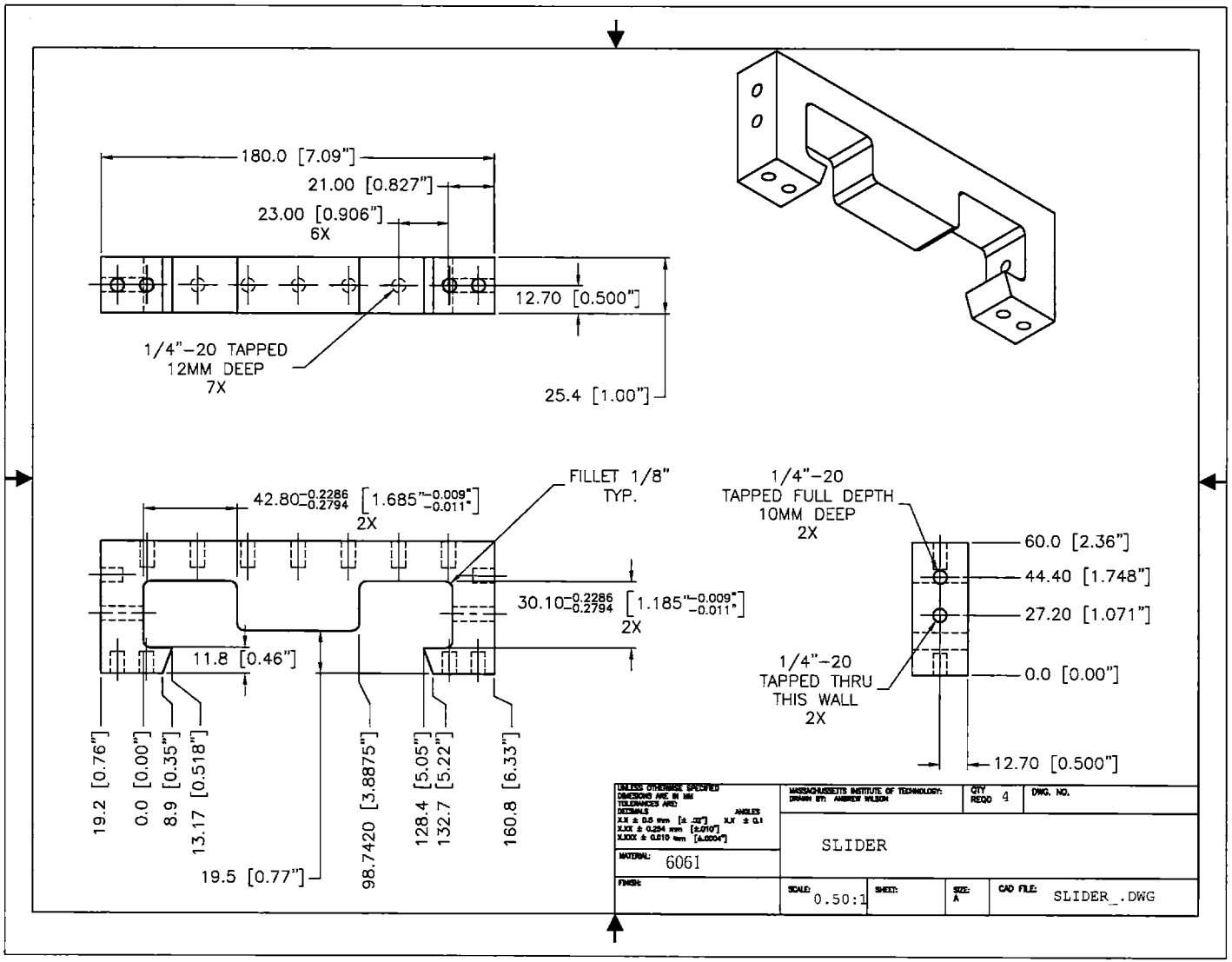
180.0 [7.09"]
21.00 [0.827"]
23.00 [0.906"]
6X
12.70 [0.500"]
1/4"-20 TAPPED
12MM DEEP
7X
25.4 [1.00"]
42.80 -0.2286 -0.2794 [1.685" -0.009" -0.011"]
2X
FILLET 1/8"
TYP.
30.10 -0.2286 -0.2794 [1.185" -0.009" -0.011"]
2X
11.8 [0.46"]
19.2 [0.76"]
0.0 [0.00"]
8.9 [0.35"]
13.17 [0.518"]
19.5 [0.77"]
98.7420 [3.8875"]
128.4 [5.05"]
132.7 [5.22"]
160.8 [6.33"]
1/4"-20
TAPPED FULL DEPTH
10MM DEEP
2X
60.0 [2.36"]
44.40 [1.748"]
27.20 [1.071"]
0.0 [0.00"]
1/4"-20
TAPPED THRU
THIS WALL
2X
12.70 [0.500"]
UNLESS OTHERWISE SPECIFIED
DIMENSIONS ARE IN MM
TOLERANCES ARE:
DECIMALS
ANGLES
X.X ± 0.5 mm [± .02"]
X.XX ± 0.254 mm [±.010"]
X.XXX ± 0.010 mm [±.0004"]
X.X ± 0.1
MATERIAL: 6061
FINISH:
MASSACHUSETTS INSTITUTE OF TECHNOLOGY:
DRAWN BY: ANDREW WILSON
QTY REQD 4
DWG. NO.
SLIDER
SCALE: 0.50:1
SHEET:
SIZE: A
CAD FILE: SLIDER_.DWG

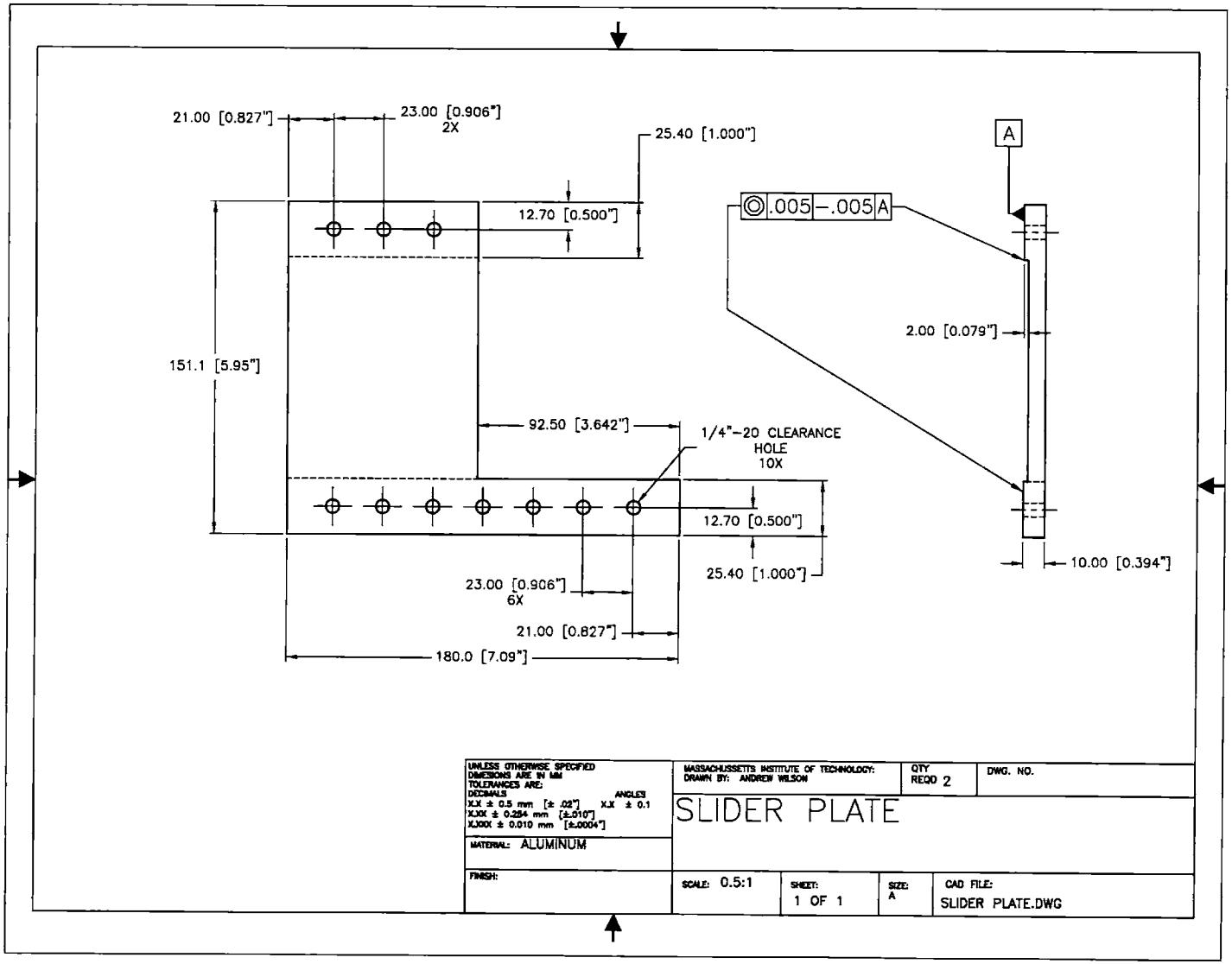
21.00 [0.827"]
23.00 [0.906"]
2X
25.40 [1.000"]
12.70 [0.500"]
151.1 [5.95"]
92.50 [3.642"]
1/4"-20 CLEARANCE
HOLE
10X
12.70 [0.500"]
25.40 [1.000"]
23.00 [0.906"]
6X
21.00 [0.827"]
180.0 [7.09"]
A
.005 -.005 A
2.00 [0.079"]
10.00 [0.394"]
UNLESS OTHERWISE SPECIFIED
DIMENSIONS ARE IN MM
TOLERANCES ARE:
DECIMALS
ANGLES
X.X ± 0.5 mm [± .02"]
X.X ± 0.1
X.XX ± 0.254 mm [±.010"]
X.XXX ± 0.010 mm [±.0004"]
MATERIAL: ALUMINUM
FINISH:
MASSACHUSSETTS INSTITUTE OF TECHNOLOGY:
DRAWN BY: ANDREW WILSON
QTY
REQD 2
DWG. NO.
SLIDER PLATE
SCALE: 0.5:1
SHEET:
1 OF 1
SIZE:
A
CAD FILE:
SLIDER PLATE.DWG

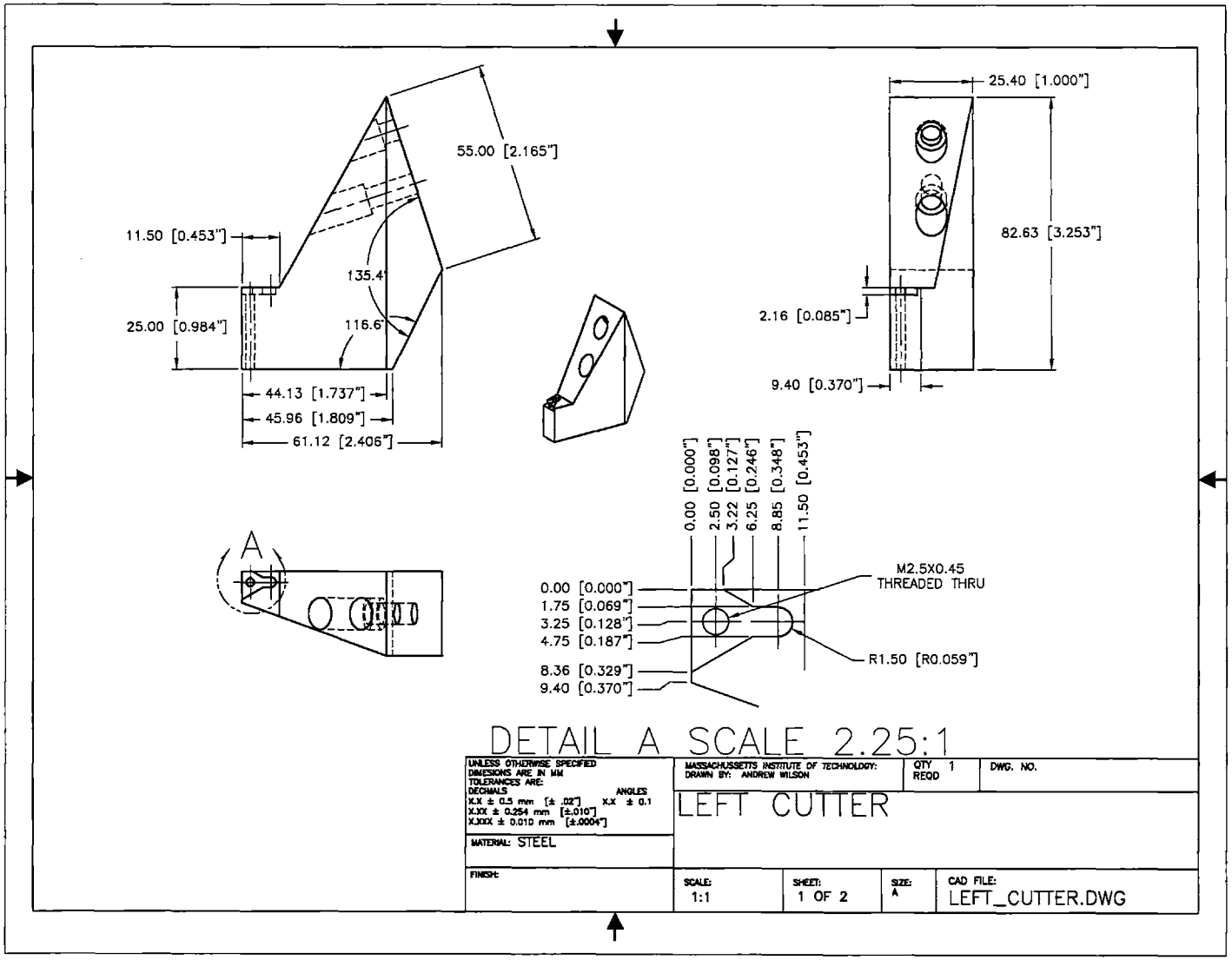
55.00 [2.165"]
11.50 [0.453"]
135.4°
25.00 [0.984"]
116.6°
44.13 [1.737"]
45.96 [1.809"]
61.12 [2.406"]
25.40 [1.000"]
82.63 [3.253"]
2.16 [0.085"]
9.40 [0.370"]
0.00 [0.000"]
2.50 [0.098"]
3.22 [0.127"]
6.25 [0.246"]
8.85 [0.348"]
11.50 [0.453"]
M2.5X0.45
THREADED THRU
0.00 [0.000"]
1.75 [0.069"]
3.25 [0.128"]
4.75 [0.187"]
8.36 [0.329"]
9.40 [0.370"]
R1.50 [R0.059"]
A
DETAIL A SCALE 2.25:1
UNLESS OTHERWISE SPECIFIED
DIMESIONS ARE IN MM
TOLERANCES ARE:
DECIMALS
ANGLES
X.X ± 0.5 mm [± .02"]
X.XX ± 0.254 mm [±.010"]
X.XXX ± 0.010 mm [±.0004"]
X.X ± 0.1
MATERIAL: STEEL
FINISH:
MASSACHUSSETTS INSTITUTE OF TECHNOLOGY:
DRAWN BY: ANDREW WILSON
QTY REQD 1
DWG. NO.
LEFT CUTTER
SCALE: 1:1
SHEET: 1 OF 2
SIZE: A
CAD FILE: LEFT_CUTTER.DWG

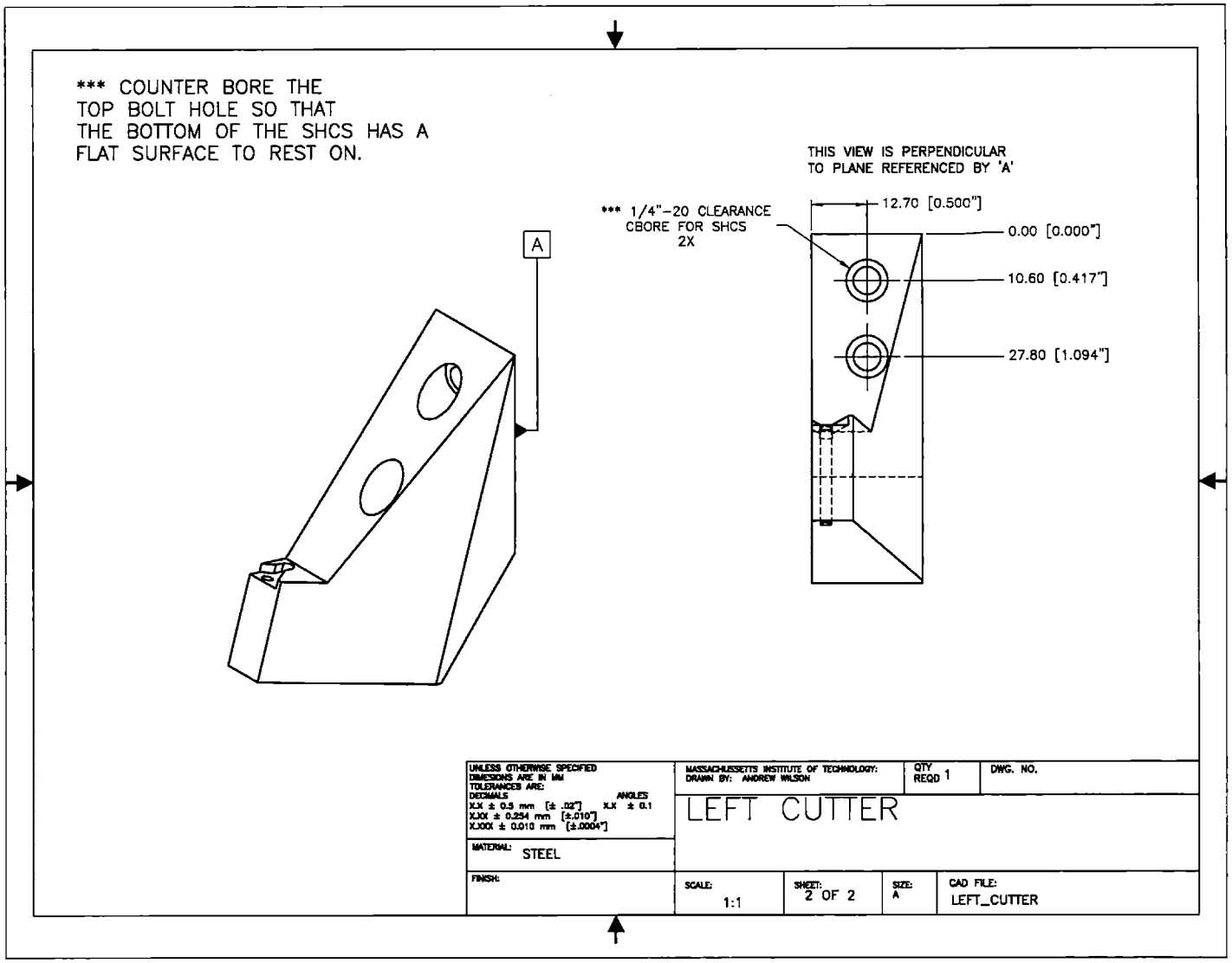
*** COUNTER BORE THE
TOP BOLT HOLE SO THAT
THE BOTTOM OF THE SHCS HAS A
FLAT SURFACE TO REST ON.
THIS VIEW IS PERPENDICULAR
TO PLANE REFERENCED BY 'A'
*** 1/4"-20 CLEARANCE
CBORE FOR SHCS
2X
A
12.70 [0.500"]
0.00 [0.000"]
10.60 [0.417"]
27.80 [1.094"]
UNLESS OTHERWISE SPECIFIED
DIMESIONS ARE IN MM
TOLERANCES ARE:
DECIMALS ANGLES
X.X ± 0.5 mm [± .02"] X.X ± 0.1
X.XX ± 0.254 mm [±.010"]
X.XXX ± 0.010 mm [±.0004"]
MATERIAL: STEEL
FINISH:
MASSACHUSSETTS INSTITUTE OF TECHNOLOGY:
DRAWN BY: ANDREW WILSON
QTY REQD 1
DWG. NO.
LEFT CUTTER
SCALE: 1:1
SHEET: 2 OF 2
SIZE: A
CAD FILE: LEFT_CUTTER

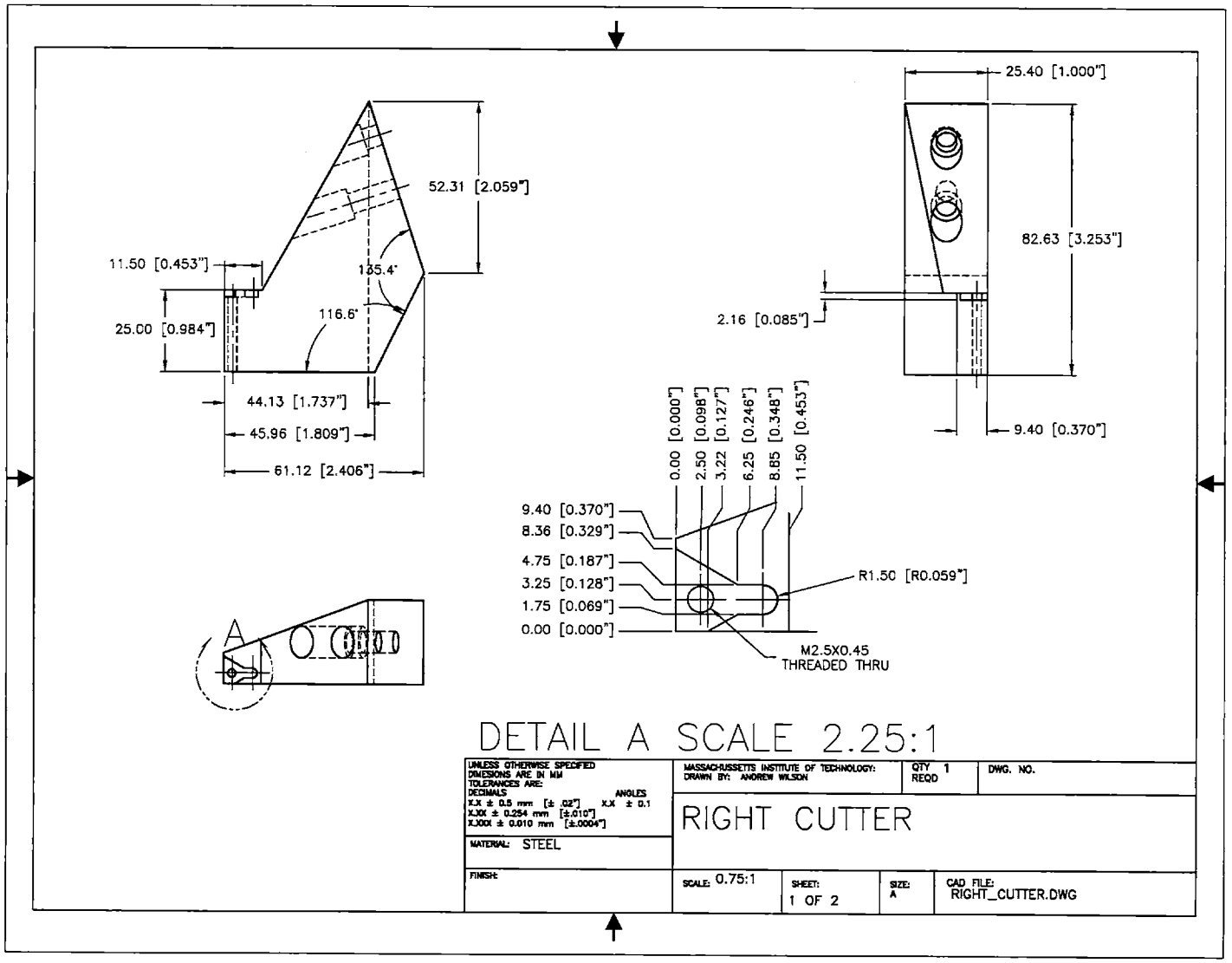
25.40 [1.000"]
52.31 [2.059"]
82.63 [3.253"]
11.50 [0.453"]
135.4°
116.6°
25.00 [0.984"]
2.16 [0.085"]
44.13 [1.737"]
45.96 [1.809"]
61.12 [2.406"]
9.40 [0.370"]
0.00 [0.000"]
2.50 [0.098"]
3.22 [0.127"]
6.25 [0.246"]
8.85 [0.348"]
11.50 [0.453"]
9.40 [0.370"]
8.36 [0.329"]
4.75 [0.187"]
3.25 [0.128"]
1.75 [0.069"]
0.00 [0.000"]
R1.50 [R0.059"]
M2.5X0.45
THREADED THRU
A
DETAIL A SCALE 2.25:1
UNLESS OTHERWISE SPECIFIED
DIMESIONS ARE IN MM
TOLERANCES ARE:
DECIMALS ANGLES
X.X ± 0.5 mm [± .02"] X.X ± 0.1
X.XX ± 0.254 mm [±.010"]
X.XXX ± 0.010 mm [±.0004"]
MATERIAL: STEEL
FINISH:
MASSACHUSSETTS INSTITUTE OF TECHNOLOGY:
DRAWN BY: ANDREW WILSON
QTY 1
REQD
DWG. NO.
RIGHT CUTTER
SCALE: 0.75:1
SHEET: 1 OF 2
SIZE: A
CAD FILE: RIGHT_CUTTER.DWG

*** COUNTER BORE
TOP HOLE SO THAT
SHCS BOTTOM HAS FLAT SURFACE
TO MOUNT ON.

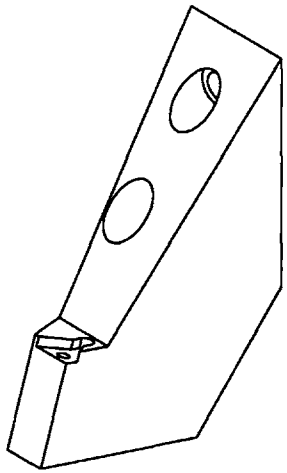

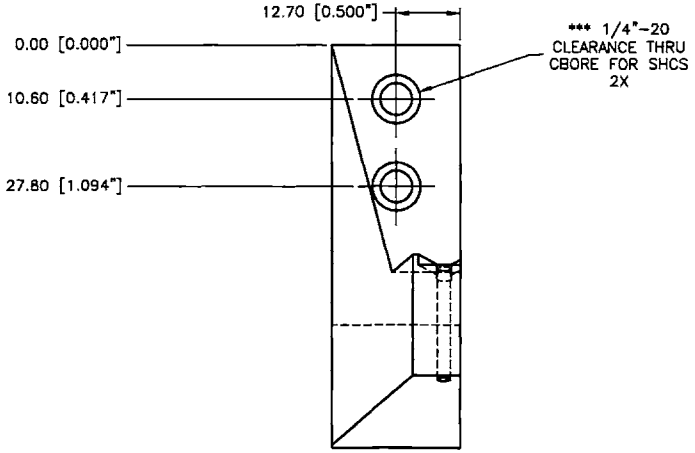

UNLESS OTHERWISE SPECIFIED DIMENSIONS ARE IN MM TOLERANCES ARE: DECIMALS ANGLES X.X ± 0.5 mm [± .02"] X.X ± 0.1 X.XX ± 0.254 mm [±.010"] X.XXX ± 0.010 mm [±.0004"]	MASSACHUSSETTS INSTITUTE OF TECHNOLOGY: DRAWN BY: ANDREW WILSON	QTY 1 REQD	DWG. NO.
	RIGHT CUTTER		
MATERIAL: STEEL			
FINISH:	SCALE: 1:1	SHEET: 2 OF 2	SIZE: A
			CAD FILE: RIGHT_CUTTER.DWG

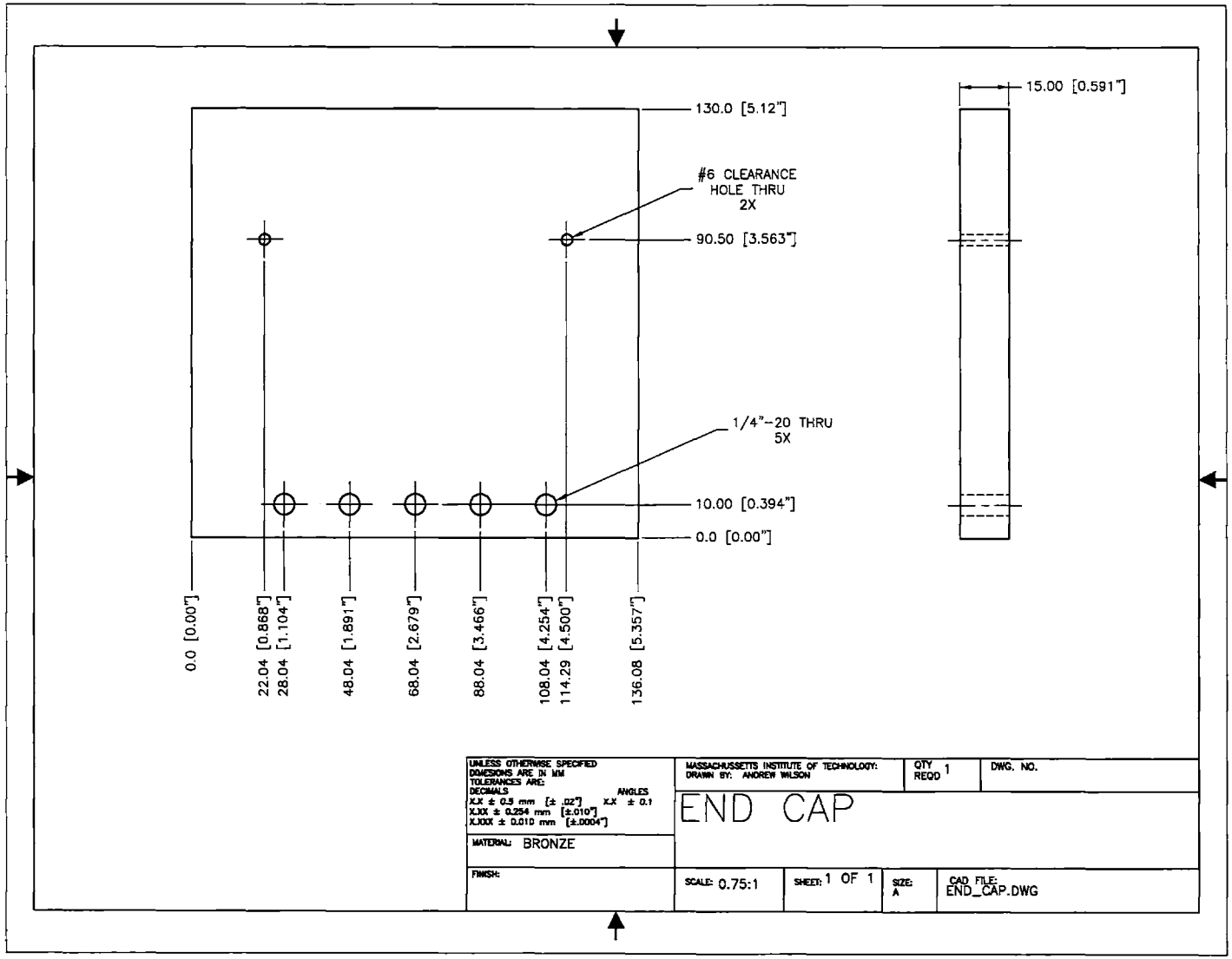
130.0 [5.12"]
#6 CLEARANCE HOLE THRU 2X
90.50 [3.563"]
1/4"-20 THRU 5X
10.00 [0.394"]
0.0 [0.00"]
15.00 [0.591"]
0.0 [0.00"]
22.04 [0.868"]
28.04 [1.104"]
48.04 [1.891"]
68.04 [2.679"]
88.04 [3.466"]
108.04 [4.254"]
114.29 [4.500"]
136.08 [5.357"]
UNLESS OTHERWISE SPECIFIED DIMENSIONS ARE IN MM
TOLERANCES ARE:
DECIMALS
ANGLES
X.X ± 0.5 mm [± .02"]
X.XX ± 0.254 mm [±.010"]
X.XXX ± 0.010 mm [±.0004"]
X.X ± 0.1
MATERIAL: BRONZE
FINISH:
MASSACHUSSETTS INSTITUTE OF TECHNOLOGY:
DRAWN BY: ANDREW WILSON
QTY REQD 1
DWG. NO.
END CAP
SCALE: 0.75:1
SHEET: 1 OF 1
SIZE: A
CAD FILE: END_CAP.DWG

0.0 [0.00"]
18.0 [0.71"]
22.75 [0.896"]
31.00 [1.220"]
39.25 [1.545"]
44.00 [1.732"]
62.0 [2.44"]
24.0 [0.94"]
19.76 [0.778"]
15.00 [0.591"]
10.0 [0.39"]
5.48 [0.216"]
0.0 [0.00"]
ø13.46 +0.5 0 [0.530" +0.020" 0.000"]
#6 THREADED FULL LENGTH 3X
7.50 [0.295"]
15.00 [0.591"]
1/4"-20 CLEARANCE THRU 2X
0.00 [0.000"]
8.00 [0.315"]
54.00 [2.126"]
UNLESS OTHERWISE SPECIFIED
DIMENSIONS ARE IN MM
TOLERANCES ARE:
DECIMALS ANGLES
X.X ± 0.5 mm [± .02"] X.X ± 0.1
X.XX ± 0.254 mm [±.010"]
X.XXX ± 0.010 mm [±.0004"]
MATERIAL: ALUMINUM
FINISH:
MASSACHUSSETTS INSTITUTE OF TECHNOLOGY:
DRAWN BY: ANDREW WILSON
QTY REQD 2
DWG. NO.
NUT BRACKET
SCALE: 1.5:1
SHEET: 1 OF 1
SIZE: A
CAD FILE: NUT_BRACKET.DWG

37.13 [1.4618"]
38.10 [1.5000"]
12.70 [0.5000"]
1/4-20
THRU BX
CBORE FOR SHCS
25.40±0.025 [1.00"+0.001 -0.001"]
38.10±0.025 [1.50"+0.001 -0.001"]
0.00 [0.0000"]
37.13 [1.4618"]
74.24 [2.9228"]
111.35 [4.3839"]
148.46 [5.8449"]
185.57 [7.3059"]
222.68 [8.7669"]
259.79 [10.2280"]
296.90 [11.6890"]
335.00 [13.1890"]
UNLESS OTHERWISE SPECIFIED
DIMENSIONS ARE IN MM
TOLERANCES ARE:
DECIMALS ANGLES
X.X ± 0.5 mm [± .02"] X.X ± 0.1
X.XX ± 0.254 mm [±.010"]
X.XXX ± 0.010 mm [±.0004"]
MATERIAL:
FINISH:
MASSACHUSSETTS INSTITUTE OF TECHNOLOGY:
DRAWN BY: ANDREW WILSON
QTY REQD 2
DWG. NO.
LINEAR BEARING
MCMASTER CARR PART # 9517K281
SCALE: 0.50:1
SHEET:
SIZE: A
CAD FILE: LINEAR_BEARING.DWG

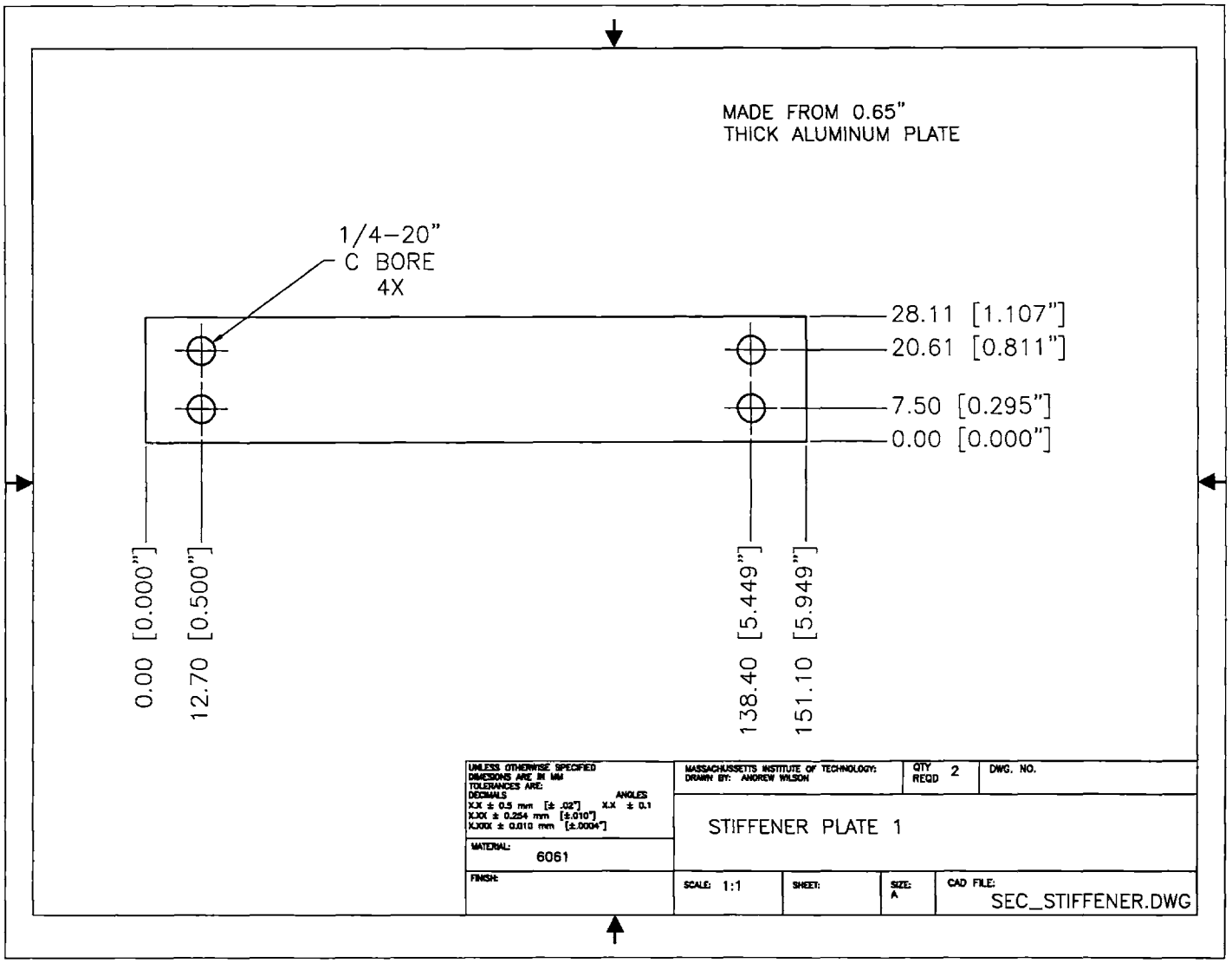
MADE FROM 0.65"
THICK ALUMINUM PLATE
1/4-20"
C BORE
4X
28.11 [1.107"]
20.61 [0.811"]
7.50 [0.295"]
0.00 [0.000"]
0.00 [0.000"]
12.70 [0.500"]
138.40 [5.449"]
151.10 [5.949"]
UNLESS OTHERWISE SPECIFIED
DIMENSIONS ARE IN MM
TOLERANCES ARE:
DECIMALS ANGLES
X.X ± 0.5 mm [± .02"] X.X ± 0.1
X.XX ± 0.254 mm [±.010"]
X.XXX ± 0.013 mm [±.0004"]
MASSACHUSSETTS INSTITUTE OF TECHNOLOGY:
DRAWN BY: ANDREW WILSON
QTY REQD 2
DWG. NO.
STIFFENER PLATE 1
MATERIAL: 6061
FINISH:
SCALE: 1:1
SHEET:
SIZE: A
CAD FILE: SEC_STIFFENER.DWG

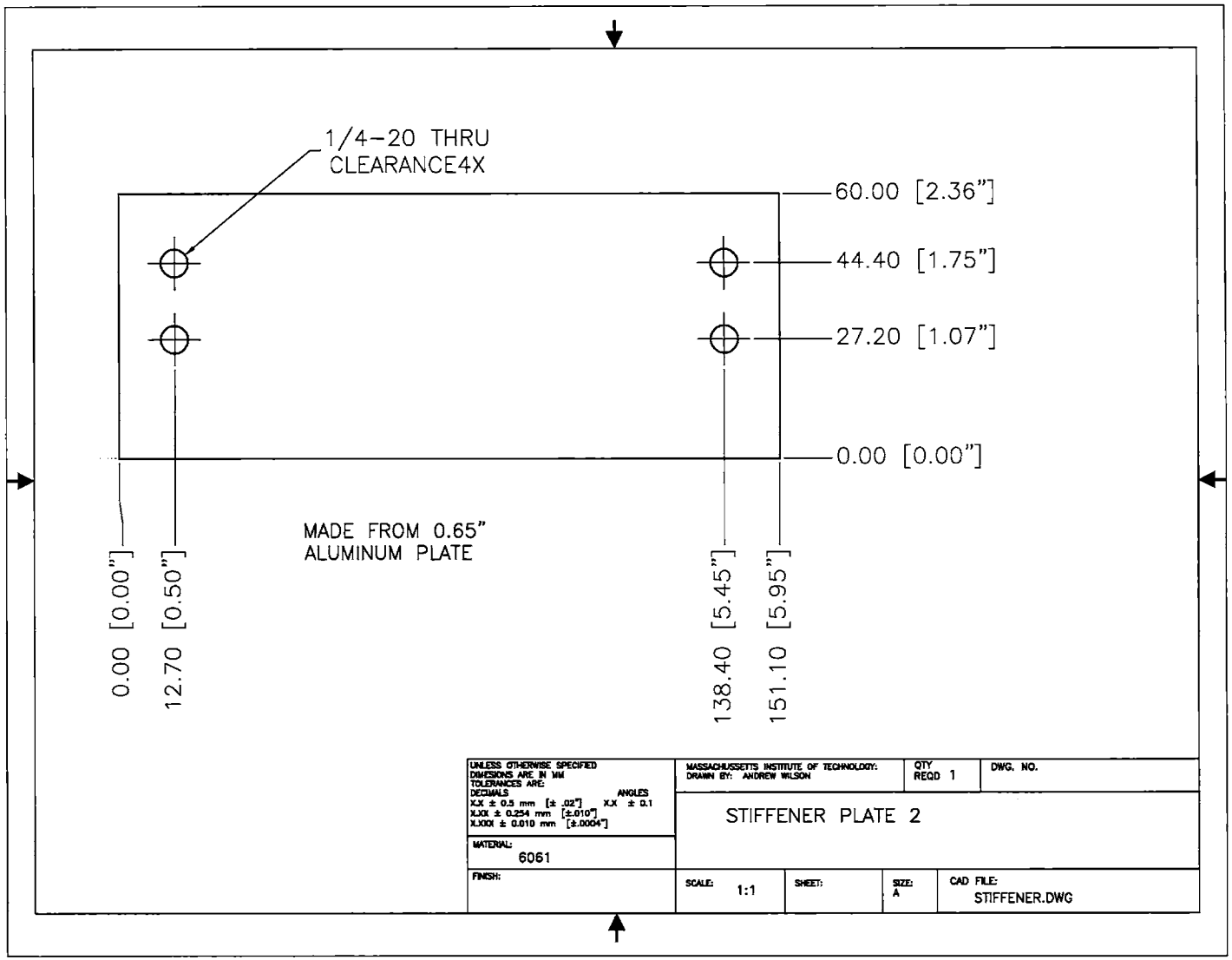
1/4-20 THRU
CLEARANCE4X
60.00 [2.36"]
44.40 [1.75"]
27.20 [1.07"]
0.00 [0.00"]
MADE FROM 0.65"
ALUMINUM PLATE
0.00 [0.00"]
12.70 [0.50"]
138.40 [5.45"]
151.10 [5.95"]
UNLESS OTHERWISE SPECIFIED
DIMESIONS ARE IN MM
TOLERANCES ARE:
DECIMALS
X.X ± 0.5 mm [± .02"]
X.XX ± 0.254 mm [±.010"]
X.XXX ± 0.010 mm [±.0004"]
ANGLES
X.X ± 0.1
MASSACHUSSETTS INSTITUTE OF TECHNOLOGY:
DRAWN BY: ANDREW WILSON
QTY
REQD 1
DWG. NO.
STIFFENER PLATE 2
MATERIAL:
6061
FINISH:
SCALE: 1:1
SHEET:
SIZE:
A
CAD FILE:
STIFFENER.DWG

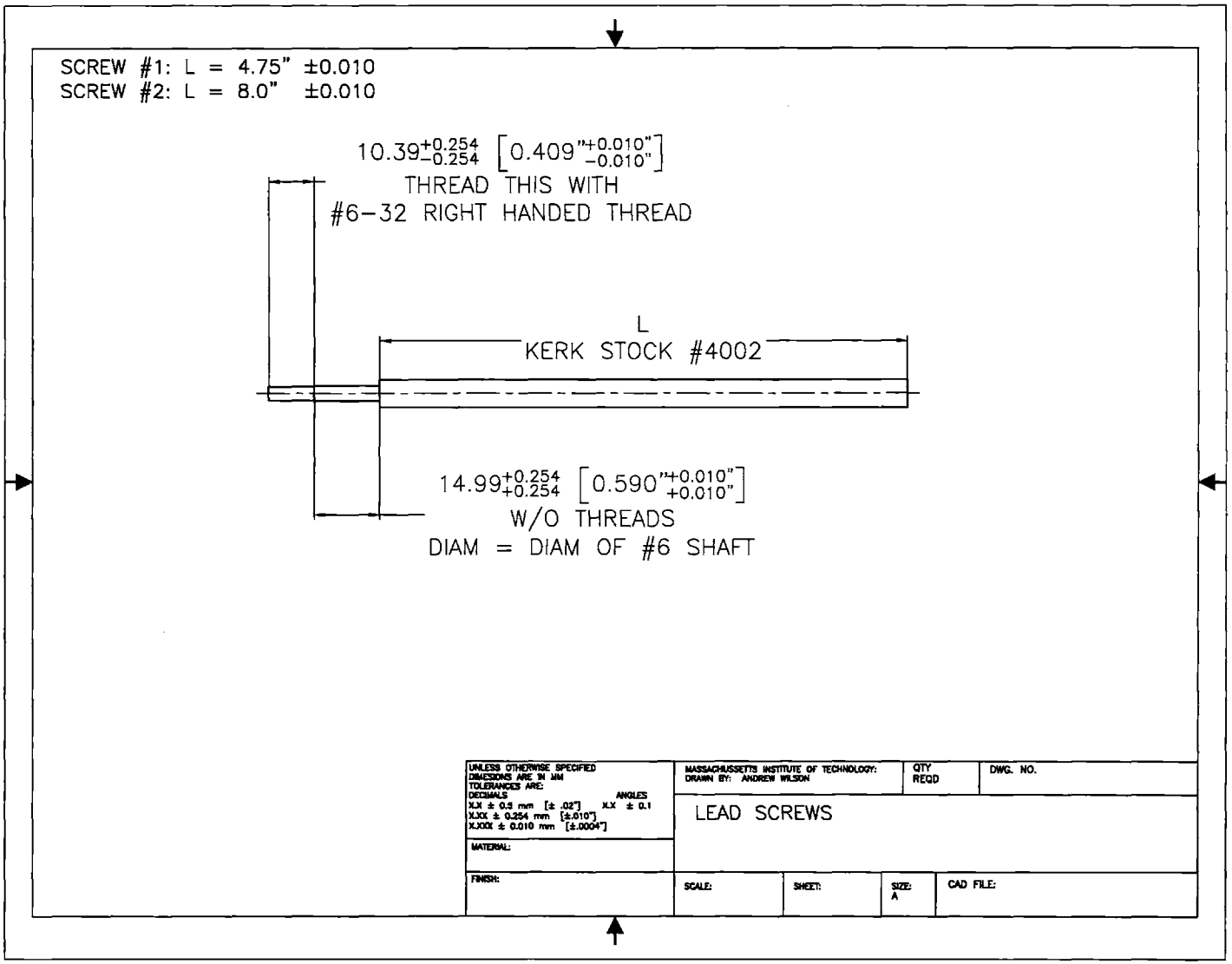
SCREW #1: L = 4.75" ±0.010
SCREW #2: L = 8.0" ±0.010
10.39 +0.254 −0.254 [0.409" +0.010" −0.010"]
THREAD THIS WITH
#6-32 RIGHT HANDED THREAD
L
KERK STOCK #4002
14.99 +0.254 +0.254 [0.590" +0.010" +0.010"]
W/O THREADS
DIAM = DIAM OF #6 SHAFT
UNLESS OTHERWISE SPECIFIED
DIMESIONS ARE IN MM
TOLERANCES ARE:
DECIMALS
X.X ± 0.5 mm [± .02"]
X.XX ± 0.254 mm [±.010"]
X.XXX ± 0.010 mm [±.0004"]
ANGLES
X.X ± 0.1
MATERIAL:
FINISH:
MASSACHUSSETTS INSTITUTE OF TECHNOLOGY:
DRAWN BY: ANDREW WILSON
QTY REQD
DWG. NO.
LEAD SCREWS
SCALE:
SHEET:
SIZE: A
CAD FILE:

Appendix C

Lead Screw Data

Two lead screws 4002 series lead screws by Kerk Motion were purchased, drawings can be seen on page 121.

Nominal Screw	**inch lead**	**Root Diameter**		**Efficiency**
Diameter		**in.**	**mm.**	**%**
1/4"	0.025	0.214	-5.44	30
(6.35 mm)				

The Nuts are NTB series 4002.

Dynamic Load	**Static Frictional Drag Torque**
10 lbs. (4.6kg)	1-3 oz.-in. (.01-.02 NM)

Anti-Backlash life

Anti-backlash life is the nut's ability to compensate for wear while maintaining its zero backlash properties. The following life data is based on 25% of the dynamic load rating. Life varies with loading, operation environment, and duty cycle.

Series	**Without TFE coating**	**With TFE coating**
ZBA	5 to 10 million (12 to 25 million)	15 to 40 million (38 to 100 million)
ZBX	40 to 60 million (100 to 150 million)	150 to 200 million (380 to 500 million)
KHD	80 to 100 million (200 to 250 million)	180 to 230 million (450 to 580 million)
NTB	100 to 125 million (250 to 315 million)	200 to 250 million (500 to 635 million)
VHD	200 to 225 million (500 to 570 million)	300 to 350 million (760 to 880 million)
B	N/A, Typical backlash, 0.003 to 0.010 (0.076 to 0.25)	N/A, Typical backlash, 0.003 to 0.010 (0.076 to 0.25)

Material Properties

Lead Screw			Nuts		
Material	**Surface Finish**		**Material**	**Tensile Strength**	**Coefficient of Expansion**
303 Stainless Steel	< 10 μinch		Polyacetal with lubricating additive	9,700 psi	6.0×10^{-5} $^{in./in.\rho}{}_F$

Torque Profile Calculation

$$T = T_f + T_v + T_l + T_j$$

T_f = nut drag = 3 oz.-in

$K_d = 0$; Dynamic coefficient of friction, nut to screw. The manufacturer does not have information on this parameter for their lead screws.

Assembly	
Standard Operating Temperature Range	**Coefficient of friction Nut to Screw**
32-200 ° F (0 – 93 ° C)	Static = 0.08 Dynamic = 0.15

$$T_l = \frac{\text{Load} \times \text{Lead}}{2\pi \times \text{Efficiency}} = 0.0060 \text{ Newton Meter}$$

Load = 1lbs. + 0.3 ×10lbs. = (weight of catamaran) + (μ preload)

Lead = 0.025"/rev.

Efficiency = 30%

J = Effective inertia $\approx 2\times$ Lead screw inertia = 2×0^{-4} oz.-in. sec^2

A = Acceleration [in/s^2]

The maximum acceleration is from Figure 2-3, is roughly 0.4 in/sec^2. Therefore the maximum required torque is 3.0002 oz.-in..

Matlab code generating the torque profile:

```
clear all;
clc;


%initial conditions
theta0=0;      %position
dtheta0=0;     %velocity
ddtheta0=0;    %acceleration


tf=6;          %finish in ten seconds
lead = 0.025; %inch per rev ->  the lead screw
dist = 6;      %travel 6 inches
```

```
%the final position data
thetaf = (dist/lead)*2*pi; %  (in/(in/rev))*(2pi rads/rev)
dthetaf=0; %we want to be stopped at the end
ddthetaf=0;% we don't want to be accellerating at the end

%these are the constraints on the trajectory
a0=theta0;
a1=dtheta0;
a2=.5*ddtheta0;
a3=(20*thetaf-20*theta0-(8*dthetaf+12*dtheta0)*tf...
    -(3*ddtheta0-ddthetaf)*tf^2)/(2*tf^3);
a4=(30*theta0-30*thetaf-(14*dthetaf+16*dtheta0)*tf...
    +(3*ddtheta0-2*ddthetaf)*tf^2)/(2*tf^4);
a5=(12*thetaf-12*theta0-(6*dthetaf+6*dtheta0)*tf...
    -(ddtheta0-ddthetaf)*tf^2)/(2*tf^5);

count = 0;

%define drag torque Tf = nut_drag
nut_drag = 3; %oz-in
Tf = nut_drag %torque from nut drag


preload = 10; %6lbs
u = 0.3; %nylon pads
Load = 1+preload*u; %1 lbs (weight of catamaran) + bearing preload
Load = Load * 15.8; %->convert to oz
Efficiency = .3; %  30%
Tl = Load*lead/(2*pi*Efficiency)  %torque due to load
```

```
%Kd = 0; %kerk motion doesn't have info on Kd


% lets double the inertia of the lead screw for effective
% interia, this over estimates it though!

density = 7.865E3 * 1/(100^3); %Kg/cm^3                          50
r = 0.25*2.54/2; %1/8"-> cm
l = 8*2.54; %8"->cm
volume = pi*r^2*l % this is cm^3
mass = density*volume % kg
I = .5*mass*r^2 %this is in Kg/m^2 we need to convert to oz-in-sec^2
I = I*(0.0141612) %now its in oz-in-sec^2, the .01416 converts to oz-in-sec^2
I=I*5 %safety factor
for t=0:tf/100:tf,
   count=count+1;
   theta(count) = polyval([a5,a4,a3,a2,a1,a0],t)*lead/(2*pi); %inches   60
   dtheta(count) = polyval([5*a5,4*a4,3*a3,2*a2,a1],t)*(1/(2*pi))*60; %this is RPM
   ddtheta(count) = polyval([4*5*a5,3*4*a4,2*3*a3,2*a2],t)*...
        lead/(2*pi);%this is inches/(sec^2)

   Tv=0; %no info on Kd so viscous torque is zero,
         %our saftey factor should take care of this
   Tja = I*ddtheta(count);
   T(count)=Tv+Tja+Tf;
end
                                                                 70
t=0:tf/100:tf;

subplot(3,1,1),plot(t,theta,'k','LineWidth',3)
```

```
title('Position');
ylabel('Position [Inches]');
subplot(3,1,2),plot(t,dtheta,'k','LineWidth',3)
title('Velocity');
ylabel('Velocity [RPM]');
subplot(3,1,3),plot(t,ddtheta,'k','LineWidth',3)
title('Acceleration');                                          80
xlabel('Time [s]')
ylabel('Acceleration [Inches/s^2]');
figure(2),plot(t,T,'k','LineWidth',3);
xlabel('Time [s]');
ylabel('Torque [oz.-inch]');
Title('Torque Curve');
```